2019-01-01

Origin And Characterization Of Intrasalt Non-Halite Lithologies Of The Neoproterozoic Patawarta Diapir, Central Flinders Ranges, South Australia

Rachelle A. Kernen
University of Texas at El Paso

ORIGIN AND CHARACTERIZATION OF INTRASALT NON-HALITE LITHOLOGIES OF THE NEOPROTEROZOIC PATAWARTA DIAPIR, CENTRAL FLINDERS RANGES, SOUTH AUSTRALIA

RACHELLE KERNEN M.S.

Doctoral Program in Geological Sciences

APPROVED:

_____
Katherine A. Giles, Ph.D., Chair

_____
Richard Langford, Ph.D.

_____
Aaron Velasco, Ph.D.

_____
J. Carl Fiduk, Ph.D.

_____
Lorena Moscardelli, Ph.D.

_____
Stephen Crites, Ph.D.
Dean of the Graduate School

DEDICATION

I dedicate this dissertation to my nephew, Rory Timothy Weiss.

You are the shining star in my life. May you grow with grace.

ORIGIN AND CHARACTERIZATION OF INTRASALT NON-HALITE LITHOLOGIES OF THE NEOPROTEROZOIC PATAWARTA DIAPIR, CENTRAL FLINDERS RANGES, SOUTH AUSTRALIA

by

RACHELLE KERNEN, B.S., M.S.

DISSERTATION

Presented to the Faculty of the Graduate School of

The University of Texas at El Paso

in Partial Fulfillment

of the Requirements

for the Degree of

DOCTOR OF PHILOSOPHY

Department of Geological Sciences

THE UNIVERSITY OF TEXAS AT EL PASO

December 2019

ACKNOWLEDGEMENTS

Thank you to Dr. Katherine Giles and Nila Matsler from the Institute of Tectonic Studies Salt-Sediment Interaction Research Consortium and Dr. James Kubicki and Dr. Annette Veilleux of the Department of Geological Sciences for their financial support throughout my career at the University of Texas El Paso. Thank you to all my committee members, Dr. J. Carl Fiduk, Dr. Richard Langford, Dr. Lorena Moscardelli, and Dr. Aaron Velasco for your service and guidance during my dissertation. Thank you to Denise Butler, Sarah Giles, Asmara Lehrmann, Piper Poe, and David Canova for being my field assistants. Special thank you to my family and global network of colleagues and friends for the encouragement and friendship.

The field research has been funded by present and past corporate sponsors of the Institute of Tectonic Studies Salt-Sediment Interaction Research Consortium, first at New Mexico State University and later at The University of Texas at El Paso (Anadarko, BHP, BP, Chevron, ConocoPhillips, Devon, ExxonMobil, Hess, Kosmos, Marathon, Nexen, Repsol, Samson, Shell, Statoil, Total), the American Association of Petroleum Geologists Grants-In-Aid David Wiman Award, the Society of Professional Earth Scientists Award, UTEP Geological Sciences Department Bruce Davidson Memorial Award, the Vernon G. and Joy Hunt Endowed Scholarship Fund in Geology, West Texas Geological Society Award, Roswell Geological Society Award, and UTEP Geological Sciences Hunt and Rowling Scholarship, PinkPetro GRIT Nomination, and numerous travel grants through UTEP, Geological Society of America, and The American Geophysical Union. Special thank you to Dr. Mike Hudec with the Applied

Geodynamics Laboratory at the Bureau of Economic Geology (University of Texas at Austin) for hosting me during summer 2017 and BP Americas for the internship experience in Houston during summer 2018.

Thank you to Bob Dalgarno, Dr. Trevor Mount, Dr. Frank Peel, and Dr. Tim Dooley for excellent technical discussions. Thank you to the Moolooloo Station Landowners, Keith and Lisa Slade, Angorichina Station Landowners Ian and Diana Fargher, and Warraweena Station Caretaker Stony Steiner, who graciously gave access to Patawarta diapir in the Flinders Ranges, South Australia.

ABSTRACT

Non-halite lithologies in salt diapirs are variously referred to as clasts, chips, rafts, stringers, sutures, and encased minibasins in the literature. Due to the complexities of gathering and processing seismic reflection data within salt bodies, non-halite intrasalt lithologies, collectively referred to as inclusions here, are often first identified while drilling wells. These wells may penetrate unexpected lithologies of unknown fluid pressure, which can result in economic failure and pose serious drilling hazards and a threat to human life. Therefore, it is imperative to identify and determine the nature of inclusions prior to drilling, and ideally during the well planning process in order to better risk the likelihood of drilling success that ultimately leads to the discovery and safe production of economic hydrocarbon accumulations. Our current understanding of intrasalt inclusions is based primarily on seismic reflection data observations and interpretations, a few well penetrations, and physical and numerical modeling, which provide limited information about the detailed nature and possible origins of intrasalt inclusions. This type of information is best derived from outcrop studies. The research results presented here aim to provide the first targeted outcrop study of intrasalt inclusions.

The exceptionally well exposed Patawarta Diapir, Flinders Ranges, South Australia contains a wide variety of intrasalt inclusion lithologies of both sedimentary and meta-igneous in origin. Patawarta Diapir provides a unique opportunity to study two different types of carbonate intrasalt inclusions in detail allowing their attributes to be documented and their origin to be determined, thus increasing our ability to identify and predict the presence of these types of inclusions in other salt diapirs. The first is present

at the margin of the diapir specifically at the salt-sediment interface, known as the Rim Dolomite and the second are a series of limestone-dominated inclusions surrounded by dolomicrite diapiric matrix and concentrated at the southern side of the diapir.

The results of field and laboratory studies of the Rim Dolomite indicate that it represents lateral dolomite caprock. The caprock developed originally in a crestal position on the Patawarta salt sheet by dissolution of halite and corresponding concentration of anhydrite insoluble residue that was subsequently altered to dolomite through processes associated with sulfate-reducing microbes. Caprock formation occurred during deposition of the Marinoan Bunyeroo Formation. Shortly after formation the dolomite caprock was rotated to a diapir-flanking (lateral) position by halokinetic drape folding associated with passive diapiric flow of the Patawarta salt sheet.

The results of field and laboratory studies of five limestone -dominated inclusions shows that the limestone was deposited as part of the post -salt Marinoan (Ediacaran) Wonoka and Bonney Sandstone formations. The inclusion strata were deposited on top of the Patawarta salt sheet as a carapace. The carapace strata were subsequently dismembered and encased in salt at an allosuture. The allosuture indicates that the mapped Patawarta Diapir actually represents two separate salt sheets that collided and superimposed one sheet over the other and incorporating the carapace of the underlying salt sheet at a suture zone as the overriding salt sheet rode over the top of the underlying salt sheet.

The two inclusion case studies from Patawarta Diapir are used to develop an inclusion classification scheme that could be used for both surface and subsurface

analysis of intrasalt inclusions. The classification system is based on the time-stratigraphic age of the inclusion lithology in relation to the depositional age of the salt layered evaporite sequence: presalt, synsalt, or post salt in age. The classification scheme is used to explore the range possible types of non-halite lithologies that could be found in a salt diapir and provides an explanation of the mechanism of inclusion incorporation into the diapir. This classification system is the first of its kind and aims to provide a useful tool in attempting to identify the origin and nature of intrasalt inclusions.

TABLE OF CONTENTS

Page

CHAPTER 1: INTRODUCTION

1.1 SIGNIFICANCE AND IMPLICATIONS

Understanding the potential hazards of drilling through salt bodies both onshore and offshore is a key component to drilling those wells safely. Salt-associated hazards may be related to the lithologic variability within the intrasalt non-halite lithologies, shear zones, and fluids within salt bodies (Davison, 2009; Dooley et al., 2017; Fernandez et al., 2017). Intrasalt, non-halite lithologies are variously referred to as clasts, chips, rafts, stringers, sutures, and encased minibasins in the literature (Dooley et al., 2012; Edwards et al., 2014; Fernandez et al. 2017; Fiduk & Rowan, 2012; Fiduk et al. 2014; Jackson et al., 2012; Moore & Douglas 2013; Neely et al. 2017; Rowan & Inman, 2011) and are collectively referred to as inclusions here. Previous 2D and 3D seismic reflection inclusion studies have focused on the identification of inclusions on datasets in various offshore salt basins like the deepwater Gulf of Mexico (Dooley et al., 2012; Edwards et al., 2014; Fiduk et al., 2014; Moore & Douglas, 2013; Neely et al., 2017; Rowan & Inman, 2011), Santos Basin (Fiduk & Rowan, 2012; Jackson et al., 2015) and Pre-Caspian Sea (Fernandez et al., 2017; Jackson et al., 2019). Fernandez et al. (2017) used 3D seismic reflection and borehole data to provide a classification of inclusion lithology types and outlined several possible modes of salt encasement to form intrasalt sediment packages specific to the Caspian Sea. Previous outcrop studies primarily focus on identifying the presence of inclusions in various onshore salt basins like the Katangan Central African Copper Belt (Cailteux et al., 2018; Jackson et al., 2004), Spanish Pyrenees (Lagabrielle et al., 2010), and Paradox Basin, Utah and

Colorado (Thompson-Jobe et al., 2019). The significance of this dissertation is that it identifies an outcrop exposure of non-halite lithologies along the salt-sediment interface and within a salt diapir, but it explores the stratigraphic origin, by using field-based principals, geochemical tools, and a classification system to further evaluate their origin.

1.2 RESEARCH OBJECTIVES

Patawarta diapir is located in the Central Flinders Ranges, South Australia, and is historically interpreted as a single diapir containing sedimentary and igneous inclusions from the autochthonous Willouran-aged Callanna Group stratigraphy (Hall, 1984). With new detailed mapping of Patawarta Diapir, a lateral caprock ('rim dolomite') is identified at the salt-sediment interface and five predominately limestone inclusions concentrated on the southern end have been re-interpreted as Ediacaran-aged Wonoka Formation and Bonney Sandstone (Wilpena Group). The Ediacaran-aged inclusions are concentrated to the southern side of the diapir where they are juxtaposed against a Willouran-aged Curdimurka Subgroup (Callanna Group) autochthonous inclusion, which is approximately 300 years older. The exceptional outcrop exposures at Patawarta Diapir provide a unique opportunity to specifically address three important topics related to intrasalt stratigraphy: 1) document the timing and nature of the rim dolomite as lateral caprock at the salt-sediment interface; 2) determine the stratigraphic origin of anomalous limestone inclusions, and 3) propose a classification scheme for all potential intrasalt inclusions and future work.

1.3 SUMMARY OF CHAPTER 2

Chapter 2 re-interprets the rim dolomite at Patawarta Diapir as a carbonate caprock using mapping relationships and presence of capstone fabrics and tests the hypothesis that the rim dolomite formed as diapir crestal caprock that was subsequently rotated to a diapir flanking ("lateral") position. The rim dolomite is named for a ridge of dolomite mapped around the margin of Patawarta Diapir at the contact of the diapir and the outboard surrounding Marinoan Bunyeroo Formation. The rim dolomite was interpreted previously as local, diapir-centric, sedimentary depositional carbonate facies within the fine-grained siliciclastic Bunyeroo Formation (Hall, 1984). The rim dolomite's lateral and vertical stratal geometries and field relationships were mapped in order to understand their stratigraphic origin. A series of 'capstone' fabric types were identified and described in order to demonstrate a caprock origin. Typically, caprock forms in a crestal position above a salt diapir. However, due to halokinetic drape-fold rotation, the caprock at Patawarta Diapir was rotated into the lateral position along with the Bunyeroo Formation.

1.4 SUMMARY OF CHAPTER 3

Chapter 3 identifies and characterizes five anomalous intrasalt limestone inclusions in the Patawarta Diapir. The inclusions were originally described as being part of the synsalt, Willouran-Torrensian age layered evaporite sequence called the Callanna Group, which regionally contains only rare limestone lithologies. This study reinterprets the carbonate inclusions as derived from the postsalt Wonoka and Bonney

formations that are approximately 300 million years younger. β13 C isotopes of the carbonate inclusions are chemostratigraphically correlated to the regional stratigraphy containing the Shuram Excursion in order to test the hypothesis that they originated from a much younger origin. Three salt encasement mechanisms are proposed as the process for incorporation of the significantly younger inclusions into the Patawarta Diapir.

1.5 SUMMARY OF CHAPTER 4

Chapter 4 proposes a classification scheme that divides intrasalt inclusions into three time-stratigraphic sequences related to the depositional age of the salt layered evaporite sequence (LES); 1) *presalt* inclusions originate from the sedimentary, igneous, and metamorphic lithologies present in the basin that are older than the layered evaporite sequence; 2) *synsalt* inclusions originate from competent interbeds in the layered evaporite sequence, including siliciclastics, carbonates, volcanic flows, and shallow sills; and 3) *postsalt* inclusions originate from the stratigraphy deposited above the layered evaporite sequence and any igneous activity that postdates the layered evaporite sequence. Modes of deposition and origin are proposed for each sequence and future work is proposed in order to address the field studies required in order to carry this work forward.

CHAPTER 2: ORIGIN OF THE RIM DOLOMITE AT PATAWARTA DIAPIR

Published in the Australian Journal of Earth Sciences (2019)

2.1 ABSTRACT

The 'rim dolomite' of South Australia's Central Flinders Ranges is a prominent ridge-forming, layered dolomitic and siliceous unit. The rim dolomite is interpreted to be a lateral caprock found exclusively at the salt–sediment interface between the Patawarta diapir and the Ediacaran-aged Bunyeroo Formation. Lateral dolomite caprock is defined by the following field relationships: 1) the rugose dolomicrite base that parallels the contact of the diapiric matrix and the bedding in the overlying stratigraphy, the exclusive presence of dolomite at the salt–sediment interface, 3) the lack of sedimentary structures or fossils (cyanobacterial laminites and stromatolites), 4) the lack of interbedded Bunyeroo lithofacies, and 5) the inability to trace the rim dolomite capstone away from the diapir margin into the outboard stratigraphy. In addition to the field relationships, the rim dolomite displays the following capstone fabrics: 1) massive—microcrystalline dolomite, 2) porphyritic—two distinct crystal sizes, one forming microcrystalline dolomite groundmass and the other forming rosettes of silica, 3) banded—microcrystalline dolomite forming pressure-dissolution layers of silica and authigenic hematite, and 4) brecciated—mosaic to disorganised, forming a microcrystalline dolomite groundmass, which locally contains remnant clasts of Callanna non-evaporite lithologies, such as quartz arenite to arkosic sandstones and basalts, surrounded by an anastomosing cement-filled vein network. All capstone fabrics contain various amounts of anhydrite, quartz, feldspar and non-evaporite grains

that represent the insoluble residue during halite dissolution and caprock accretion. Three different genetic models for the lateral caprock are described and tested, and that of these, only the halokinetically rotated caprock model fits the data. The field relationships and capstone fabrics of the rim dolomite match other lateral caprocks in salt basins such as the Paradox Basin and Gulf Coast, USA.

2.2 INTRODUCTION

The Patawarta diapir is a Neoproterozoic allochthonous salt sheet exposed in the Flinders Ranges of South Australia (Figure 1a). Locally exposed along the margin of the diapir is an enigmatic carbonate unit mapped as the 'rim dolomite' (Figure 1b). The rim dolomite forms a resistant, linear carbonate ridge, less than 100m wide and up to 500m long. Coats (1964) interpreted the rim dolomite as a metamorphic differentiation of dolomitic material from carbonate breccia, with apparent bedding interpreted as a flow structure from the moving diapir (Figure 2). Hall (1984) and Lemon (1988) interpreted the rim dolomite as a local, diapir-centric, carbonate depositional facies within the adjacent fine-grained siliciclastics of the Bunyeroo Formation. Several other origins have been hypothesized including: 1) a rubble zone generated during advance of the salt sheet, 2) a large clast or a bedded unit of dolomite on top of the salt from the Callanna Group that was pushed and rotated to the margin of the diapir during internal salt flow, 3) a diagenetic alteration halo or concretion in the Bunyeroo Formation, and 4) a carbonate caprock (Figure 2; Giles et al., 2012). This study provides detailed documentation of the field relationships originally established by Giles et al.,

(2012) and new detailed stratigraphic and petrographic documentation of the rim dolomite.

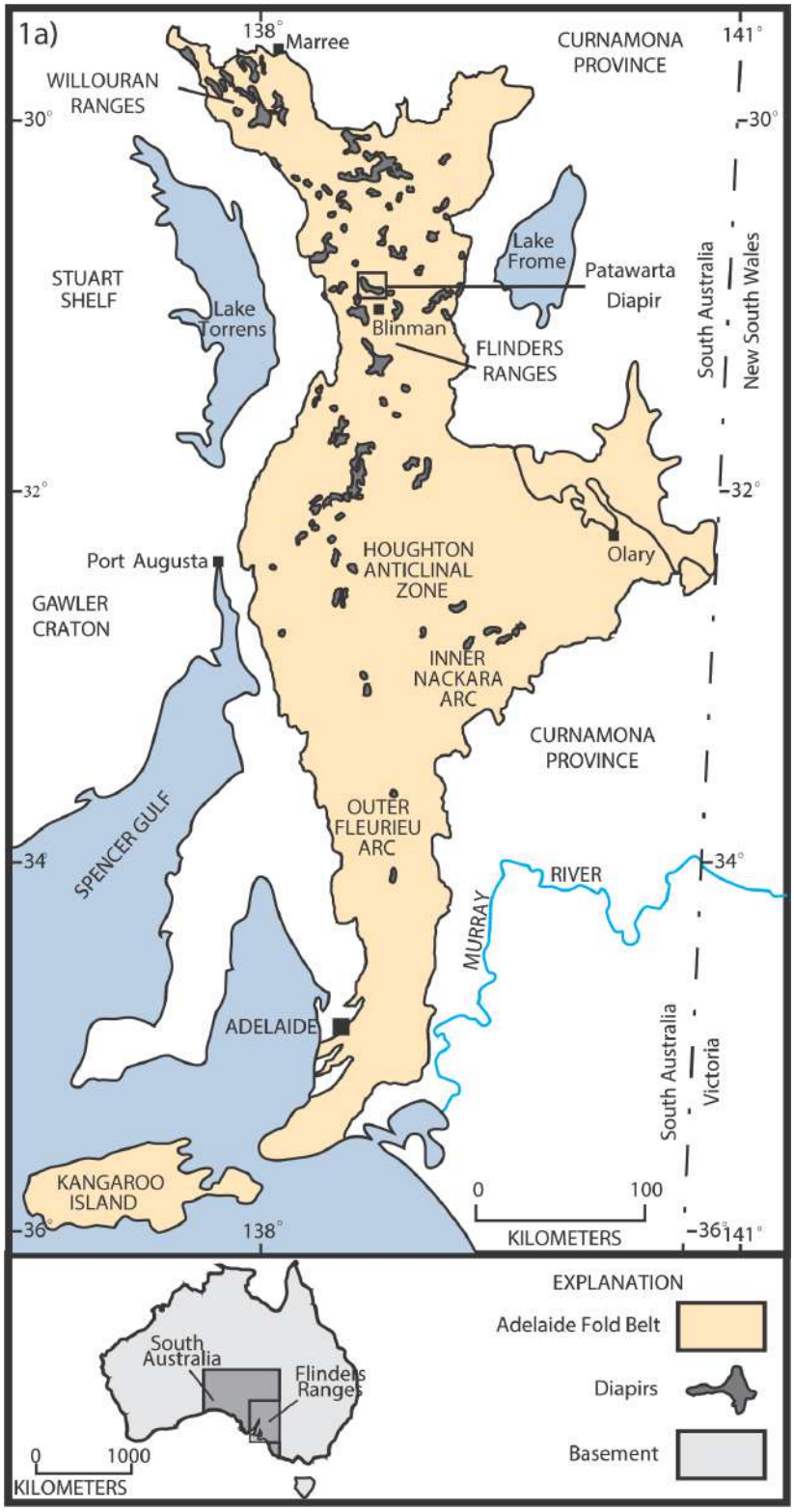

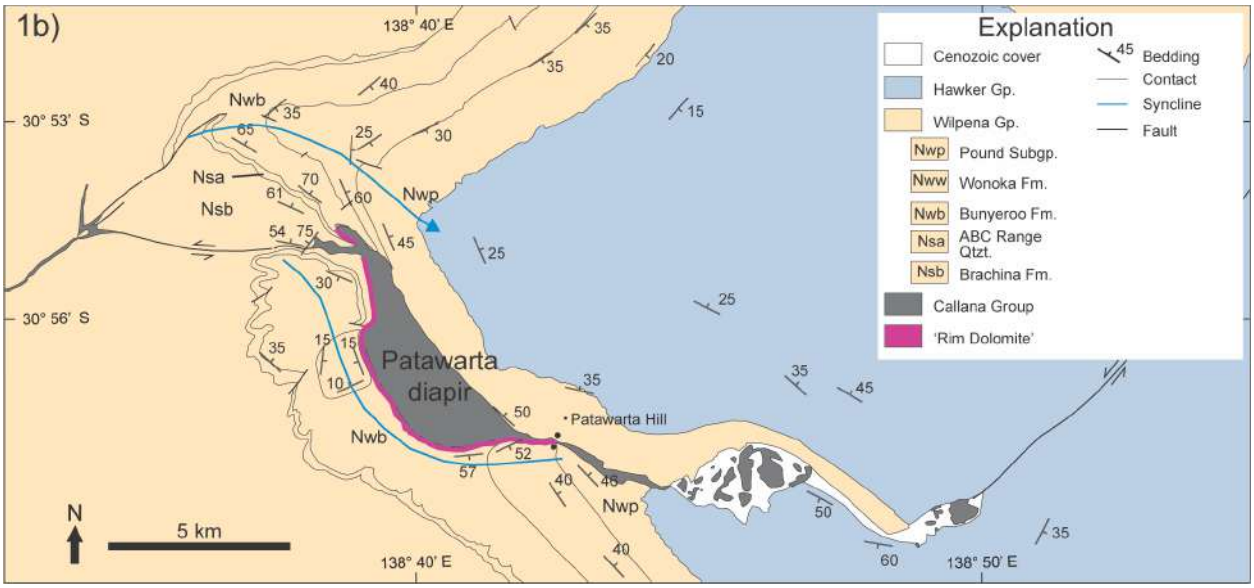

Figure 1: a) Map of the Adelaide Foldbelt of South Australia displaying the location of major salt diapirs, including the Patawarta diapir in the Central Flinders Ranges (modified from Kernen, 2011; after Dalgarno & Johnson, 1968); and b) location of rim dolomite adjacent to the Patawarta diapir (modified from Hearon et al., 2015b).

Figure 2: Rim dolomite at the salt–sediment interface at the Patawarta diapir.

Salt diapir caprocks form by dissolution of halite and the cross flow of halite-undersaturated waters that leaves an insoluble residue of the non-halite minerals accreting along the salt–sediment interface (Figure 3; Kyle & Posey, 1991). The insoluble residue is dominated by sulfate minerals (anhydrite and gypsum) that progressively accrete downward with ongoing halite dissolution during diapiric inflation, a process referred to as 'underplating' (Kyle & Posey, 1991). Early in this process, microbe sulfate reduction (up to 85 ^{o}C) or thermochemical sulfate reduction (100–135 ^{o}C) reduce organic compounds such as dead organic matter, carbohydrates, kerogen, crude oil, bitumen, dissolved or gaseous organic compounds (Machel, 1989).

Sulfate is reduced to sulfide (H2S, HS–, and S2–) and to elemental sulfur while the organic compounds are oxidized to bitumen, bicarbonate, and/or carbon dioxide (Machel, 1989). A number of minerals may precipitate if the specific cations are available in sufficient amounts: these include calcite, dolomite, siderite, ankerite, pyrite, sphalerite, galena, and other minerals (Machel, 1989). Secondary and tertiary porosity, as well as solution-collapse brecciation, may occur owing to the dissolution of solid sulfates and/or carbonates (Machel, 1989). As a result, a vertically zoned sequence of anhydrite, gypsum, and/or limestone is formed along the salt–sediment interface and referred to as caprock (Figure 3; Kyle & Posey, 1991). Caprock associated with salt bodies can be found in both crestal and lateral positions adjacent to salt bodies (Evans, Nunn, & Hanor, 1991; Giles et al., 2012; Jackson, & Lewis, 2012; Kyle & Posey, 1991; Mast, 2016; Schwerdtner & Troeng, 1978).

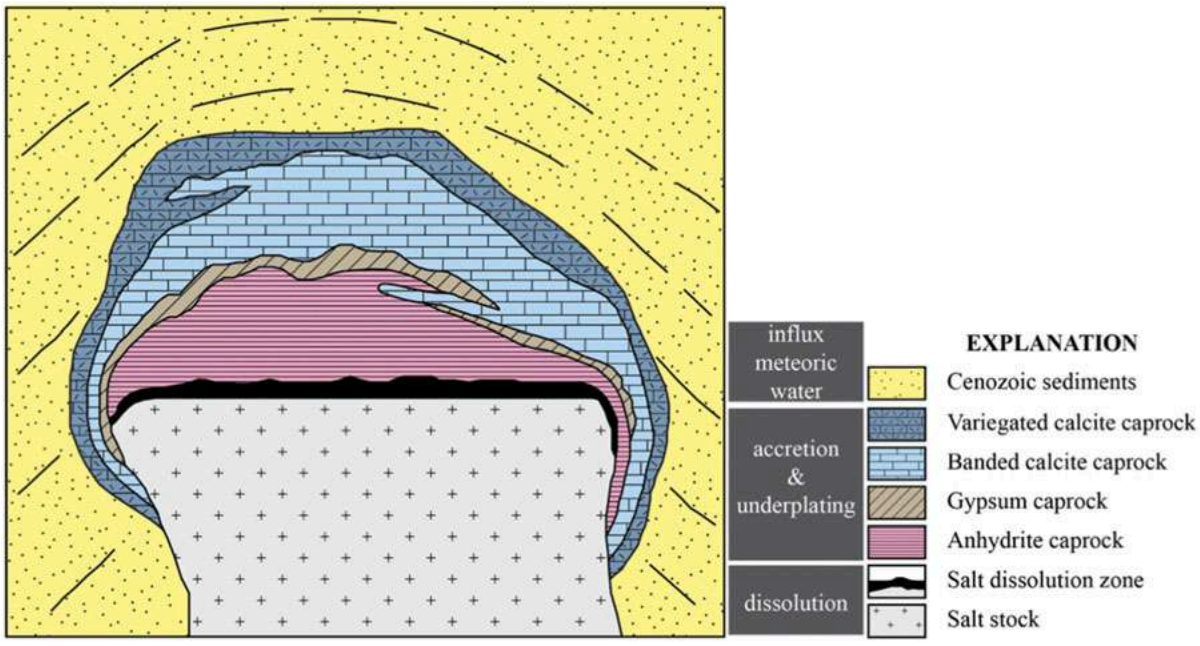

Figure 3: Generalized cross-section of a typical Texas Gulf Coast diapiric carbonate caprock assemblage (modified from Kyle & Posey, 1991).

Using new detailed field mapping, stratigraphic and petrographic analysis of the rim dolomite and adjacent stratigraphy, we reinterpret the rim dolomite as lateral carbonate caprock that developed roughly coeval to the deposition of the Ediacaran Bunyeroo Formation. This study provides the first outcrop documentation of lateral carbonate caprock at the salt–sediment interface of an allochthonous salt sheet. A set of criteria is proposed for recognizing lateral carbonate caprock that can be applied to evaluating the origin of diapir-centric carbonate bodies in salt basins worldwide. We derive the capstone definition and classification from outcrop and thin-section observations by Poe et al. (2018).

2.3 GEOLOGICAL SETTING

The Adelaide Rift Basin formed during the breakup of the Rodinia supercontinent in the Neoproterozoic (Dyson, 1996; Jenkins, 1990; Preiss, 2000; Sprigg, 1952). The pre-rift basement (Pre-Adelaidean) is of Archean–Paleoproterozoic age. The rift fill (Figure 4) consists of syn- to post-rift Callanna and Wilpena group sediments of Neoproterozoic (Adelaidean) age, overlain by Cambrian Hawker Group. The rift basin was inverted in the late Cambrian to Ordovician to create the Adelaide Foldbelt (Figure 1a) during the Delamerian Orogeny (Forbes & Preiss, 1987; Preiss, 2000). The basal rift fill unit, the Callanna Group, of Willouran age, includes a layered evaporite sequence consisting of siliciclastic, carbonate, and evaporite sediments (Dyson, 1996; Forbes & Preiss, 1987; Preiss, 2000; Webb, 1960). Passive diapirism sourced from this interval began in latest Willouran to early Torrensian time period, continuing throughout the

deposition of the basin fill, and giving rise to more than 180 salt diapirs seen in outcrop in the Adelaide Foldbelt (Dalgarno & Johnson, 1968; Dyson, 1996; Forbes & Preiss, 1987; Rowan & Vendeville, 2006). The salt bodies range from simple diapirs to allochthonous salt sheets (Coats, 1973; Dyson 1998, 2004, 2005; Hearon, Lawton, & Hannah, 2010; Hearon et al., 2015a; Kernen, Giles, Lawton, Rowan, & Hearon, 2012; Lemon, 2000; Rowan et al., 2019; Williams, 2017).

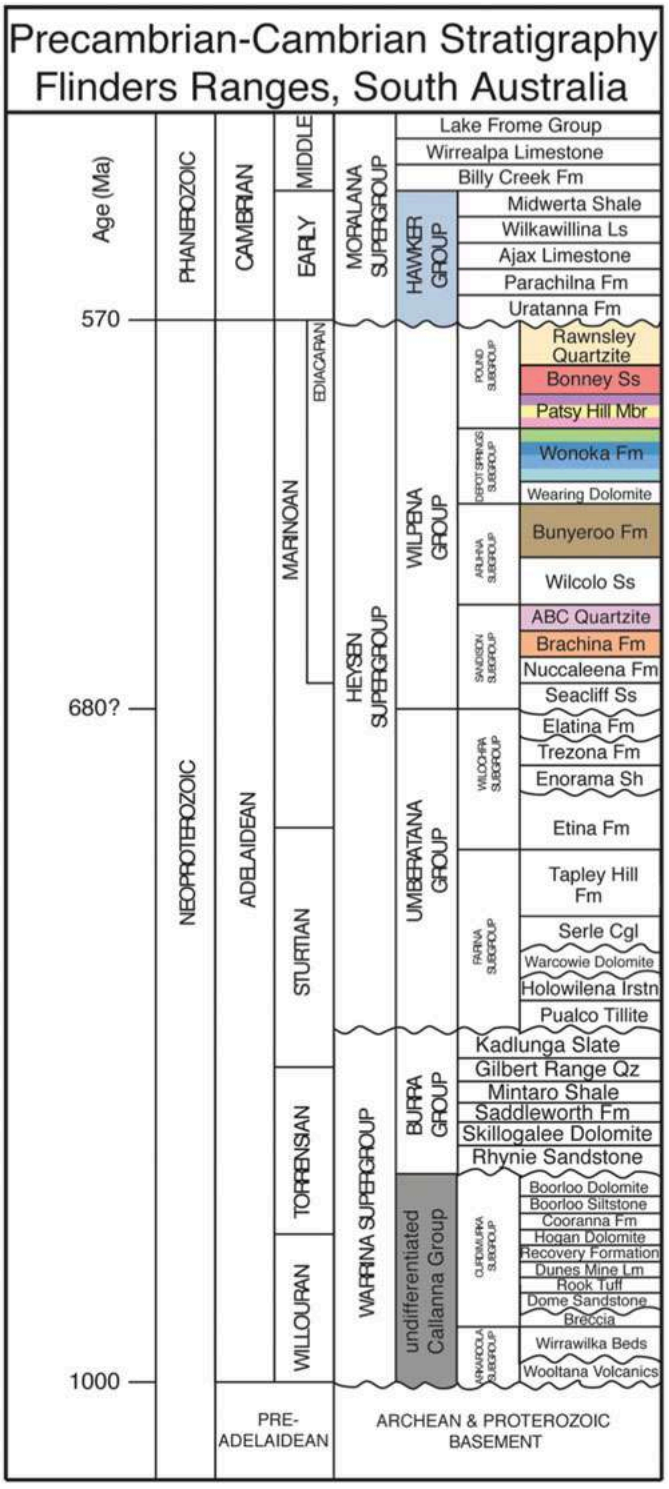

Figure 4: Precambrian–Cambrian stratigraphy of the Flinders Ranges, South Australia (modified from Preiss, 1987). Colored units correspond to the stratigraphic units documented at the Patawarta diapir in map view and cross-section. The

undifferentiated Callanna Group represents the remaining siliciclastic, carbonate and volcanic clasts of a former evaporate-dominated unit and the diapiric matrix.

The Patawarta diapir is located approximately 15 km north of the Blinman township. It contains decimeter- to kilometer-scale clasts of non-evaporite lithologies derived from the autochthonous Callanna Group, which includes fine-grained siliciclastics, carbonate and dolerite (fine- and coarse-crystalline basalt), and clasts of silty carbonates and shales from the Ediacaran Wilpena Group (Kernen, Giles, & Rowan, 2018). The Patawarta diapir, like all diapir outcrops in the Flinders Ranges, does not contain the original halite or other evaporite minerals, but has been intensely modified by strong halokinetic deformation, dissolution, igneous intrusion(s), and diagenetic alteration, so that it now consists of a dolomicrite breccia referred to as 'diapiric matrix' (Preiss, 1987). The diapiric matrix is located in zones around the siliciclastic, carbonate and dolerite Callanna and Wilpena group clasts. The Patawarta diapir forms an allochthonous salt sheet (Figure 1b; Hearon et al., 2015a; Jackson & Talbot, 1991; Kernen et al., 2012; Rowan et al., 2019), whereby the surface map view represents an oblique cross-sectional view of the diapir. The southern and western margins contain a subsalt minibasin while the northern and eastern margins contain a suprasalt minibasin (Gannaway, 2014; Kernen et al., 2012; Rowan et al., 2019). Ediacaran Wilpena Group through Cambrian Hawker Group stratigraphy is present in both the subsalt and suprasalt minibasins (Figure 4).

The nomenclature and subdivision of stratigraphic units in the Wilpena Group have a long and variable history (Figure 5). The earliest stratigraphic studies of the Wilpena Group in the Flinders Ranges are from Selwyn (1860), who describes the units as being 'olive-brown and blue sandy shales, and thin calcareous shales lying beneath thick sandstones and quartzites.' This description refers to the Bunyeroo and Wonoka formations, which are overlain by the Bonney Sandstone. Over half a century later, Mawson (1938, 1939, 1941) defined stratigraphic units equivalent to the Brachina Formation (lower Wilpena Group) through the uppermost Cambrian (Lake Frome Group).

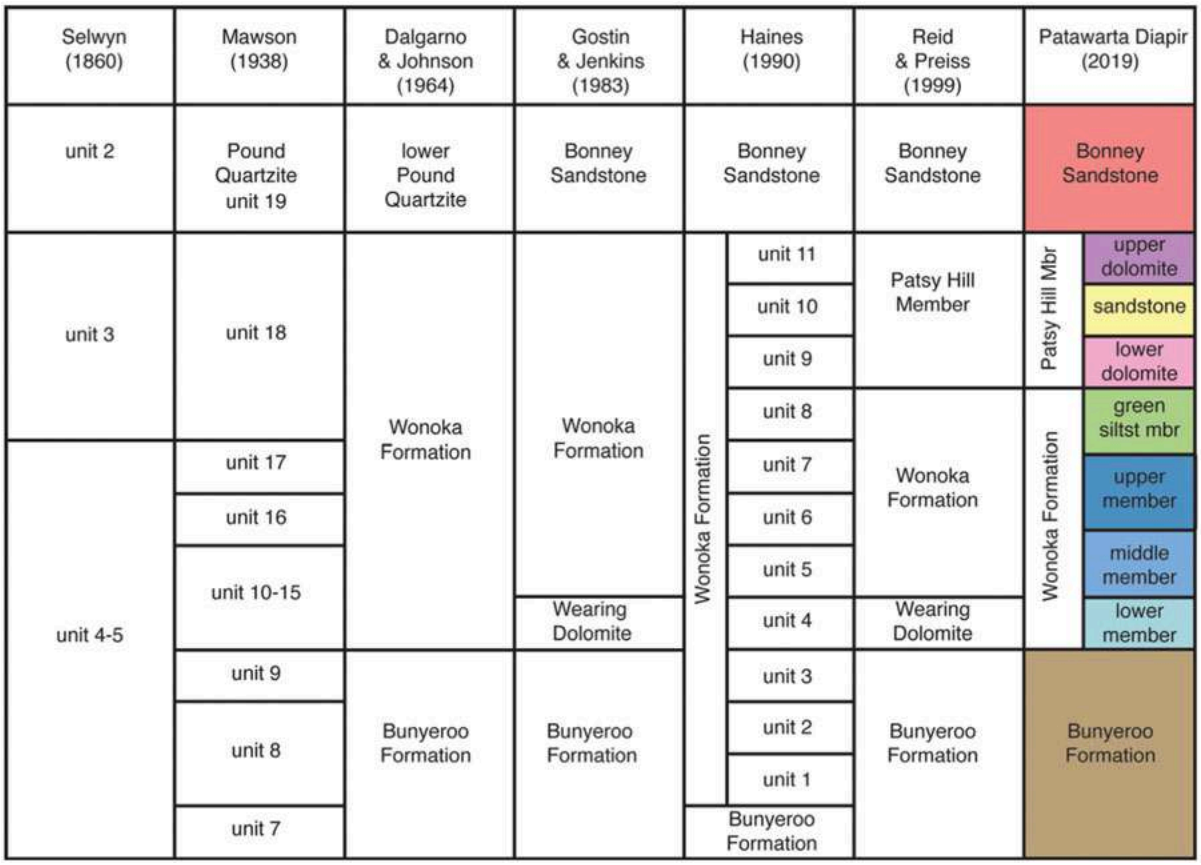

Figure 5: Evolution of the Bunyeroo and Wonoka formations, Patsy Hill Member, and Bonney Sandstone stratigraphic nomenclature though time (Kernen, 2011).

The Bunyeroo Formation is present in both the suprasalt minibasin to the northeastern side and the subsalt minibasin to the southwestern side of the Patawarta diapir (Figure 6). The Bunyeroo Formation has a sharp basal contact with the underlying ABC Range Quartzite, and an upper, more gradational contact with the overlying Wonoka Formation. The Bunyeroo Formation is composed of red, maroon, purple, green, yellow, tan, orange-brown, massive, thin-bedded (0.5–10 cm) laminated beds of shale and siltstone. The Bunyeroo Formation covers the rim dolomite on the northern and southern sides of the diapir (Figure 7; Lemon, 1988). On the northern side, the lower Bunyeroo Formation is composed of red to purple shale and siltstone that locally grades into lenses of conglomeratic sandstone containing granule to pebble-sized clasts of the rim dolomite (Gannaway, 2014). The rounded, moderately well-sorted sandstones consist of dominantly quartz with 5–10% feldspar grains (Gannaway, 2014). The western and southern margins display conglomerate and sandstones that occur as broad, lense-like outcrops. These outcrops thin away from the diapir and grade into the dominantly shale and siltstone lithologies of the Bunyeroo Formation (Figures 6 & 7). Above the halokinetic sequence boundary in the subsalt minibasin (Figures 6 & 7; Section E) stacked channelized lenses containing clasts of red Bunyeroo Formation, rim dolomite and dolerite exist and thus record periods of exposure and erosional reworking of the diapir, the rim dolomite, and Bunyeroo Formation roof strata (Figure 6). The Bunyeroo Formation is a homogenous calcareous siltstone (Figure 8a) with silt- to shale-sized grains of angular quartz. The upper member of the Wonoka Formation (Figure 8b) is a silty limestone containing iron-stained cyanobacterial

laminites. The Patsy Hill Member of the Bonney Sandstone contains oblong to circular peloids of an unknown origin (Figure 8c). The overlying Bonney Sandstone contains composite oncoids in rare carbonate beds towards the base of the units that are immediately adjacent to the Patawarta diapir (Figure 8d). These depositional carbonates in the outboard stratigraphy are distinctly different from the rim dolomite.

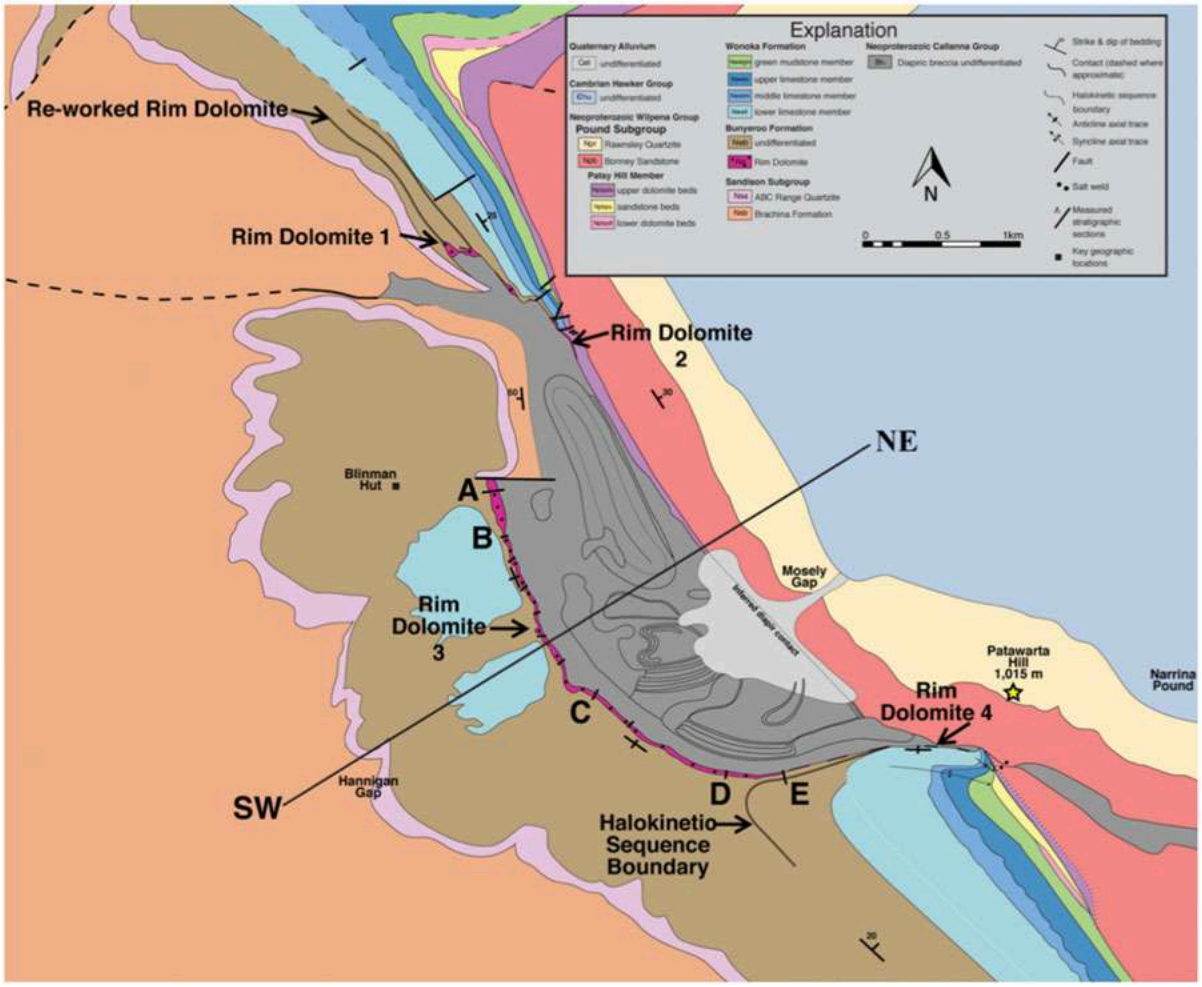

Figure 6: Geological map of the Patawarta diapir. Rim dolomite (hot pink) is located in the suprasalt crestal position (1, 2) and subsalt lateral position (3, 4). Black line represents location of cross-section in Figure 7.

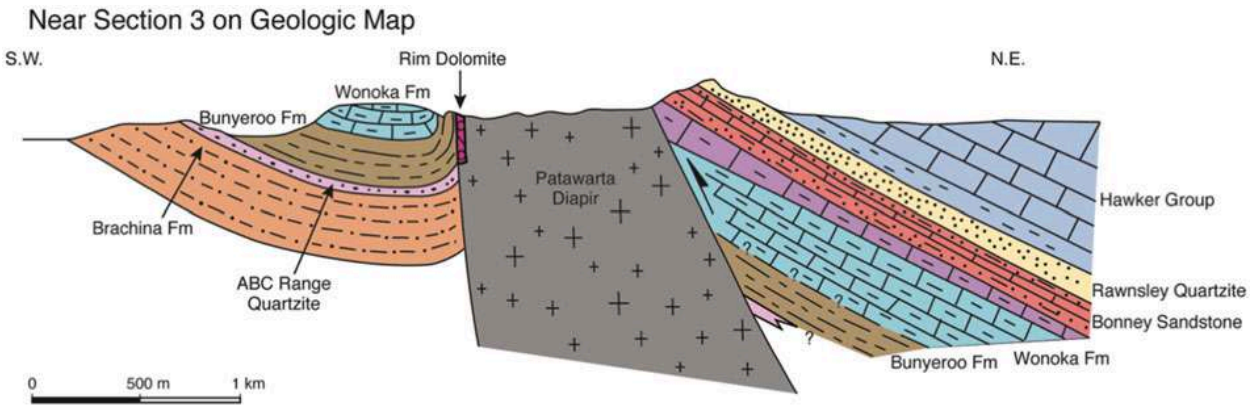

Figure 7: Cross-section through the rim dolomite (labelled 'rim dolomite 3' on Figure 6; modified from Lemon, 1988).

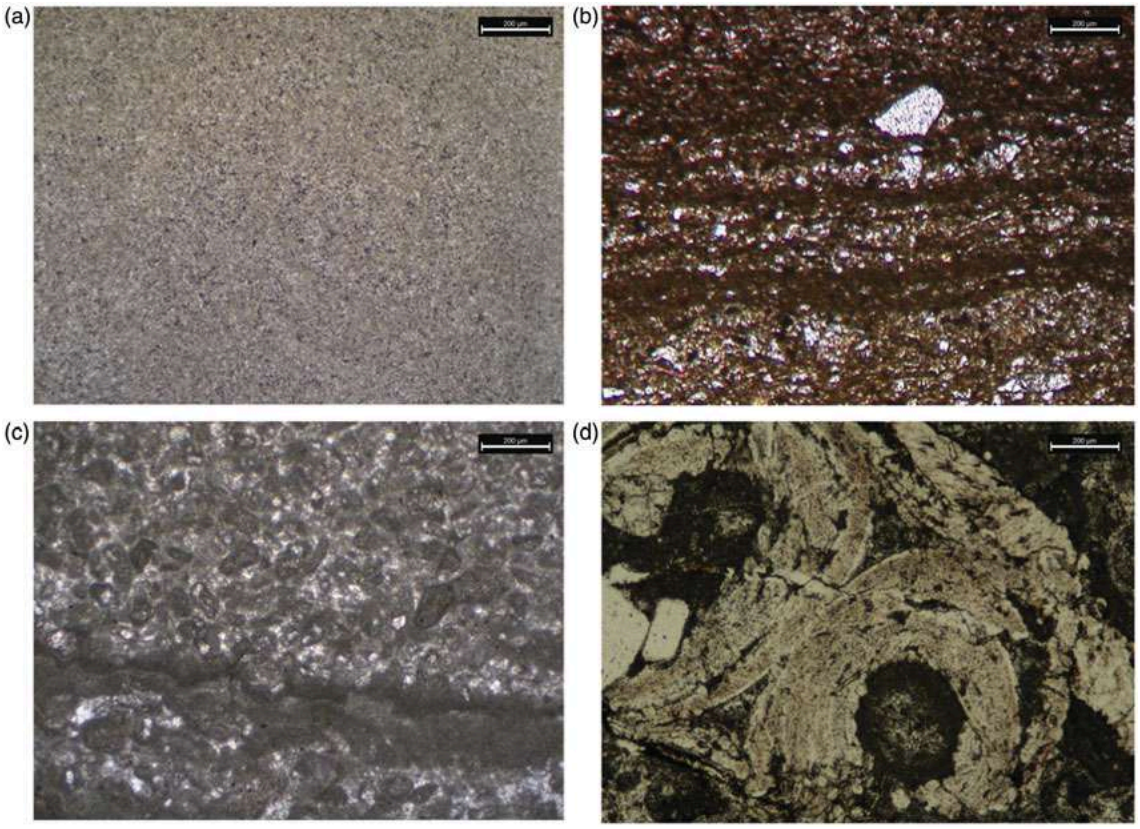

Figure 8: Photomicrographs in plane light of (a) siltstone from the Bunyeroo Formation, (b) algal laminite from the upper member of the Wonoka Formation, (c) peloids from

Patsy Hill Member of the Bonney Sandstone and (d) composite oncoids from the Bonney Sandstone.

The Bunyeroo Formation was originally interpreted by Mawson and Segnit (1949) as a loessite deposit based on the homogeneity, great thickness, minimal presence of coarse-grained sediments, and the absence of sedimentary structures. The depositional environment of the Bunyeroo Formation was later reinterpreted as a deep basinal shale to outer shelf setting below fair-weather and storm wave base (Dyson, 1992, 1996; Gannaway, 2014; Gostin & Jenkins, 1983; Preiss, 1987; von der Borch, Grady, Eickhoff, Dibona, & Christieblick, 1989). The age of the Bunyeroo Formation is constrained by the Acraman impactite layer (Gostin, McKirdy, Webster, & Williams, 2010), which constrains it as Ediacaran age (580 Ma).

The Wonoka Formation type section is approximately 620m thick at Bunyeroo Gorge (approximately 80 km south of the Patawarta diapir) in the Central Flinders Ranges (Haines, 1990). The depositional environment of the Wonoka Formation was a shallow marine, subtidal carbonate shelf that shallows upward from the lower shoreface to the foreshore (Haines, 1990). Reid and Preiss (1999) redefined the base of the Bonney Sandstone to include the shallow-water carbonates, formerly included in the uppermost Wonoka Formation, which is now referred to as the Patsy Hill Member of the Bonney Sandstone (Figure 5; Preiss, 2000). Preiss (1987) suggested the carbonate and sandstones within the Patsy Hill Member represent the interfingering of tidally influenced carbonate and clastic facies as the shallow water clastics prograded over the

deeper carbonate shelf. Mawson (1938) defined the Pound Quartzite, which was later subdivided into the Bonney Sandstone and Rawnsley Quartzite by Forbes (1971). Forbes (1971) suggested that the depositional environment of the Bonney Sandstone was tidally influenced marginal marine with local estuary type deposits. The Bonney Sandstone consists of flaggy to medium-bedded, silty and feldspathic sandstone, mostly fine to medium-grained but occasionally coarse-grained, interbedded with siltstone and rare limestone (Forbes, 1971). Common sedimentary structures preserved in the Bonney Sandstone are trough and planar crossbedding, lenticular and wavy bedding, ripple marks, soft-sediment deformation, mudcracks and parting lineations (Preiss, 1987).

2.4 METHODS

Figure 6 is a geological map of the Patawarta diapir, including the rim dolomite, and adjacent Wilpena and Hawker groups at 1:36 000. The 1:60 000 COPLEY and 1:250 000 ANGEPENA geological map sheets (Coats, 1973, 2009), aerial photographs, Quickbird 4-band (60 cm resolution), HYMAP 126-band (4m resolution) satellite imagery, and Google Earth imagery were used as base materials for the geological map. In order to document thickness and changes in the capstone of the rim dolomite adjacent to the Patawarta diapir (Coats, 1973, 2009), five stratigraphic sections were measured (Figures 6 & 10; Sections A–E) along the lateral subsalt exposures. For each measured section, the lithology, grainsize, fresh and weathered colors, capstone type, bedding and formation contacts were documented. A correlation diagram of the rim

dolomite was created from the stratigraphic sections, using the contact between the diapiric matrix and the rim dolomite as a datum and extending a few meters into the overlying Bunyeroo Formation (Figure 10). Approximately 100 samples were collected in order to document the range of capstones and varying mineralogies (Figures 11–16). Petrographic thin-sections were stained for calcite and iron with alizarin red-S and potassium ferricyanide, respectively. The rim dolomite photomicrographs were petrographically analyzed in both plane and polarized light for groundmass, cements and grain mineralogy. We derive the capstone definition and classification from Poe et al. (2018) from the outcrop and thin-section observations.

2.5 RESULTS: Rim Dolomite Attributes

The rim dolomite crops out at the salt–sediment interface at the Patawarta diapir (Figure 9). The rim dolomite is a meter-scaled layered, partly silicified dolomitic unit that separates the Callanna diapiric breccia from the outboard stratigraphy of the Bunyeroo and Wonoka formations and the Patsy Hill Member of the Bonney Sandstone (Figure 6; Coats, 1973, 2009; Haines, 1987, 1988; Giles et al., 2012; Read, 1971). The suprasalt diapir margin (north to northeast) contains isolated outcrops of the rim dolomite with chaotic internal layering displaying variable orientations (labeled ‘rim dolomite 1’ on Figure 6). The isolated rim dolomite outcrops are onlapped by the suprasalt Bunyeroo and Wonoka formations (Figure 6). Isolated outcrops of rim dolomite are present where the Bunyeroo and Wonoka formations are erosionally removed at the subsalt–sediment

interface. The rim dolomite is directly overlain by the upper dolomite beds of the Patsy Hill Member of the Bonney Sandstone (labeled ‘rim dolomite 2’ on Figure 6). The most laterally continuous exposure (>5 km) of rim dolomite is formed adjacent to the subsalt Bunyeroo Formation (western and southern margin) where it ranges in thickness from 3 to 90m (labeled ‘rim dolomite 3’ on Figure 6). Here the orientation of internal layering within the rim dolomite mimics that of the outboard Bunyeroo Formation. At the southeastern subsalt margin, the rim dolomite forms isolated pods adjacent to the subsalt Wonoka Formation (labeled ‘rim dolomite 4’ on Figure 6). At all locations, the rim dolomite lacks sedimentary structures and fossils (e.g. cyanobacterial laminites and stromatolites), which are instead present in the directly adjacent stratal units (Bunyeroo and Wonoka formations and Bonney Sandstone; Figure 8).

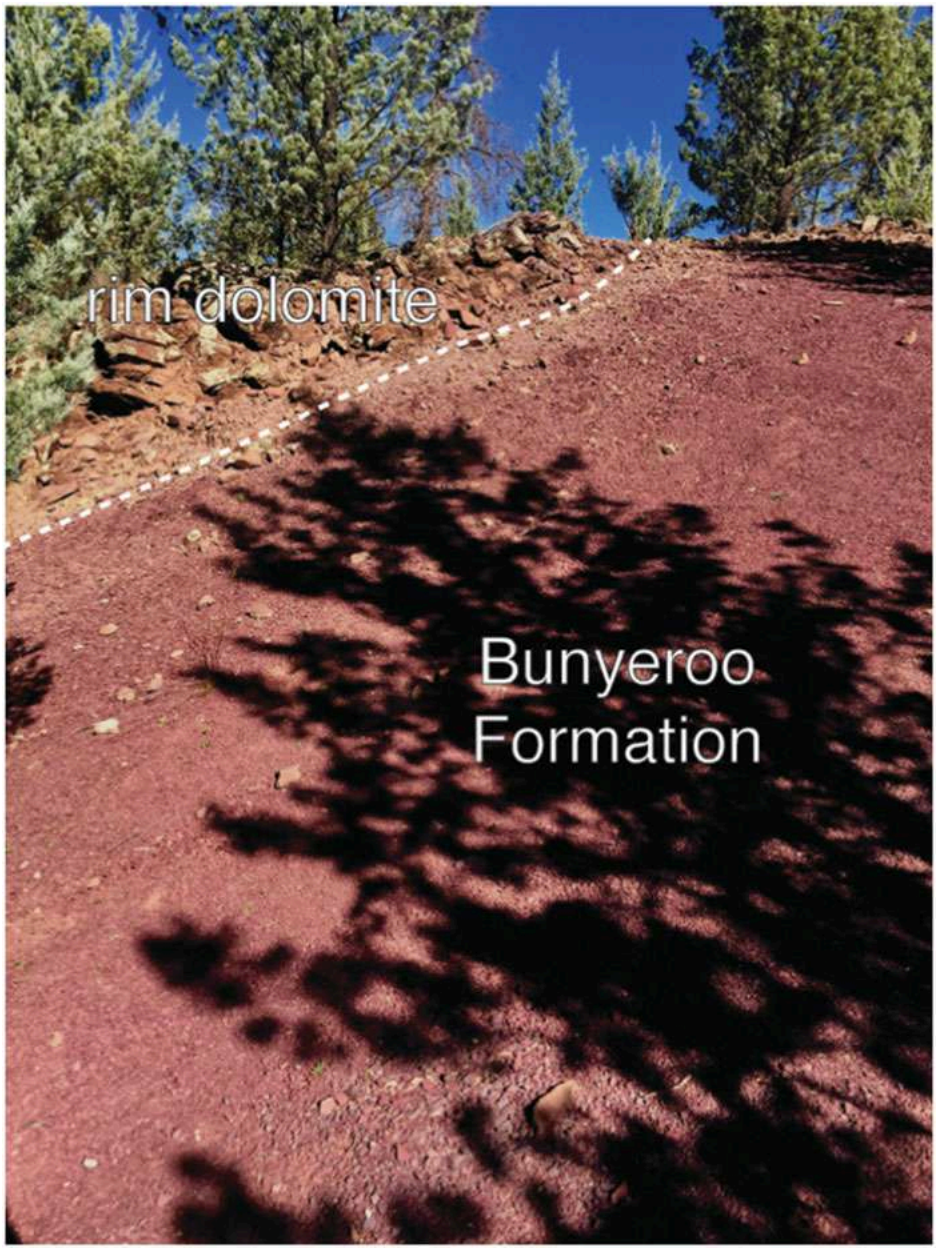

Figure 9: Rim dolomite adjacent to the Bunyeroo Formation; 'rim dolomite 1' on Figure 5.

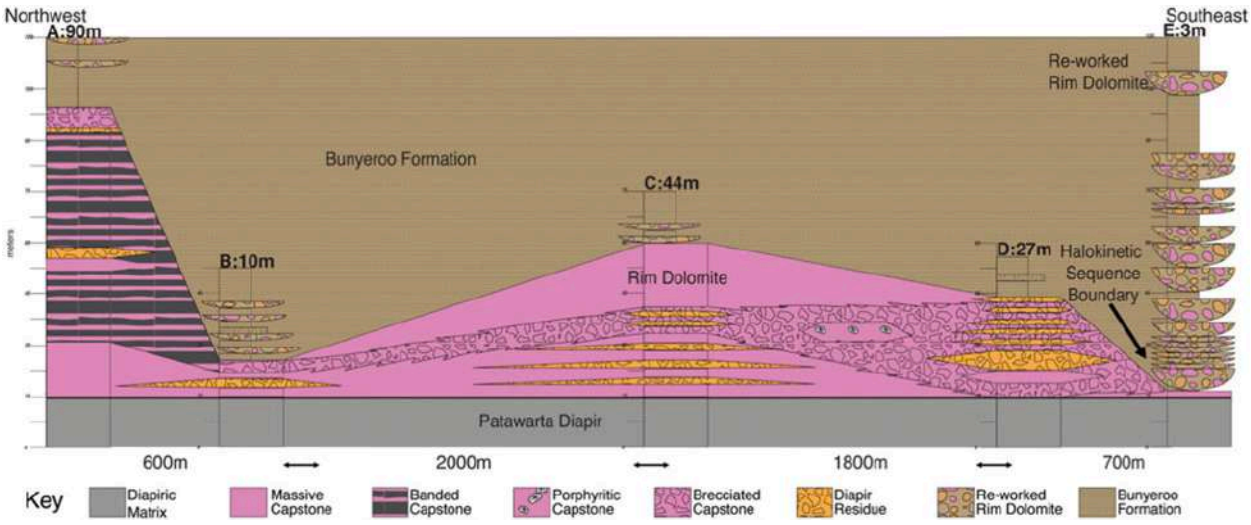

Figure 10: Fence diagram of the lateral rim dolomite on Figure 6.

The rim dolomite includes a blue-grey to grey, yellowtan, and pink micritic dolomite (Figure 9). The rim dolomite displays four distinct capstone types match descriptions by Poe et al. (2018) of caprocks found along the salt–sediment interface in the Paradox Basin (Utah) and the Gulf Coast (Texas). The four rim dolomite capstone types are: 1) massive—microcrystalline dolomite; 2) porphyritic— two distinct crystal sizes, one forming microcrystalline dolomite groundmass and the other forming rosettes of silica; 3) banded—microcrystalline dolomite forming pressure-dissolution layers of silica and authigenic hematite; and 4) brecciated—mosaic to disorganized subfabrics forminga microcrystalline dolomite groundmass. All capstones contain various amounts of anhydrite, quartz, feldspar and non-evaporite grains.

Massive Capstone

Massive capstone is the most common type and consists of a homogenous, microcrystalline dolomite groundmass with up to 5–25 vol% angular, silt to fine-grained sand-sized quartz, 5–25 vol% angular, fine-grained sand-sized feldspar, and up to 5 vol% highly birefringent platy mica grains (Figure 11). Iron-oxide staining appears in clusters and along veins.

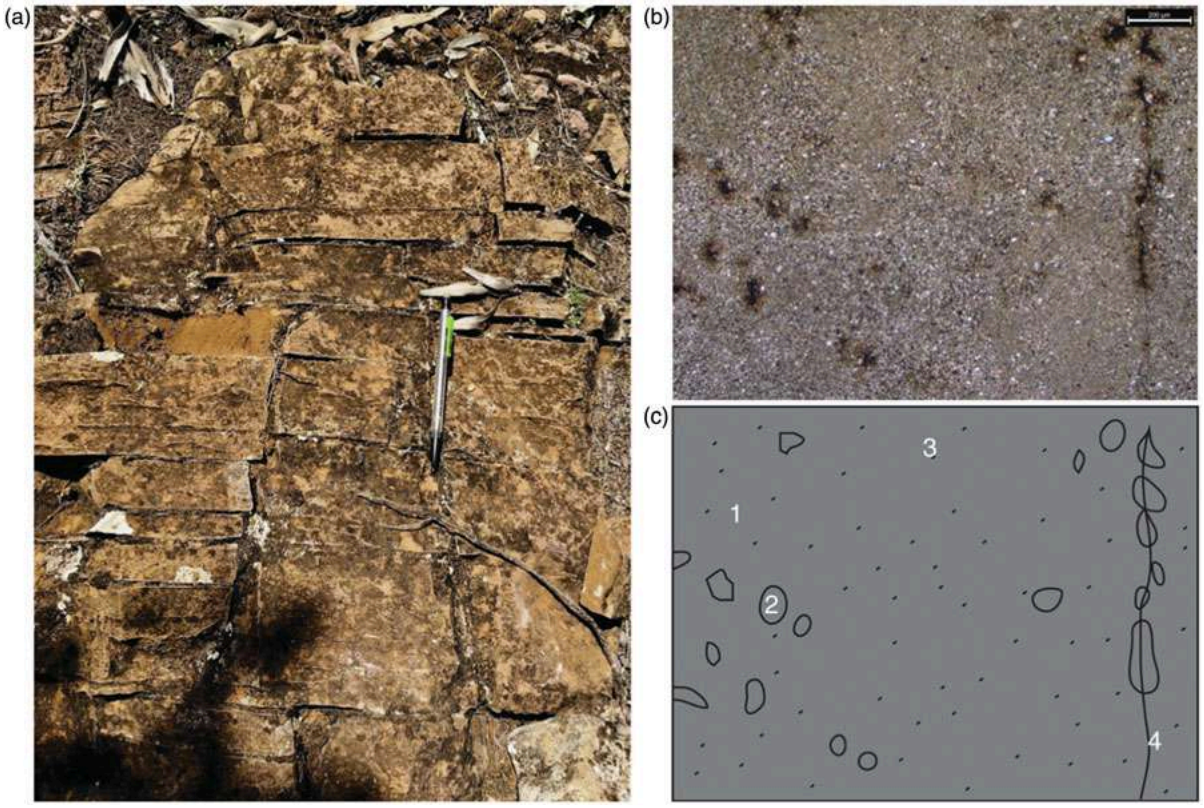

Figure 11: Rim dolomite displaying the massive capstone (sample 24-17). a) Outcrop, b) photomicrograph in polarized light, and c) sketch of capstone attributes including: 1, dolomite groundmass; 2, iron-oxide stain; 3, detrital quartz, feldspar, clay minerals; 4, vein with iron-oxide stain.

Porphyritic Capstone

Porphyritic capstone is rare; it was found in one small pod along the western margin (Figure 12). It displays two distinct crystal sizes; one forming a rosette of quartz crystals and the other forming a microcrystalline groundmass of dolomite. Iron-oxide veins crosscut the dolomite matrix and locally contain later calcite cements. We interpret the porphyritic capstone to have initially contained rosettes of gypsum that were later replaced by silica (Milliken, 1979).

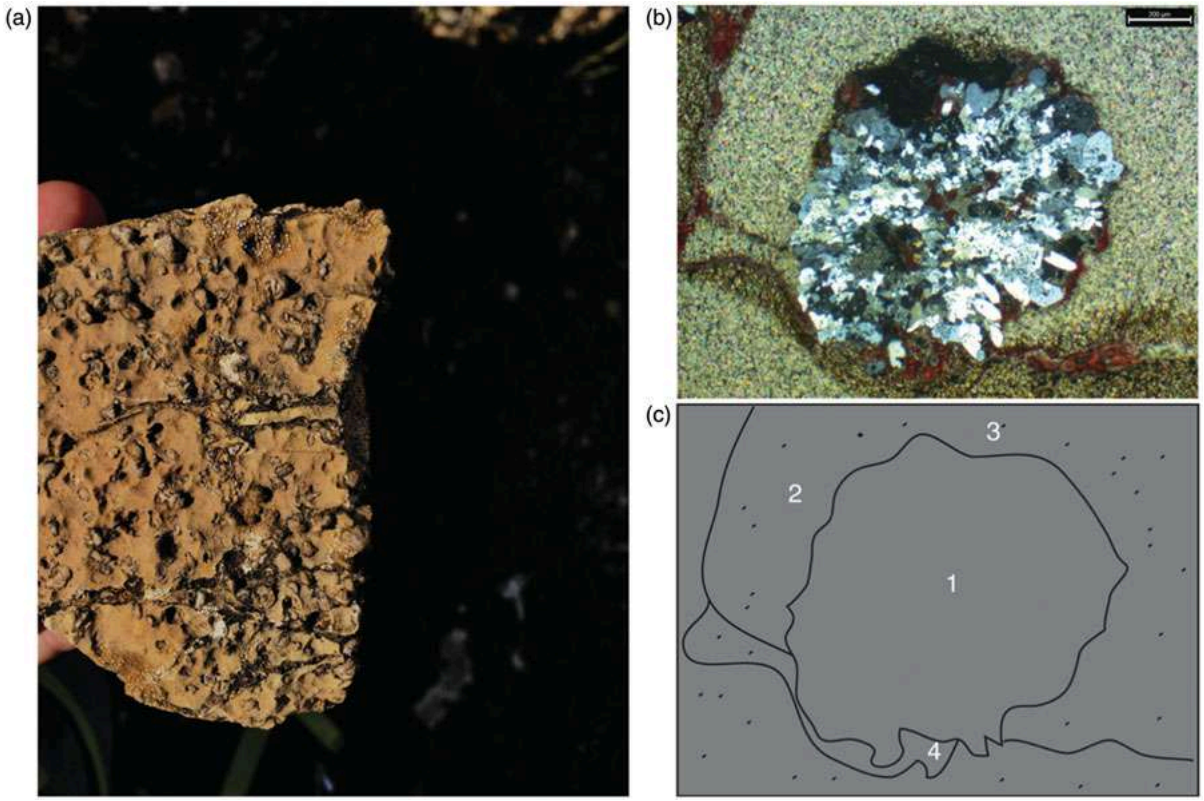

Figure 12. Rim dolomite displaying the porphyritic capstone (sample 34-17). (a) Outcrop, (b) photomicrograph in polarized light, and (c) sketch of capstone attributes including: 1, rosette of silica; 2, dolomite groundmass; 3, detrital quartz, feldspar, clay minerals; 4, vein with calcite.

Banded Capstone

Banded capstone consists of 1mm to 1 m-thick layers of microcrystalline dolomite groundmass alternating light tan to dark brown. A concentration of authigenic minerals is located at the base of a stylolitic pressure-dissolution surface, authigenic quartz needles, few highly birefringent clay minerals, and silt to fine-grained sand-sized quartz grains with etched edges (Figure 13). The pressure-dissolution surface is parallel to the diapir margin and is concentrated with hexagonal, opaque authigenic hematite crystals and forms the bands that range in width from 1mm to 1 m. Diagenetically altered fractures form perpendicular to the banded capstone and their origin have yet to be determined.

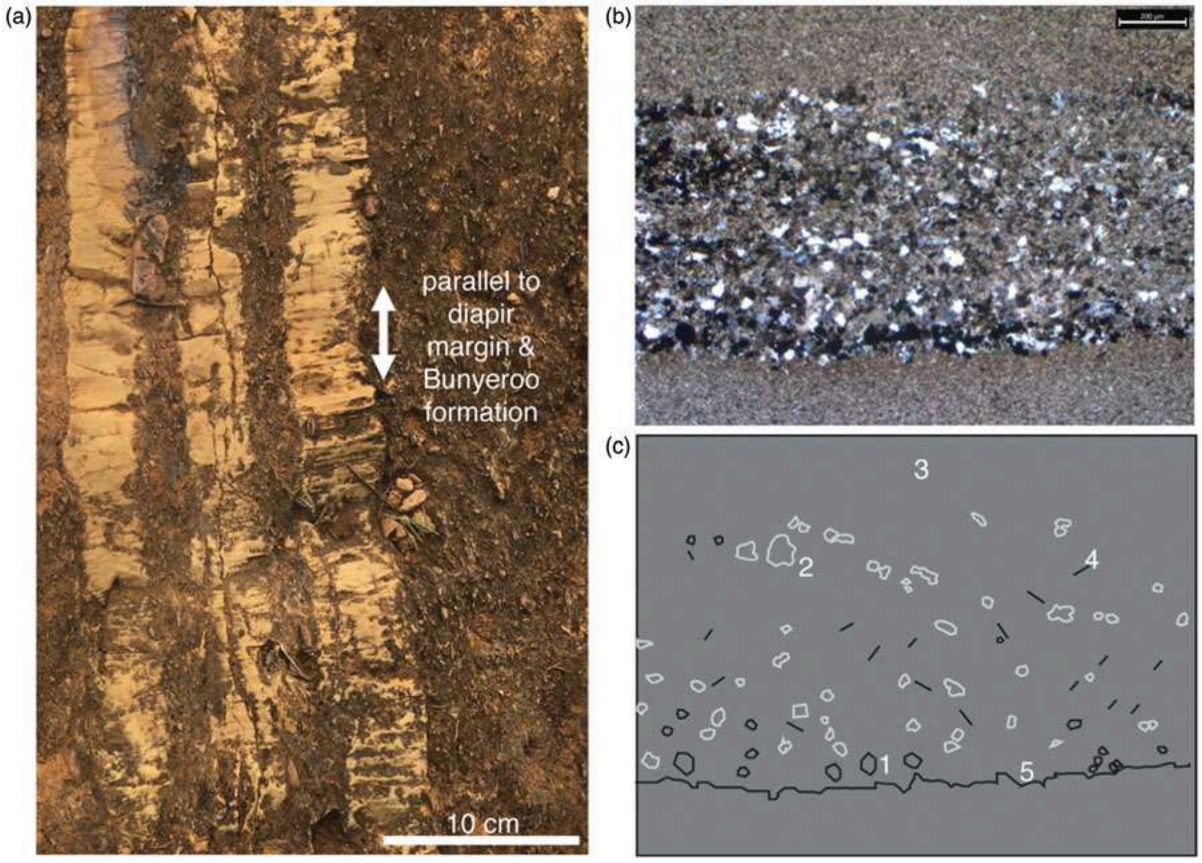

Figure 13. Rim dolomite displaying the banded capstone (sample 08-17). (a) Outcrop, (b) photomicrograph in polarized light, and (c) sketch of capstone attributes including: 1, authigenic hematite hexagon; 2, detrital quartz grain; 3, dolomite groundmass; 4, authigenic quartz needle; 5, pressure-dissolution surface.

Brecciated Capstone

Brecciated capstone is subdivided into mosaic-brecciated (Figure 14) and disorganized-brecciated (Figure 15). The mosaic-brecciated capstone consists of angular clasts of microcrystalline dolomite that contain 5–25 vol% silt to fine-grained sand-size quartz, feldspar and clay minerals. Anastomosing veins form the boundaries between clasts. These boundaries are filled with hematite-stained, coarse-crystalline dolomite rhombohedra, silica and late-stage calcite cements. Mosaic brecciated capstone clasts show little displacement while the disorganized-brecciated capstone consists of angular to subrounded clasts of microcrystalline dolomite that contain 20–25 vol% silt to fine-grained sand-size quartz, feldspar and clay minerals. The disorganized-brecciated clasts float in a matrix of iron-oxide stained microcrystalline dolomite. Coarse crystalline dolomite rhombohedra, silica and late-stage calcite are cements filling vugs within the disorganized-brecciated capstone. The brecciated capstone transitions gradationally from mosaic to disorganized throughout the rim dolomite.

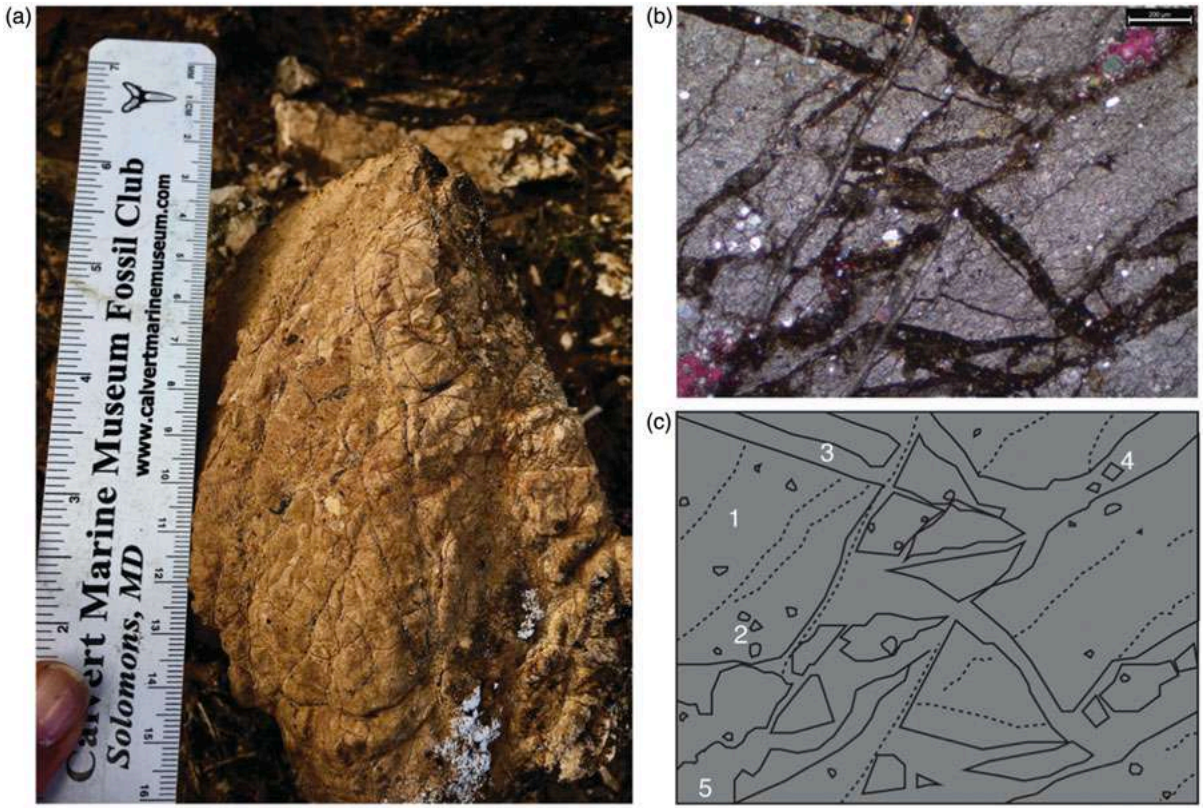

Figure 14. Rim dolomite displaying the mosaic-brecciated capstone (sample 48b-17). (a) Outcrop, (b) photomicrograph in polarized light, and (c) sketch of capstone attributes including: 1, angular clast of dolomite groundmass; 2, detrital quartz grains; 3, iron-oxide vein fill; 4, dolomite cement; 5, calcite cement (modern caliche).

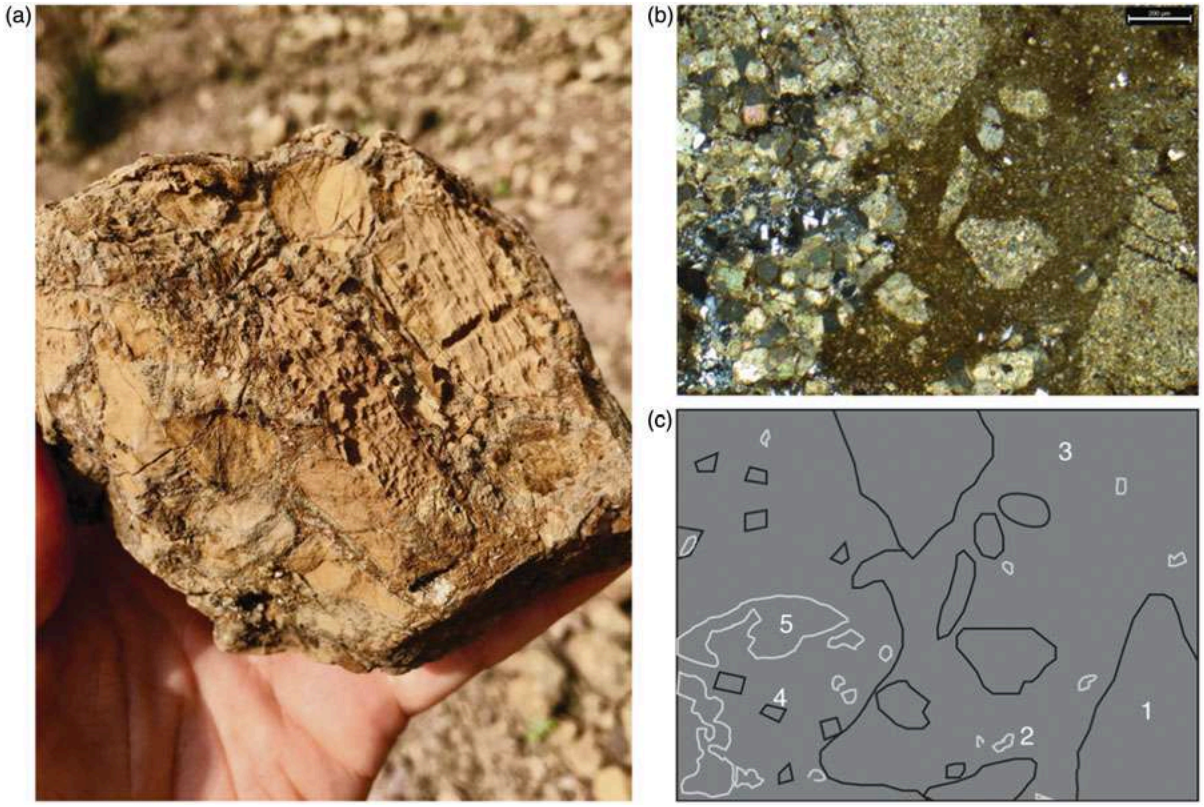

Figure 15. Rim dolomite displaying the disorganized-brecciated capstone (sample 45a-17). (a) Outcrop, (b) photomicrograph in polarised light and (c) sketch of capstone attributes including: 1, subrounded clast of dolomite groundmass; 2, detrital quartz; 3, iron-oxide stained cement; 4, coarse-crystalline rhombohedral dolomite; 5, silica cement.

'Insoluble Residue'

The insoluble residue is composed of rounded to subrounded, fine-grained to pebble-sized arkosic to quartz arenite clasts, and rounded to subrounded, medium-grained to pebble-sized basalt clasts (Figure 16). The residue is not laterally consistent and does not display sedimentary structures such as imbrication, crossbedding, laminations

or beds, inverse or normal grading, ripple marks or channelized lenses. Early-stage calcite cement replaced by dolomite forms rims around the clasts with later-stage quartz veins cross-cutting the basalt grains and coarse-crystalline dolomite groundmass.

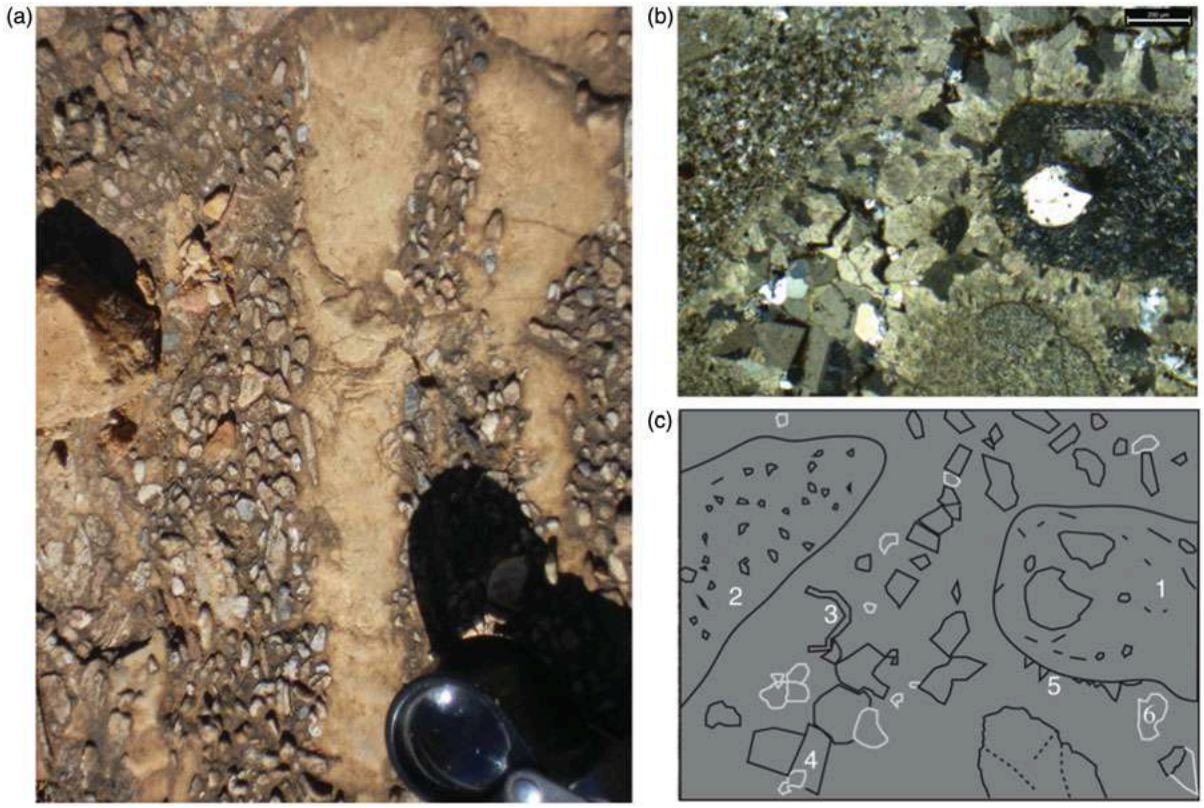

Figure 16. Rim dolomite residue (sample 41a-17). (a) Outcrop, (b) photomicrograph in polarised light and (c) sketch of capstone attributes including: 1, basalt clast; 2, sandstone clast; 3, iron-oxide stained dolomite cement; 4, coarse-crystalline rhombahedral dolomite; 5, calcite pseudomorph replaced with dolomite; 6, silica cement.

Interpretation

Correlation of the capstone types along the western–southern margin (Figure 6) demonstrates that the rim dolomite abruptly transitions from the thickest section

(Section A; 90 m), which are massive and banded capstones, to thinner sections (Section B–D; 10–45 m), which are dominated by massive and brecciated capstones. Section E contains the thinnest section of rim dolomite (3 m) and is composed of massive capstone. Section E is erosionally truncated by a tapered composite halokinetic sequence boundary (Figure 6; Kernen et al., 2012). Establishing the presence of capstone types allow for the rim dolomite to be interpreted as a carbonate caprock. Additionally, we interpret the rim dolomite as carbonate caprock based on the following field relationships: 1) the rim dolomite is present exclusively at the salt–sediment interface between the Patawarta diapir and the Bunyeroo Formation, which matches with Kyle and Posey's (1991) criteria of crestal caprock; 2) the rim dolomite does not interfinger with the outboard Bunyeroo Formation stratigraphy, and such interfingering might be expected if it were a depositional carbonate facies (Walther, 1894); 3) lack of sedimentary structures or fossils of cyanobacterial mats, which is present in sedimentary dolomite facies of this age (Knoll, 1985); 4) presence of a distinctive carbonate facies that is not found in depositional carbonate facies of the outboard Bunyeroo and Wonoka formations, or Patsy Hill Member, rather this distinctive facies are equivalent to that of typical capstone recognized in caprock elsewhere (Poe et al., 2018); 5) presence of stylolitic or pressure solution banding in the banded capstone, indicating prolonged dissolution processes (Grover, 1968, 1969); 6) presence of silica-replaced gypsum rosettes in the porphyritic capstone indicating a precursor gypsum mineralogy, a common caprock mineral (Kyle & Posey, 1991); and 7) clasts of massive dolomicrite in the brecciated capstone, which is evidence of

autobrecciation that results from mass volume changes taking place within the caprock and perhaps associated with the transition from gypsum to anhydrite, Mn- to Mg-bearing dolomite, or the dissolution of solid sulfates and/or carbonates (Fyfe & Bischoff, 1965; Machel, 1989; Zdanovsky, 1956).

There are currently three published models on the formation of lateral caprock: 1) the in-situ model, 2) the rotated layered evaporite sequence model and 3) the halokinetically rotated caprock model. The in-situ model, proposed by Evans et al. (1991) and applied by Jackson and Lewis (2012), states the emplacement of lateral caprock is the result of undersaturated basinal water that flows upward along the flanks of the diapir (Figure 17). The outward-dipping geometries of the surrounding strata focus buoyancydriven fluid flow towards the diapir, resulting in preferential dissolution of halite and accretion of calcium sulfate minerals in place at depth. Large volumes of halite, which are dissolved along the salt–sediment interface by deep, warm, basinal brines, have implications for understanding the patterns and vigor of fluid flow in sedimentary basins. Seismic interpretation of the salt–sediment interface of vertical diapirs may be miscalculated by several hundred meters if time-migrated seismic reflection data are used. This hypothesis is unlikely because the rim dolomite is only present adjacent to the Bunyeroo Formation at the Patawarta diapir. If the in-situ model was likely, the rim dolomite would exist at the salt–sediment interface at other permeable stratigraphic levels adjacent to the Patawarta diapir.

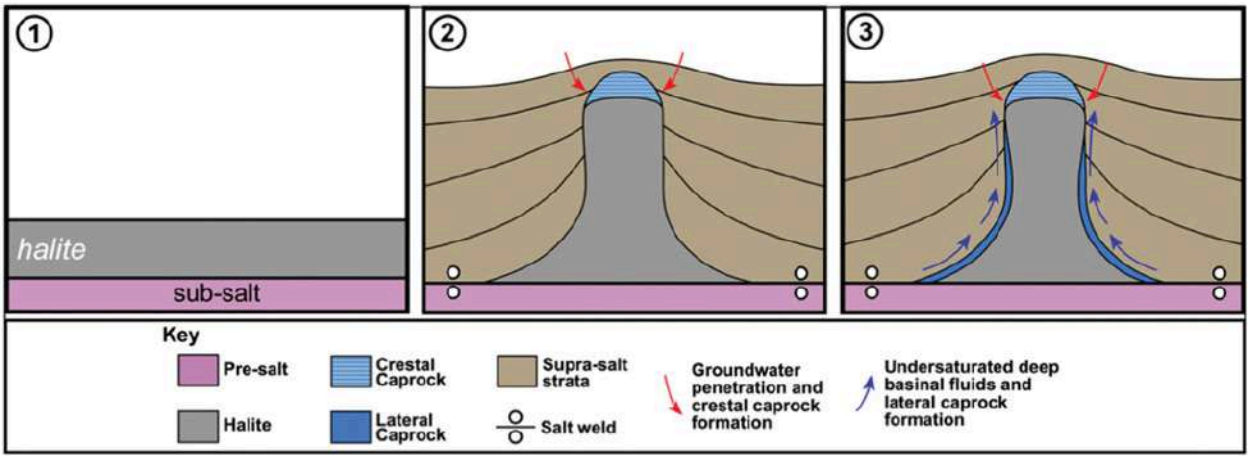

Figure 17. Models of lateral caprock formation, in situ model proposed by Evans et al. (1991) and applied by Jackson and Lewis (2012).

The rotated layered evaporite sequence model, proposed by Schwerdtner and Troeng (1978), is an anhydrite- dominated evaporite sequence at the top of the depositional salt that has been rotated against the flank of the diapir during diapiric rise, resulting in a lateral caprock (Figure 18). This type of diapir-centric carbonate is coeval or slighter younger than the layered evaporite sequence. This results in a non-halite lithological sequence that is misinterpreted as a carbonate caprock or an outboard depositional lithological stratigraphic unit. The hypothesis that the rim dolomite is a Callanna Group clast from the layered evaporite sequence (Schwerdtner & Troeng, 1978) is unlikely because the lithostratigraphy of the rim dolomite does not match the carbonate lithologies in the Callanna Group.

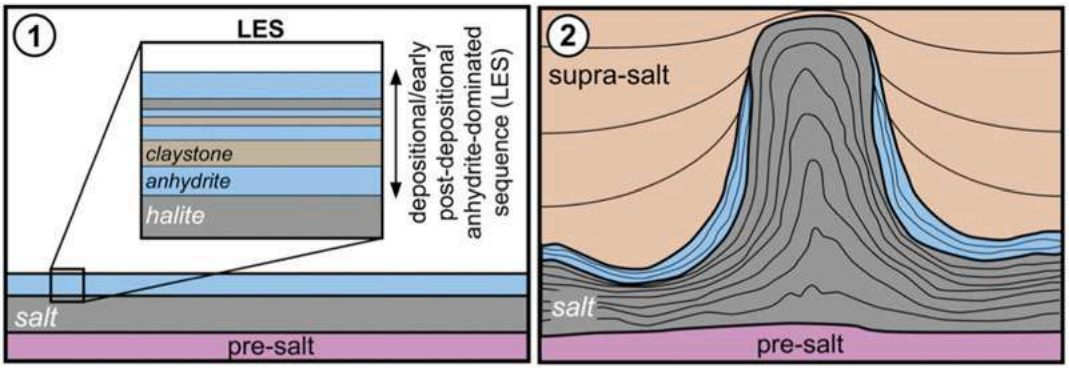

Figure 18. Models of lateral caprock formation, layered evaporite sequence (LES) model (from Jackson, Lewis, & Mannie, 2013); modified from Schwerdtner and Troeng (1978).

The halokinetically rotated caprock model suggests that caprock develops in a crestal position, which is then rotated during the drape-folding of the roof strata (Figure 19; Giles & Lawton, 2002; Giles & Rowan, 2012, Rowan, Lawton, Giles, & Ratliff, 2003). The mechanical boundary between strong and weak rock shifts from the top of the diapir to the base of the caprock, so the competent caprock detaches from the underlying halite-dominated diapir and rotates off the crest of the diapir into a lateral position. Stratigraphic thinning of the Bunyeroo Formation towards the Patawarta diapir indicates that the diapir formed a topographic high during deposition of the Bunyeroo Formation in a shallow water to subaerial environment (Kernen et al., 2012). This setting enables a halite-undersaturated system to come in contact with the top of the Patawarta diapir and begin the dissolution of halite and accretion of insoluble residue (Figure 19; Steps 1 and 2). Ongoing diapir inflation results in the attenuation of the crestal carbonate caprock, forming laterally discontinuous outcrops along >5km of the

top salt–sediment interface (Figure 19; Step 3). The topography generated by inflation of the diapir exceeds the sedimentation rates of the adjacent minibasin, resulting in erosional thinning of the roof. Subsequent stripping of the diapiric roof strata exposes the rim dolomite to erosion and reworks it into the surrounding upper Bunyeroo fine-grained siliciclastics at the halokinetic sequence boundary (Figure 19; Step 4). The remaining rim dolomite was onlapped by the Wonoka Formation (Figure 19; Step 5). Subsequently, continued halokinetic folding rotated the original top salt (and rim dolomite) into a vertical to overturned lateral position (Figure 7). Increasing rates of sedimentation relative to diapiric rise leads to onlap and formation of an overlying halokinetic sequence, which may or may not develop a new crestal caprock assemblage.

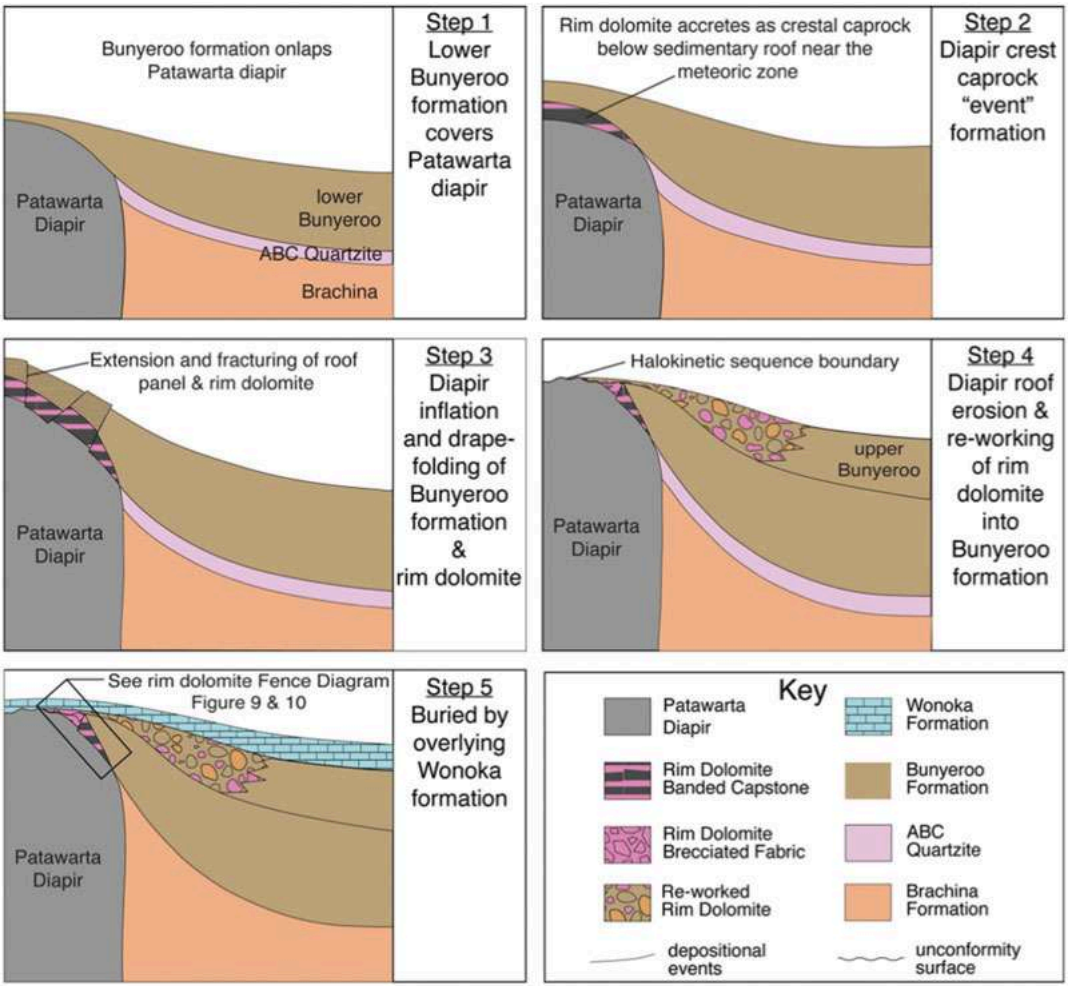

Figure 19: Models of lateral caprock formation, halokinetically rotated caprock (modified from Mast, 2016; after Giles et al., 2012); 1) Lower Bunyeroo Formation is deposited and covers the Patawarta diapir; 2) rim dolomite develops as a crestal caprock; 3) diapir inflation causes extension and fracturing of roof panel and rim dolomite; 4) continued diapir inflation causes erosion of the roof and rim dolomite, clasts of which are subsequently deposited in the overlying Bunyeroo Formation; 5) the rim dolomite is subsequently buried by the Wonoka Formation forming a halokinetic sequence boundary. With further halokinetic rotation (Figure 7), the rim dolomite becomes vertical to overturned in a lateral position.

2.6 DISCUSSION

We can recognize a halokinetically rotated caprock model as the origin for other diapir-centric carbonates found in the Flinders Ranges by applying the field relationships outlined in the 'rim dolomite attributes' section above. Carbonate caprock has been identified along the salt–sediment interface adjacent to the Bunyeroo and Wonoka formations at the South Angepena diapir at Warraweena Station, the Pinda diapir on Pinda Station, and the Beltana diapir on Beltana Station; B. Dalgarno (personal communication, 2017) suggested that it may be present adjacent to the Cambrian Hawker Group stratigraphy at the Wirrealpa diapir on Angorichina Station. These occurrences imply that the development of carbonate caprock was confined to specific stratigraphic intervals within the Wilpena and Hawker groups in the Flinders Ranges. This could be an indication that carbonate caprock development coincides with a shallow water or subaerial depositional environment (presence of phreatic meteoric groundwater to dissolve the halite-rich diapir and introduce the magnesium ions needed to diagenetically form dolomite). It may provide insight to the depositional environment of the Bunyeroo Formation adjacent to the Patawarta diapir being deposited in a shallow water or subaerial environment as a loessite as Mawson and Segnit (1949) originally suggested. Caprock has a high porosity at the salt–sediment interface that may serve as a hydrocarbon reservoir and/or conduit for fluids. Understanding the origin of caprock allows for a better understanding of the mineralogical and porosity distribution and where hydrocarbons can migrate or be trapped. How and when these caprocks form can provide a timeline for the petroleum-system elements. Identifying

caprock can improve seismic interpretation along the salt–sediment interface, which aids in identifying drilling hazards during the well planning process (Jackson & Lewis, 2012; Kernen et al., 2017).

2.7 CONCLUSIONS

Four distinctive capstone fabrics (massive, porphyritic, banded and brecciated) are documented at the salt–sediment interface at the Patawarta diapir and is known as the rim dolomite. The rim dolomite displays the following field relationships: 1) a rugose dolomicrite base that parallels the contact of the diapiric matrix and the bedding in the overlying stratigraphy, 2) the exclusive presence of dolomite at the salt–sediment interface, 3) the lack of sedimentary structures or fossils (cyanobacterial laminites and stromatolites), 4) the lack of interbedded Bunyeroo lithofacies, and 5) the inability to trace the rim dolomite capstone away from the diapir margin into the outboard stratigraphy. These field relationships and fabric types are interpreted to represent a carbonate caprock that accreted as an insoluble residue at the top of the Patawarta diapir while it was covered by the Bunyeroo Formation. Through diapir inflation, the carbonate caprock and overlying Bunyeroo Formation was uplifted, rotated, and eroded forming a debris apron of diapiric matrix, carbonate caprock and Bunyeroo Formation at the halokinetic sequence boundary in the adjacent subsalt minibasin. We interpret the rim dolomite at the Patawarta diapir to be a halokinetically rotated carbonate caprock that formed at the salt–sediment interface in a diapir-crestal position that was

subsequently rotated into a lateral position. This interpretation is supported by the detailed field mapping, stratigraphic and petrographic observations presented in this study.

CHAPTER 3: ORIGIN OF CARBONATE INCLUSIONS AT PATAWARTA DIAPIR

To be submitted for publication in Precambrian Research

3.1 ABSTRACT

Patawarta salt diapir is located in the Central Flinders Ranges, South Australia, and historically is interpreted as a single allochthonous salt sheet containing sedimentary and igneous intrasalt inclusions derived from the autochthonous Willouran-aged Callanna Group stratigraphy. Using new detailed mapping, lithostratigraphic and chemostratigraphic analysis, five primarily silty limestone inclusions (0.5-2km^2) are interpreted here to be Ediacaran-aged Wonoka Formation and Patsy Hill Member of the Bonney Sandstone (Wilpena Group) inclusions within Patawarta diapir, which is approximately 2-6km^2. Lower Wonoka Formation sedimentary inclusions as well as surrounding minibasin stratigraphy are shown to contain part of the Shuram δ^{13} C and δ^{18} O stable isotope excursion with δ^{13} C as light as -6.7‰. This method of correlating intrasalt inclusions to the regional stratigraphy is the first of its kind in the Adelaide Rift Complex. The Ediacaran-aged inclusions are concentrated to the southern side of the diapir where they are juxtaposed against a Willouran-aged Curdimurka Subgroup (Callanna Group) autochthonous inclusion 1-2km^2 in size, which is approximately 300 million years older. The carbonate inclusions in Patawarta diapir represent a suprasalt condensed section forming a carapace composed of Wonoka Formation and lower beds of the Patsy Hill member (Bonny Sandstone) and Patawarta diapir is composed of two separate salt bodies that encase the suprasalt carapace at an allosuture. This study represents the first documented example of salt tectonic encasement of suprasalt strata

for the origin of the silty limestone inclusions in the salt diapirs in the Flinders Ranges, South Australia.

3.2 INTRODUCTION

Understanding the origin and nature of non-halite lithologies in salt diapirs is a key component to drilling wells safely because they are a common salt-associated drilling hazard. Salt-associated drilling hazards may be related to the lithologic variability, shear zones, and fluids within the intrasalt non-halite lithologies (Davison, 2009; Dooley et al., 2017; Fernandez et al., 2017). Non-halite lithologies in salt diapirs are variously referred to as inclusions, clasts, chips, rafts, stringers, sutures, and encased minibasins in the literature (Dooley et al., 2012; Edwards et al., 2014; Fernandez et al. 2017; Fiduk & Rowan, 2012; Fiduk et al. 2014; Jackson et al., 2015; Moore & Douglas 2013; Neely et al. 2017; Rowan & Inman, 2011). Non-halite sedimentary inclusions are particularly hazardous because they vary widely in mechanical strength depending on the lithology and often contain fluids that are over- or under-pressured resulting in a pressure kick or a loss in drilling mud when penetrated by the drill bit (Dooley et al., 2012; Hudec, 2014). Borehole instability related to salt creep and shear, by salt moving at a peak rate of approximately 100mm yr^{-1} (Weijermars et al., 2014) can cause fluid and/or pressure leakage issues (Gloyna & Reynolds, 1961). Salt bodies may contain pockets of brine that cause a pressure kick while the drill bit is penetrating the salt body (Davison, 2009). The pockets of brine are thought to be sourced from matured hydrocarbon in shale inclusions that were originally

deposited within the depositional layered evaporite sequence (LES; Davison, 2009). The presence of bitumen or tar in salt is an indication that overpressure forces are present, which can result in significant drilling delays, may necessitate sidetracks or worst-case, well abandonment and subsequent financial loss (Han et al., 2008; Kukla et al., 2011b).

Previous 2D and 3D seismic reflection studies of sedimentary inclusions have focused on the identification of intrasalt lithologies on datasets in various offshore salt basins like the deepwater Gulf of Mexico (Dooley et al., 2012; Edwards et al., 2014; Fiduk et al., 2014; Moore & Douglas, 2013; Neely et al., 2017; Rowan & Inman, 2011), Santos Basin (Fiduk & Rowan, 2012; Jackson et al., 2015) and Pre-Caspian Sea (Fernandez et al., 2017; Jackson et al., 2019). Fernandez et al. (2017) used 3D seismic reflection and borehole data to provide a classification of inclusion lithology types and outlined several possible modes of salt encasement to form intrasalt sedimentary inclusions. Previous outcrop sedimentary inclusion studies primarily focused on identifying the presence of inclusions in various onshore salt basins like the Katangan Central African Copper Belt (Cailteux et al., 2018; Jackson et al., 2004), Spanish Pyrenees (Lagabrielle et al., 2010), and Paradox Basin, Utah and Colorado (Thompson-Jobe et al., 2019).

Because seismic imaging within salt bodies is often of poor resolution and biostratigraphic data is either not collected in inclusions or is unavailable for public use, little is known about the stratal geometry or stratigraphic origin (age) of the non-halite sedimentary strata within salt bodies (Helgesen et al., 2013; Huang et al., 2012; Li et al.,

2011; Peles et al., 2004; Roy & Chazalnoel, 2011). This study provides a detailed lithologic, stratigraphic, and geochemical description of Precambrian anomalous silty limestone sedimentary inclusions in the Patawarta diapir that are correlated to the regional stratigraphy of the Flinders Ranges, South Australia (Marinoan (Ediacaran)-aged Wonoka Formation and Patsy Hill Member of the Bonney Formation) using lithostratigraphic and chemostratigraphic methods. We postulate the incorporation of the Wonoka Formation inclusions occurred at a suture zone within an allochthonous salt canopy.

Correlating the sedimentary inclusions to the regional stratigraphy is not difficult if the inclusions have fossil assemblages (biostratigraphy), however, correlating Precambrian inclusions (like those in the Flinders Ranges) can be very difficult, hence the significance of our study using other stratigraphic methods. The workflow used in this study could potentially be used to determine the stratigraphic origin (age) of sediment inclusions at other field locations where a conventional biostratigraphic correlation is not possible. Once the stratigraphic origin (age) of the inclusions is determined and correlated to the regional stratigraphy, the overall depositional environment of the non-halite sedimentary inclusions can be interpreted, and salt tectonic encasement hypotheses can be proposed.

3.3 GEOLOGIC SETTING

The Adelaide rift basin of South Australia developed through a series of continental rifting events as western Laurentia and Australia separated during the

breakup of the Neoproterozoic Rodinian supercontinent (Figure 1; Dyson, 1996; Preiss, 2000; Sprigg, 1952). It is a failed rift that trends north- south extending almost 800km northward from the area of Adelaide, SA through the Flinders Ranges where it bifurcates into the Willouran and Gammon ranges. The rift basin contains rift-fill sediments that were deposited contemporaneously with long-lived (>250 m.y.), widespread passive salt diapirism (Dyson, 1996; Forbes & Preiss, 1987; Rowan & Vendeville, 2006). After rifting ceased in the Late Neoproterozoic to early Cambrian, a major episode of crustal shortening and metamorphism followed, known as the Delamerian Orogeny, which resulted in the inversion of the failed rift system during the Late Neoproterozoic to Ordovician (~500 Ma). Shortening and inversion of the failed rift system created the Adelaide Rift Complex (Fig. 1; Forbes & Preiss, 1987; Preiss, 2000).

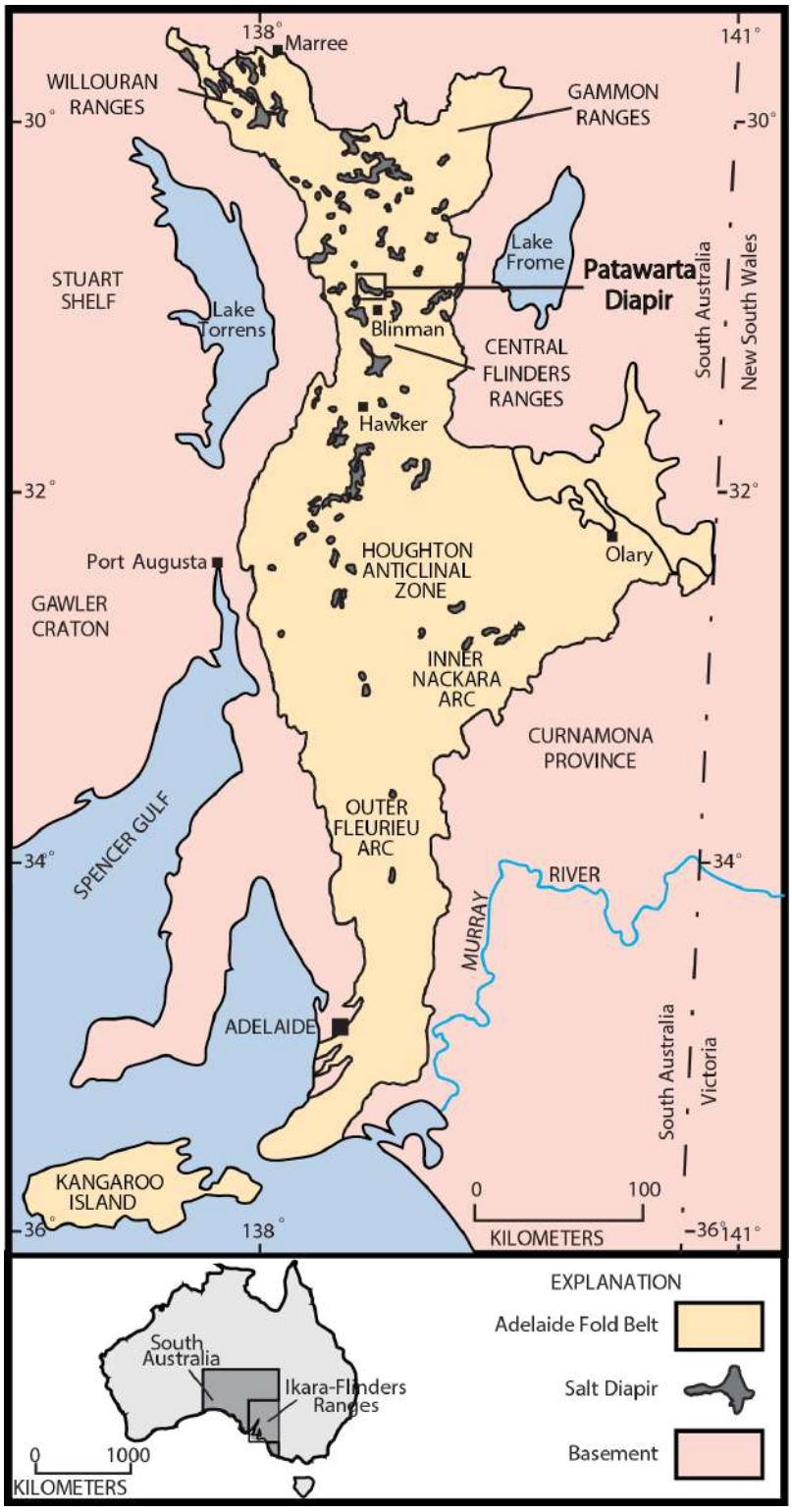
138°
Marree
141°
WILLOURAN RANGES
GAMMON RANGES
30°
30°
Lake Frome
Patawarta Diapir
STUART SHELF
Lake Torrens
Blinman
CENTRAL FLINDERS RANGES
South Australia
New South Wales
Hawker
32°
32°
Port Augusta
HOUGHTON ANTICLINAL ZONE
Olary
GAWLER CRATON
INNER NACKARA ARC
CURNAMONA PROVINCE
OUTER FLEURIEU ARC
SPENCER GULF
34°
34°
RIVER
MURRAY
ADELAIDE
South Australia
Victoria
KANGAROO ISLAND
0
100
KILOMETERS
36°
138°
141°
EXPLANATION
Adelaide Fold Belt
Salt Diapir
Basement
South Australia
Ikara-Flinders Ranges
0
1000
KILOMETERS

Figure 1: Map of the Adelaide Foldbelt of South Australia displaying the location of major salt diapirs, including the Patawarta salt diapir in the Central Flinders Ranges (modified from Kernen, 2011; after Dalgarno & Johnson, 1968).

The Adelaide rift basin contains a thick succession of strata (up to 24,000m) that provides one of the most complete sedimentary records of Upper Proterozoic through Lower Cambrian depositional systems in South Australia (Preiss, 1987). The Callanna Group at the base of the rift sequence, above Archean and Proterozoic igneous and metamorphic basement (Figures 2 & 3) is approximately 130-8400m thick. It contains the layered evaporite sequence (LES) that is composed of Willouran to Torrensian-aged interlayered evaporites (halite and gypsum in the subsurface), halite-cast bearing siliciclastics, carbonates (mostly dolomite), and mafic igneous rocks (Figure 2; Dyson, 1996; Forbes & Preiss 1987; Preiss, 2000). The Callanna Group was deposited in a highly restricted marginal marine sabkha environment during the early stages of rifting (Figure 2; Preiss, 1987). It is overlain by the Torrensian to Sturtian Burra Group that is 3000-8000m thick and composed of shale, siltstone, heavy-mineral laminated sandstones, and dolomites (Figure 2; Preiss, 1987). The basal Burra Group was deposited in lagoonal to open marine settings and deepens upward into the lower shoreface (Figure 2; Preiss, 2000). The Burra Group is overlain by the Sturtian to Marinoan marine shelf strata. The overlying Umberatana Group is 10-6000m thick and composed of diamictite, conglomerate, sandstone, and laminated siltstone (Fig. 2; Preiss, 2000). The Umberatana Group was variously deposited in a glacial, interglacial,

and post-glacial marine shelf settings (Figure 2; Preiss, 2000). It is overlain by the Marinoan Wilpena Group that is 40-7000m thick and composed of dolomite, limestone, calcareous sandstone, calcareous siltstone, siliceous siltstone, and shale (Figure 2; Preiss, 1987). The Wilpena Group was deposited in primarily open marine, siliciclastic and carbonate shelfal depositional system with minor near shore and fluvial facies (Figure 2; Preiss, 1987).

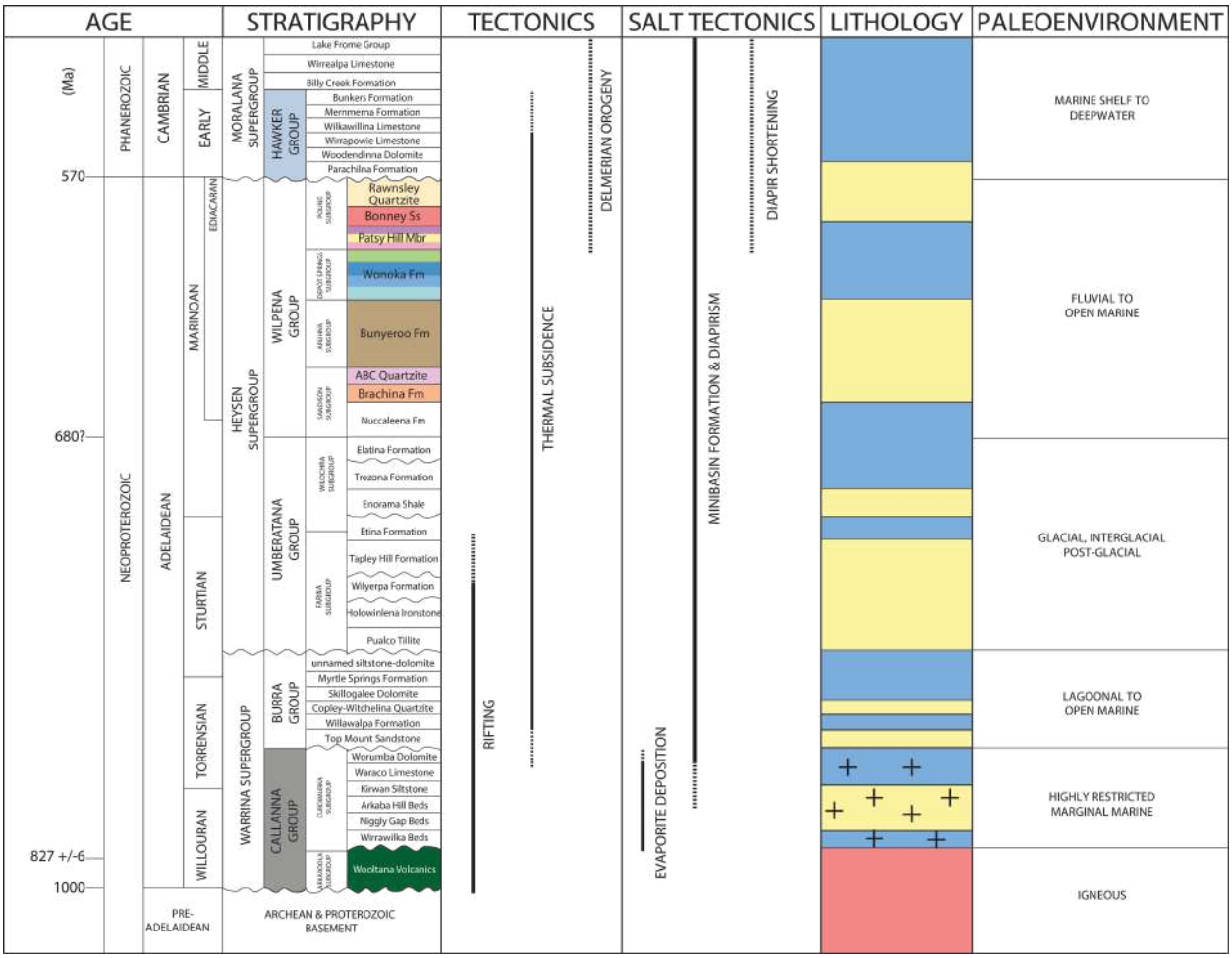

Figure 2: Precambrian–Cambrian stratigraphy of the Flinders Ranges, South Australia (modified from Preiss, 1987). The colors on the stratigraphic column correspond to the map units on Figure 5a. Under 'Lithology' blue corresponds to a dominate carbonate

lithology, yellow corresponds to a dominate siliciclastic lithology, and red corresponds to a dominate evaporite lithology. The regional tectonics, salt tectonics, lithology, and paleoenvironment of the Adelaide Foldbelt.

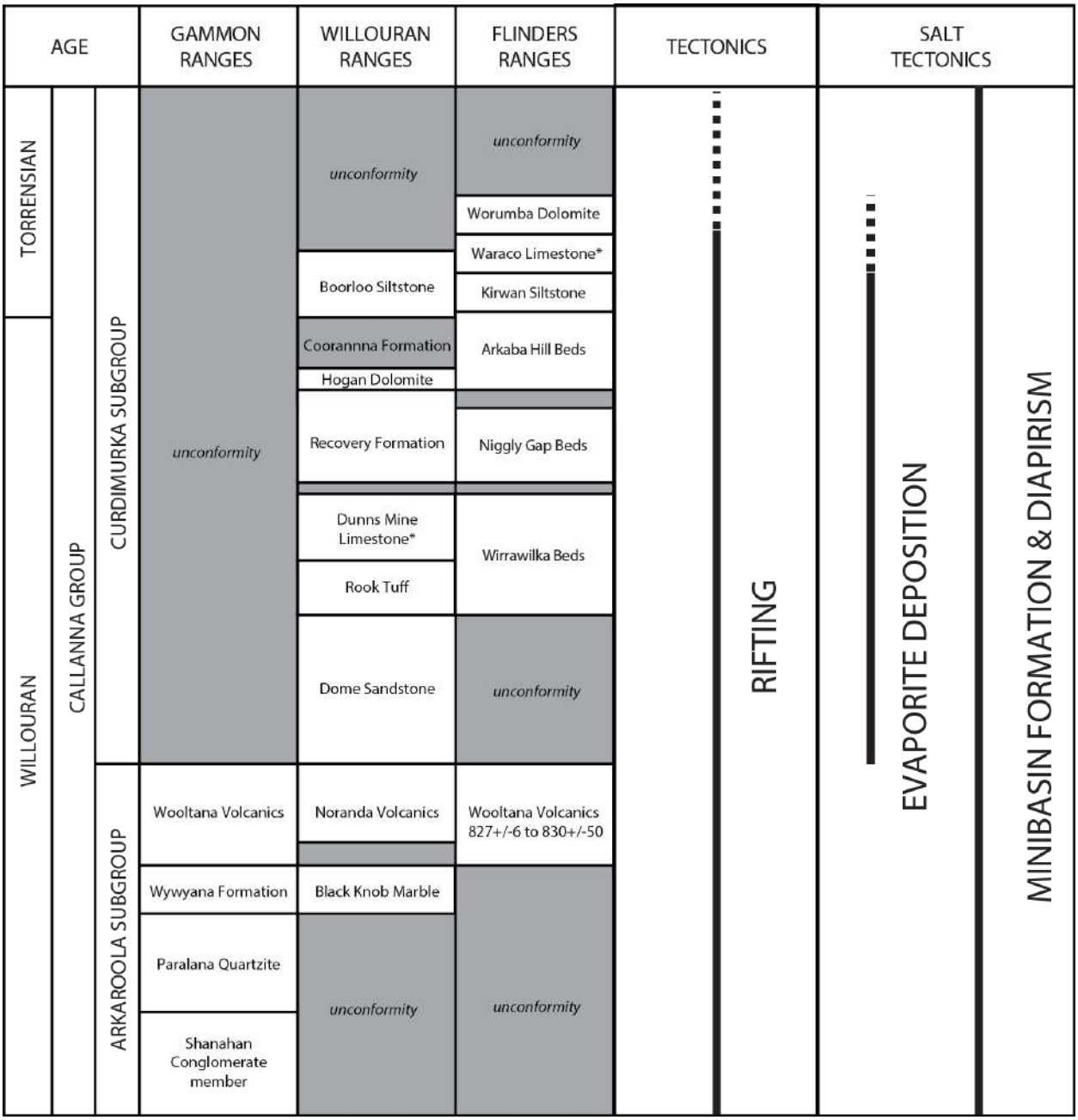

Figure 3: Stratigraphy, tectonics, and salt tectonics of the Callanna Group layered evaporite sequence in the Gammon, Willouran, and Flinders Ranges (modified from

Preiss, 1987). The Callanna Group strata in the Gammon and Willouran Ranges are located in their original layered evaporite sequence. The Callanna Group strata in the Flinders Ranges are located in the salt diapirs as inclusions.

The Adelaide Rift Complex (ARC) contains over 180 exposed salt diapirs (Figure 1; Dalgarno & Johnson, 1968; Lemon, 1988). The exposed diapirs do not have halite or gypsum present at the surface but contain inclusions of non-evaporite lithologies that are surrounded by a diagenetic dolomicrite matrix. The diagenetic dolomicrite matrix surrounds pebble to kilometer-scale inclusions of non-evaporite lithologies generally thought to be derived entirely from the Callanna Group LES that was subsequently stratigraphically dismembered and carried with the salt during diapirism (Figure 2; Preiss, 1987). Both the inclusions and dolomicrite matrix are collectively mapped as 'diapiric breccia' (Preiss, 1987). Mobilization of the Callanna Group evaporites and initiation of passive salt diapirism in the Adelaide Rift Complex began in the latest Willouran to early Torrensian (Figure 2; Dalgarno & Johnson, 1968). Allochthonous salt (meaning diapiric salt whose flow is lateral as appose to vertical; Jackson & Talbot, 1989) in the Adelaide Rift Complex was first extensively recognized by Dalgarno & Johnson (1968) and further documented during deposition of the Burra, Umberatana, Wilpena and Hawker groups (Figure 3) by Dyson (1998, 2004, 2005), Lemon (2000), Hearon et al. (2010), Kernen et al. (2012), Hearon et al., (2015a), Williams (2017), and Rowan et al. (2019).

Parts of the Callanna Group LES remaining at the autochthonous level are preserved in the Willouran and Gammon ranges. The lower part of the Callanna Group is called the Arkaroola Subgroup (Figure 3), which outcrops primarily in the Gammon Ranges near Mount Painter and Arkaroola. Within the Arkaroola Subgroup the Wooltana Volcanics in the Gammon and Flinders ranges have been radiometrically dated at 827 +/-6 to 830 +/-50 million years (Figure 3; Coats & Preiss, 1987). The relatively younger part of the Callanna Group is called the Curdimurka Subgroup, which outcrops in the Willouran Ranges (Figure 3; Preiss, 1987). The Flinders Ranges do not contain exposures of the Callanna Group LES at the autochthonous level. Here, the Callanna stratigraphic units are only preserved in inclusions within the diapiric breccia. Because the inclusions are no longer in their original depositional position, stratigraphic correlation from the Flinders Ranges diapiric Callanna to the *in-situ* autochthonous Callanna LES in the Willouran and Gammon ranges is problematic (Figure 3; Preiss, 1987). Because the Callanna Group stratigraphy in the Flinders Ranges are preserved only in inclusions they have different stratigraphic names than the proposed age-equivalent units in the Willouran and Gammon Ranges (Figure 3; Preiss, 1987).

Within the autochthonous Callanna stratigraphic units, very few carbonates and specifically limestones have been documented (Figure 3). The Dunns Mine Limestone has been documented in the Willouran Ranges and the slightly younger Waraco Limestone in the Flinders Ranges (Preiss, 1987). The Dunns Mine Limestone varies between 50-200m in thickness and is composed of dark gray dolomites interbedded with calcareous shales and siltstones and lenses of sandstone (Murrell, 1977).

Additionally, chalcedonic nodules are found in the dolomites in the lower part of the section (Murrell, 1977). The Waraco Limestone is composed of pale gray to cream stromatolitic dolomite and calcitic and dolomitic marble (Preiss, 1987). The lack of limestone units in the Callanna Group stratigraphy are significant because they are compared to the common, large silty limestone inclusions mapped and analyzed at Patawarta diapir for this study.

Previous Work Patawarta Diapir

Patawarta diapir, the subject of this diapir inclusion study, outcrops in the Central Flinders Ranges and has been interpreted as an allochthonous salt sheet covering roughly 4km^2 (Figures 1, 4-6; Hearon et al., 2015a; Kernen et al., 2012; Rowan & Vendeville, 2006; Rowan et al., 2019). The map view represents an oblique cross-sectional view of a ramping allochthonous salt sheet (*see Figure 8 in* Hearon et al., 2015a; Kernen et al., 2012; Rowan & Vendeville, 2006; Rowan et al., 2019). An interpreted subsalt minibasin is located below the allochthonous salt sheet along the southeastern margin (Kernen et al., 2012; Kernen et al., 2018) of Patawarta diapir and an interpreted suprasalt minibasin is located above the allochthonous salt sheet along the northern and eastern margin of Patawarta diapir (Gannaway, 2014). The subsalt minibasin contains Wilpena Group strata of the upper Bunyeroo Formation, Wonoka Formation (lower-upper members & green siltstone members), Patsy Hill member of the Bonney Sandstone (lower-upper dolomite beds, lower-upper sandstone beds), and the lower Bonney Sandstone. All of these stratigraphic units thin and upturn toward the

diapir recording the passive halokinetic growth history of the southern margin of the diapir (Figures 4 & 5; Hearon et al., 2015; Kernen, 2011; Kernen et al., 2012). The suprasalt minibasin along the northern margin of Patawarta diapir was described and correlated to the subsalt minibasin by Gannaway (2014). It contains the same stratigraphic units as the subsalt basin; however, they are substantially thicker in the suprasalt minibasin (Table 1). The suprasalt units thin and upturn toward the diapir where they progressively onlap the top of the diapir. (Table 1; Gannaway, 2014).

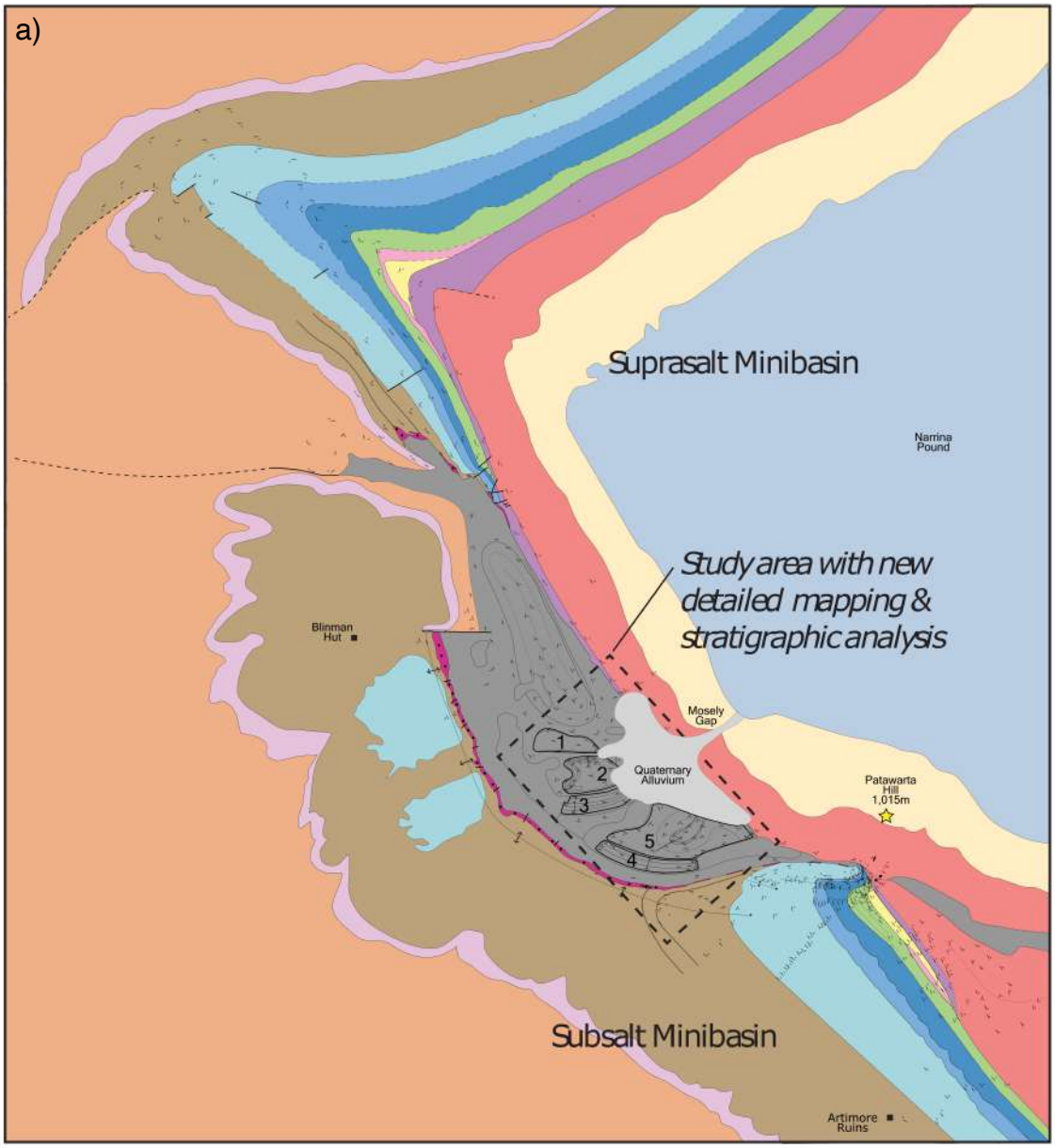
a)
Suprasalt Minibasin
Narrina Pound
Study area with new detailed mapping & stratigraphic analysis
Blinman Hut
Mosely Gap
Quaternary Alluvium
Patawarta Hill 1,015m
1
2
3
4
5
Subsalt Minibasin
Artimore Ruins

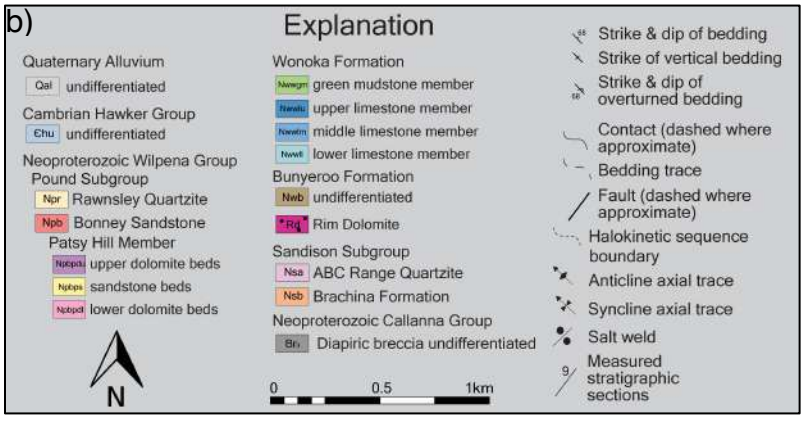
b)
Explanation
Quaternary Alluvium
Qal undifferentiated
Cambrian Hawker Group
Chu undifferentiated
Neoproterozoic Wilpena Group
Pound Subgroup
Npr Rawnsley Quartzite
Npb Bonney Sandstone
Patsy Hill Member
upper dolomite beds
sandstone beds
lower dolomite beds
N
Wonoka Formation
green mudstone member
upper limestone member
middle limestone member
lower limestone member
Bunyeroo Formation
Nwb undifferentiated
Rim Dolomite
Sandison Subgroup
Nsa ABC Range Quartzite
Nsb Brachina Formation
Neoproterozoic Callanna Group
Diapiric breccia undifferentiated
0
0.5
1km
Strike & dip of bedding
Strike of vertical bedding
Strike & dip of overturned bedding
Contact (dashed where approximate)
Bedding trace
Fault (dashed where approximate)
Halokinetic sequence boundary
Anticline axial trace
Syncline axial trace
Salt weld
Measured stratigraphic sections

Figure 4: a) Geologic map of Patawarta diapir in the Flinders Ranges, South Australia (modified from Gannaway, 2014; Kernen et al., 2012). Study area located in the dashed box where numbers 1-5 depict inclusions—see Figure 8, b) Explanation of geologic map of Patawarta diapir.

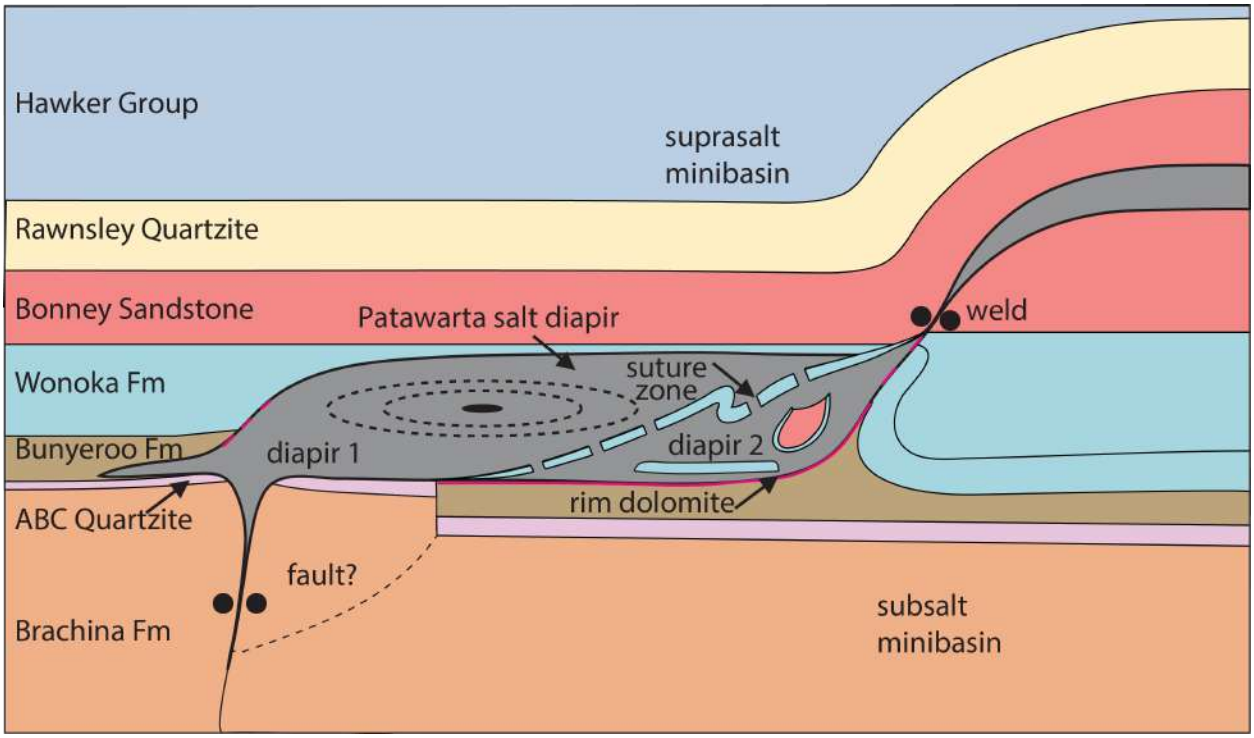

Figure 5: Schematic diagram of the Wonoka formation and Patsy Hill member inclusions inside the Patawarta salt diapir (modified from Hearon et al., 2015a). Diapir 1 represents the northern updip salt body and diapir 2 represents the southern salt body separated by a suture zone referred to as an allosuture (Dooley et al., 2012).

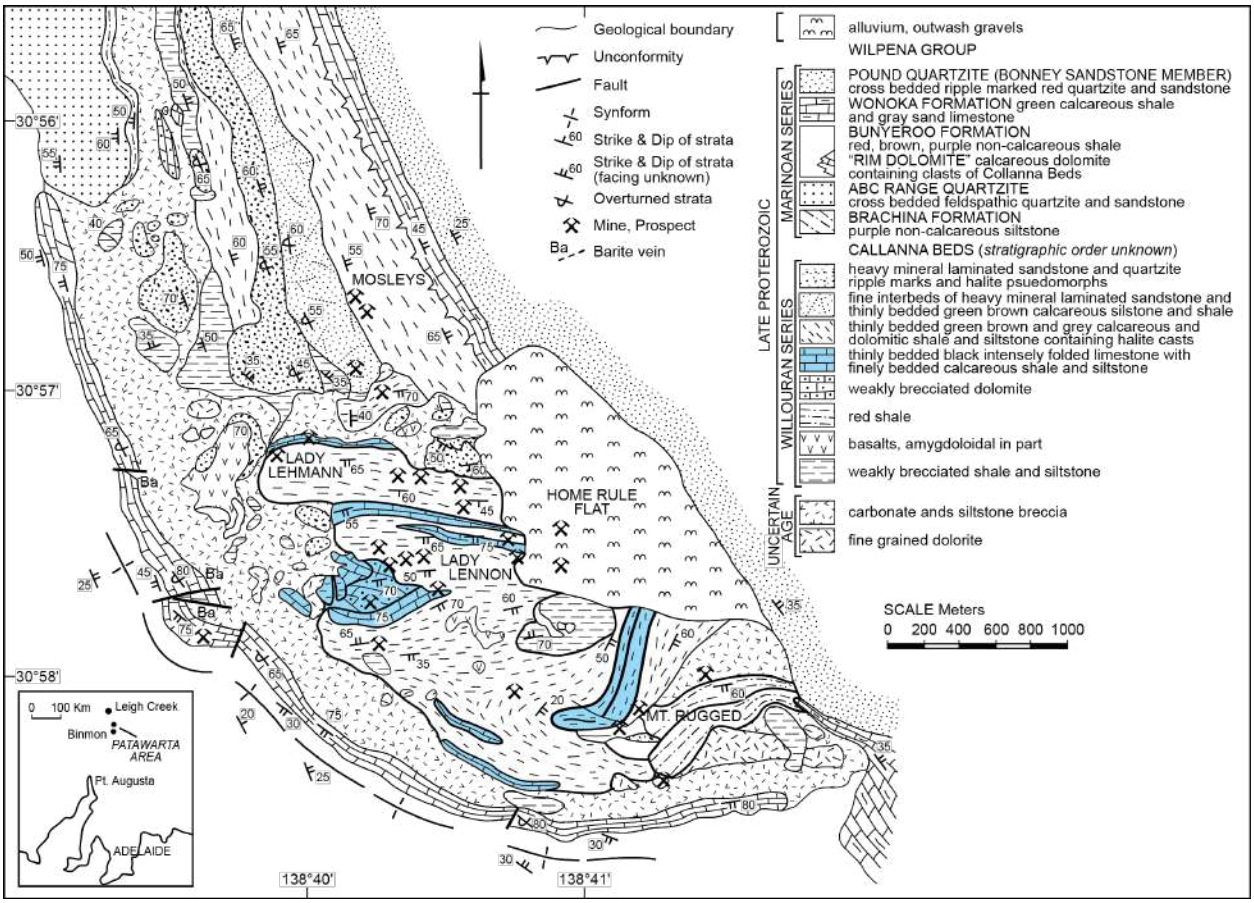

Figure 6: Geologic map of the Patawarta diapir showing variable lithologies of inclusions in the diapiric breccia. The anomalous limestone and calcareous siltstones and shales are highlighted in the blue (modified from Hall, 1984).

Table 1: Stratigraphic unit thicknesses variations of the suprasalt and subsalt minibasins that are compared to thickness trends of the carbonate inclusions in the Patawarta diapir (modified from Gannaway, 2014; Kernen et al., 2012). All units are in meters.

Stratigraphy		Map Unit	SUPRASALT MINIBASIN (Gannaway, 2014)				SUBSALT MINIBASIN (Kernen et al., 2012)				INTRASALT MINIBASIN (*this study*)					
			Thickest Section	Thinnest Section	Lateral distance of thinning toward diapir	Percentage of thinning	Thickest Section	Thinnest Section	Lateral distance of thinning toward diapir	Percentage of thinning	Thickest Section	Location of Thickest Section	Thinnest Section	Location of Thinnest Section	Lateral distance of thinning	Percentage of thinning
Bonney Ss		Npb	*isopachous*				40	25	covers entire area	relatively constant	*absent*					
	Patsy Hill Member	Npbpdu	105	20	5800	81	55	15	2 isolated lens	73						
		Npbps	156	69	isolated lens	56	40	9	590	78						
		Npbpdl	43	19	2100	55	40	18	isolated lens	55	30	3	3	1	unknown	90
Wonoka Formation		Nwwgm	230	97	3000	58	130	7	323	95	200	5	6	1	unknown	97
		Nwwlu	246	36	3300	85	80	20	457	75	70	3	6	1	unknown	91
		Nwwlm	383	30	3800	92	215	20	457	91	55	3	30	4	unknown	45
		Nwwll	779	247	4200	96	550	70	457	87	60	3	22	4	unknown	63
Bunyeroo Formation		Nwb	1588	32	5000	98	*dip-section syncline-data not availible*				*absent*					

Patawarta diapir contains abundant intrasalt inclusions (Figures 4 & 5) that were generally mapped by Hall (1984). The inclusions contain the following lithologies: heavy mineral laminated sandstone and quartzite containing ripple cross-lamination and halite pseudomorphs, thin interbeds of heavy mineral laminated sandstone and thinly bedded green brown calcareous siltstone and shale, thinly bedded green brown and gray calcareous and dolomitic shale and siltstone containing halite casts, thinly bedded black limestone with finely bedded calcareous shale and siltstone, weekly brecciated dolomite, red shale, amygdaloidal basalt and fine-grained dolerite (Figures 6 & 7; Hall, 1984). The thinly bedded black limestone and calcareous siltstones and shales are not lithologies documented in the age equivalent autochthonous Callanna LES in the Willouran Ranges, however they are common inclusion lithologies in the southern part of the Patawarta Diapir (Figures 6 & 7).

Figure 7: Outcrop photographs of Callanna Group inclusions a & b) heavy mineral laminated sandstone and quartzite ripple marks and halite pseudomorphs, c) fine interbeds of heavy mineral laminated sandstone and thinly bedded green brown calcareous siltstone and shale, d) finely bedded green black calcareous shale and siltstone, e) amygdaloidal basalt and f) dolerite.

Kernen et al. (2012) and Gannaway (2014) measured stratigraphic sections (A through Z; excluding sections J, K, L, M), through the lower limestone member of the Wonoka Formation in both the suprasalt and subsalt minibasins (Figures 8-10; Table 1).

The lower limestone member thins toward the diapir in both the subsalt and suprasalt minibasins and is composed of red, purple and light green lime mudstone, silty lime mudstone, micaceous siltstone, and rare lithic arkosic sandstones near the base of the unit. The lime mudstone is thinly laminated (1-3 mm thickening upward to 1 cm-20 cm thick). The silty lime mudstone and micaceous siltstone beds are 1-5 cm thick and occur every 5 m at the base to 0.3 m at the top of the member. Sedimentary structures present in the lime mudstone include horizontal laminae/bedding, mud drapes, reduction spots, and flute casts. Sedimentary structures within the silty lime mudstone and micaceous siltstone include hummocky cross-stratification, dolomitized symmetrical ripples with mud drapes, low angle crossbedding, asymmetrical and symmetrical ripples, flute casts, climbing ripples, and mud limestone rip-up clasts.

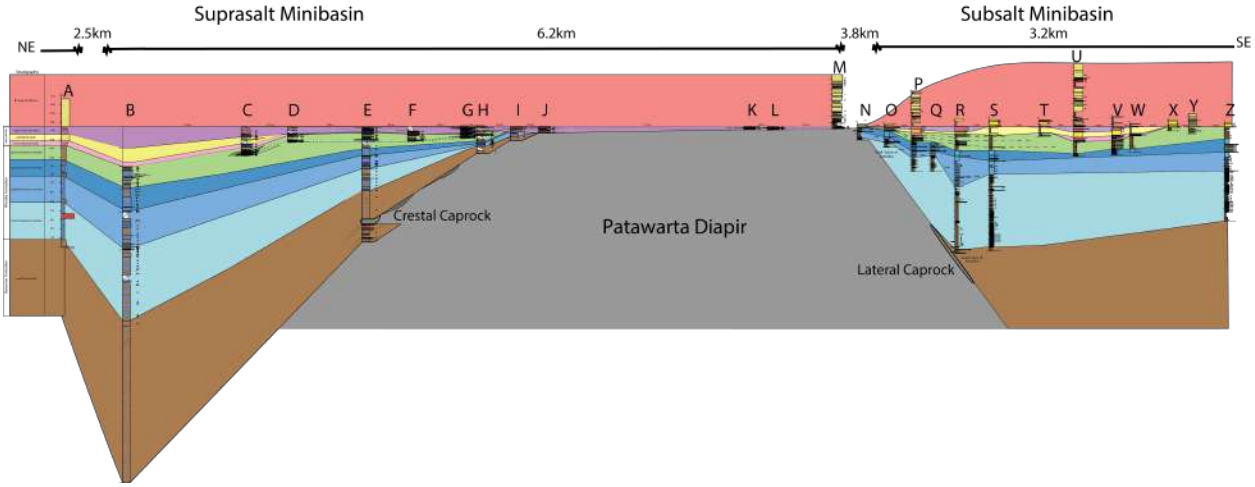

Figure 8: Fence diagram of the thickness changes in the suprasalt and subsalt minibasins (modified from Gannaway, 2014; Kernen et al., 2012).

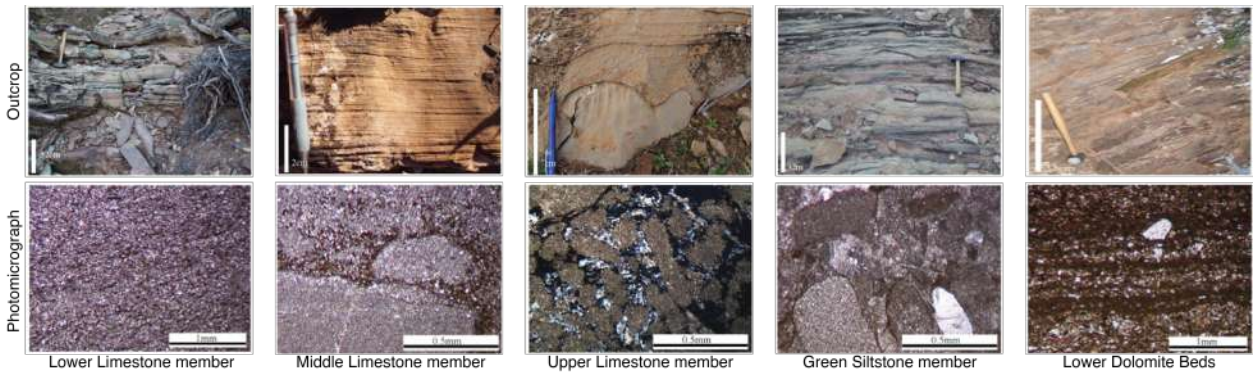

Figure 9: Subsalt minibasin Wonoka Formation and Patsy Hill member (from Kernen, 2011).

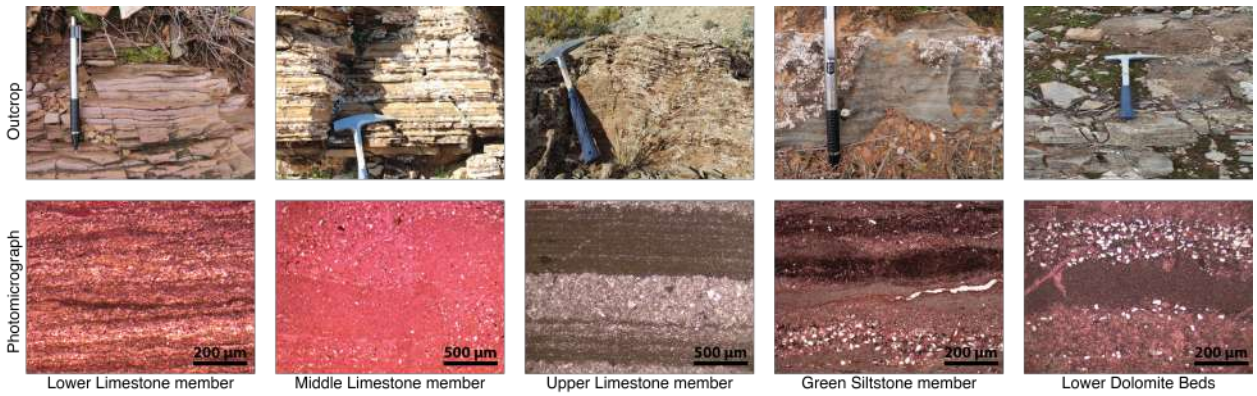

Figure 10: Suprasalt minibasin Wonoka Formation and Patsy Hill member (from Gannaway, 2014).

Based on the previous work of Kernen et al. (2012) and Gannaway (2014), the middle limestone member of the Wonoka Formation was measured in stratigraphic section A through Z (excluding sections I, J, K, L, M) in the suprasalt and subsalt minibasins (Figures 8-10; Table 1). The middle limestone member in the suprasalt and subsalt minibasins thin toward the diapir and are composed of blue gray to red lime mudstone, calcareous siltstone, and quartz arenite sandstones. The lime mudstone is

thin to medium bedded (1-30 cm thick) decreasing to thinly laminated (1-2 mm thick). The calcareous siltstone is 1 mm- 5 m thick and occurs every 0.3 m at the base to every 5-10 cm toward the top. The quartz arenite sandstones are located toward the top of the member in beds 0.3 m to 1 m thick and contain medium-grained, well sorted, subangular to subrounded grains of quartz and less than 10% lithics composed of calcareous siltstone. Sedimentary structures within the lime mudstone are horizontal laminae and lime mudstone drapes on the calcareous siltstone beds. Sedimentary structures within the calcareous siltstone are hummocky cross-stratification, planar lamination, asymmetrical and symmetrical ripples, flute casts, and lime mudstone rip up clasts. Sedimentary structures within the quartz arenite sandstones are horizontal laminae, low angle cross bedding, asymmetrical and symmetrical ripples, and lime mudstone rip-up clasts.

According to Kernen et al. (2012) and Gannaway (2014), the upper limestone member of the Wonoka Formation was measured in stratigraphic section A through Z (excluding sections J, K, L, M) in the suprasalt and subsalt minibasins (Figures 8-10; Table 1). The upper limestone member in the suprasalt and subsalt basins thin toward the diapir and are composed of blue gray to purple lime mudstone and litharenite sandstones. The lime mudstone beds are 0.3-2 m thick. The litharenite sandstones are medium grained, well sorted, well rounded and contain lithic grains of lime mudstone. The lime mudstone beds display soft-sediment deformation with the overlying litharenite sandstones. The litharenite sandstones form stylonodular texture (stylolite formed

during diagenesis along a pre-existing fracture from soft sediment deformation; Haines, 1988) and low angle crossbedding.

Kernen et al. (2012) and Gannaway (2014) documented the green mudstone member of the Wonoka Formation in stratigraphic section A through Z (excluding sections I, J, K, L, M, N) in the suprasalt and subsalt minibasins (Figures 8-10; Table 1). The green mudstone member in the suprasalt and subsalt basins thin toward the diapir and are composed of green to yellow calcareous siltstone, lime mudstone, with local litharenite and sublitharenite conglomeratic sandstone beds. The base of the member contains calcareous siltstone that is thinly laminated (1 mm to 1 cm) and interbedded with lime mudstone. The top of the lime mudstone becomes interbedded with litharenite to sublitharenite conglomeratic sandstone.

Based on the previous work of Kernen et al. (2012) and Gannaway (2014), the Patsy Hill lower dolomite beds were measured in stratigraphic section A-D and O-R, U, and V in the suprasalt and subsalt minibasins (Figures 8-10; Table 1). The lower dolomite beds in the suprasalt and subsalt basins are composed of dark gray dolomite, crypt-algal laminite, black fetid shale, litharenite and subarkose sandstones, and quartzite pebble conglomerate. The dark gray dolomite beds contain round to irregular-shaped, stacked concretions and are rhythmically interbedded with black fetid shale. Locally imbricated pink quartzite granule to pebble beds overlie erosional scour surfaces. The crypt-algal laminate forms 4-6 cm thick beds interbedded with litharenite and subarkosic sandstones and quartzite pebble conglomerate. The litharenite beds form sand stringers in the crypt-algal laminate and are composed of angular to rounded,

poorly sorted, silt to pebble size clasts of chert, granite, siltstone, and lime mudstone. The subarkose beds also form sand stringers in the crypt-algal laminite and are angular to round, poorly sorted, silt to pebble size clasts (bi-modal) of feldspar and less than 10% lithic grains of chert and lime mudstone.

Haines (1988), Kernen et al., (2012) and Gannaway, (2014) interpreted the subsalt and suprasalt minibasins to be deposited in a shallowing upward wave dominated shelfal setting (Lower Wonoka-Green Siltstone member) to a tidally dominated tidal inlet setting (Patsy Hill member; Table 2). Gannaway (2014) has similar observations and interpretations as Kernen et al., (2012) however, she recognized shelfal turbidites Bouma B & C in the lower member of the Wonoka Formation. The Patsy Hill Member of the Bonny Sandstone is interpreted to represent a slightly different depositional environment than the subsalt stratigraphy, mostly likely due to the changes in accommodation from the uplift of Patawarta diapir and subsidence of the suprasalt minibasin (Gannaway, 2014). The lower dolomite beds in the suprasalt minibasin are karsted and display a supratidal flat depositional environment rather than a tidal channel inlet (Gannaway, 2014; Kernen et al., 2012). The lower sandstone beds are interpreted to be a barrier bar akin to the subsalt stratigraphy, however the suprasalt barrier bar contains calcareous sandstones, which are not present on the subsalt side (Gannaway, 2014; Kernen et al., 2012). The upper dolomite beds are akin to the subsalt stratigraphy and interpreted to be lagoonal setting with washover fan and flood tidal delta deposits (Gannaway, 2014; Kernen et al., 2012; Table 2).

Table 2: Compilation of the stratigraphic units surrounding Patawarta diapir and their depositional environments, depositional, and halokinetic sequence stratigraphy for intrasalt, suprasalt, and subsalt (modified from Gannaway, 2014; Kernen et al., 2012).

Stratigraphy			Map Unit	Depositional Environment			Depositional Sequence Stratigraphy	Halokinetic Sequence Stratigraphy		
				Intrasalt Clasts (this study)	Suprasalt Minibasin (Gannaway, 2014)	Subsalt Minibasin (Kernen et al., 2012)		Intrasalt Clasts (this study)	Suprasalt Minibasin (Gannaway, 2014)	Subsalt Minibasin (Kernen et al., 2012)
Bonney Sandstone			Npb	absent	middle shelf lower shoreface		Transgressive-Highstand Systems Tracts	absent	Minimal halokinetic deformation	Minimal halokinetic deformation
Bonney Sandstone	Patsy Hill Member	unit 11	Npbpdu	absent	lagoon with washover fans & flood tidal delta	lagoon/bay	*Transgressive Surface* Lowstand Systems Tract		*CHS Boundary* Tapered CHS rim syncline	*CHS Boundary* Tapered CHS rim syncline
Bonney Sandstone	Patsy Hill Member	unit 10	Npbps	absent	barrier island	barrier bar				
Bonney Sandstone	Patsy Hill Member	unit 9	Npbpdl	lagoon/ lacustrine	intertidal tidal flat	main tidal channel inlet	*Sequence Boundary*			
Wonoka Formation		unit 8	Nwwgm	coastal plain	lagoon & subtidal to intertidal upper shoreface to foreshore	coastal plain	Highstand Systems Tract	carapace		
Wonoka Formation		units 6-7	Nwwlu	coastal plain	foreshore upper shoreface	foreshore upper shoreface				
Wonoka Formation		unit 5	Nwwlm	coastal plain	upper shoreface lower to middle shoreface	foreshore lower to upper shoreface				
Wonoka Formation		units 1-4	Nwwll	coastal plain	lower shoreface outer shelf	lower shoreface outer shelf	*Maximum Flooding Surface*		*CHS Boundary* Tapered CHS	*CHS Boundary* Tapered CHS
Bunyeroo Formation			Nwb	absent	outer shelf or terrestrial(?)		Transgressive Systems Tract	absent		

Chemostratigraphic Setting

Carbon isotope compositions of unaltered carbonates (δ^{13}Ccarb) precipitated in equilibrium with seawater reflects the composition of dissolved inorganic carbon (DIC) reservoir in the oceans, as precipitation of carbonates involves little isotopic fractionation relative to the DIC pool (Hayes & Waldbauer, 2006; Halverson et al., 2010; Schmid, 2017). Carbon isotopes constrain primary productivity and organic matter burial where the organisms prefer to uptake light carbon isotopes ^{12}C against ^{13}C during chemical reactions. Therefore, organic material will be enriched in light carbon isotope compared to the original pool of carbon. Dissolved organic carbon (DOC) pool is controlled by organic carbon burial and water column stratification. As a result, positive δ^{13}Ccarb excursions are driven by nutrient inputs in the surface oceans leading to an increase of light ^{12}C intake by organisms or an increase in burial efficiency of organic

matter. Negative δ^{13}Ccarb excursions are the result of decreased burial of organic matter from either a loss of primary productivity or lower burial efficiency. Abrupt changes in the δ^{13}C ratios are known as carbon isotope excursion events that are used as a correlation tool to a known basin wide event. Those excursion events are typically given a name and are compared to excursions and sequence stratigraphy in other sedimentary basins.

The oldest documented Neoproterozoic carbon isotope excursion in the Tonian (Willouran and Torrensian) is called the 'Bitter Springs' excursion which is located in the Amadeus Basin Bitter Springs Formation (Limestone) near Alice Springs (Figure 11; Klaebe, 2015). The Bitter Springs excursion is approximately δ^{13} C -3‰ to -4‰ (PDB) and the stratigraphic equivalent formation in the Willouran or Flinders Ranges is not clear as a proper correlation is yet to be discovered and described (Stueken et al., 2019). The second oldest carbon isotope excursion is called the 'Islay' excursion which becomes the most negative at δ^{13} C -9‰ (PDB) however, there is an unconformity at at this time in the Willouran and Flinders ranges and strata of that age are not found (Figure 11; Condon et al., 2015). The 'Keele Peak' in the Marinoan Umberatana Group is the only positive carbon isotope excursion at δ^{13} C +12‰ (PDB) (Figure 11; Condon et al., 2015). The 'Trezona' excursion in the Marinoan Umberatana Group becomes the most negative at δ^{13} C -7‰ (PDB) and is documented in the Flinders Ranges stratigraphy (Figure 11; Condon et al., 2015). The youngest Marinoan excursion is referred to as the Ediacaran-aged Shuram excursion (Fike et al., 2006; Grotzinger, et al., 2011; Husson et al., 2015; Le Guerroué ., 2010), which has δ^{13} C values as low as -

12‰ (PDB), thus constituting the most negative δ^{13} C excursion known in Earth's history (Figures 11 & 12; Husson et al., 2015). Our goal is to use the δ^{13} C values in the limestone inclusions in Patawarta Diapir as a chemostratigraphic correlation tool to the regional stratigraphy of the Adelaide Rift Complex.

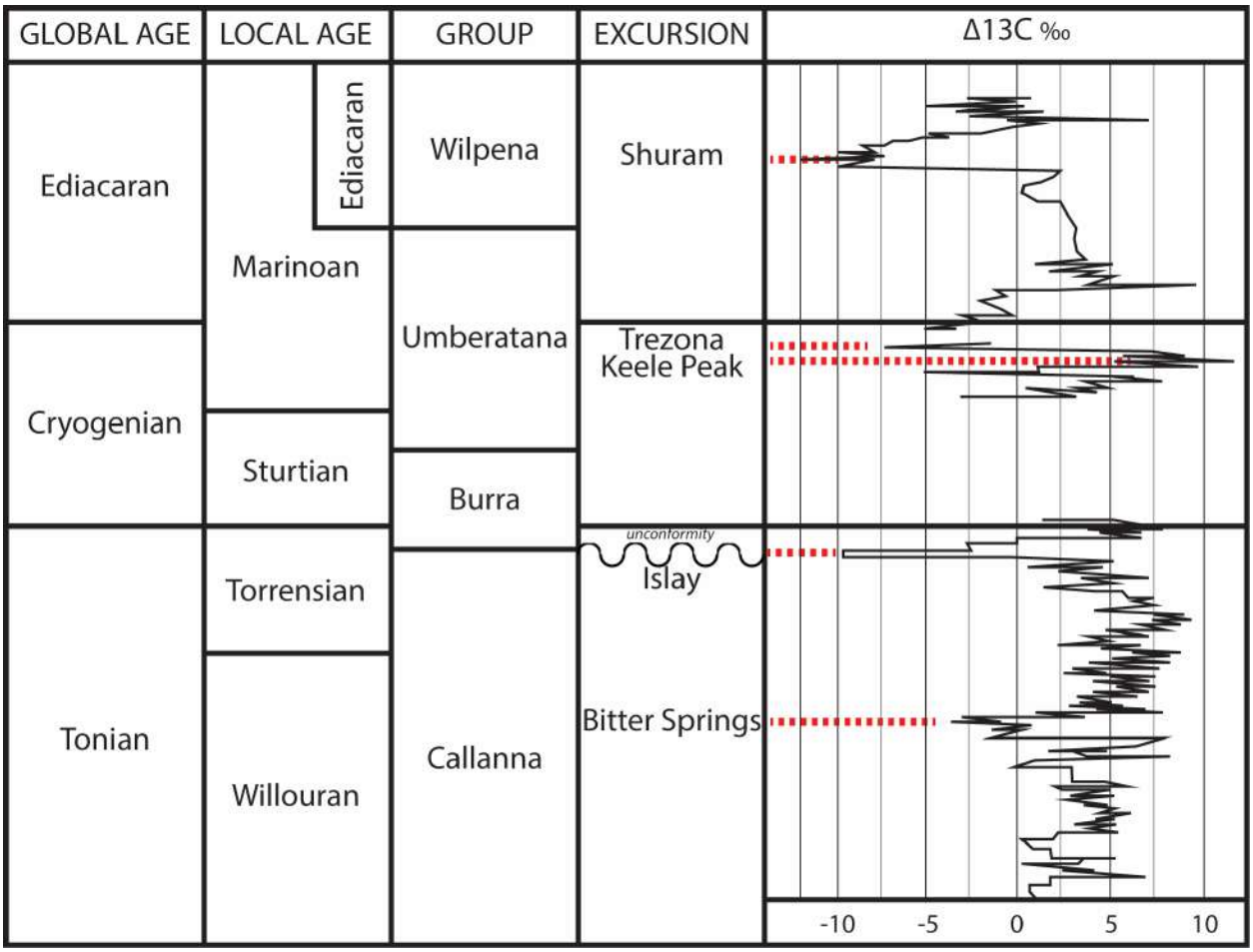

Figure 11: Global delta 13 Carbon Isotope Curve for the Neoproterozoic and early Cambrian stratigraphy (modified from Condon et al., 2015). Possible carbon negative isotope excursions in the Flinders Ranges inclusions could be from the Synsalt Bitter Springs, Postsalt Trezona, or Postsalt Shuram. The Islay excursion is not found in the Flinders Ranges and the Keele Peak is a positive carbon isotope excursion (our study is interested in the negative excursions).

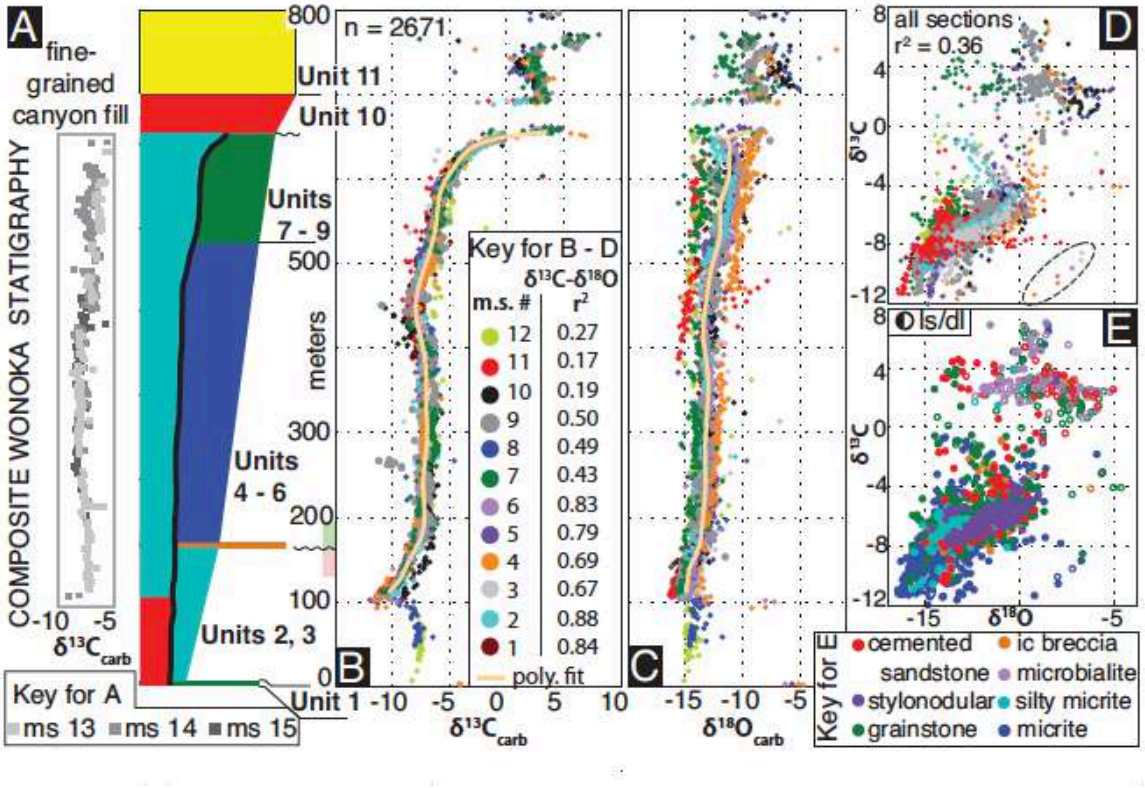

Figure 12: δ¹³C (Shuram Excursion) & δ¹⁸O from Husson et al., (2015) where a) is a generalized stratigraphic column where sampling took place, b) compilation of the δ¹³ C isotope values, c) compilation of the δ¹⁸ O isotope values, d) graph of δ¹³ C verses δ¹⁸ O and, e) highlighted portion (elliptical from d). This study is used as a chemostratigraphic basis for establishing the Shuram excursion in the inclusion stratigraphy at Patawarta diapir.

Husson et al., (2015) measured 15 stratigraphic sections throughout the Flinders Ranges and collected hundreds of Wonoka Formation and Patsy Hill Member samples measuring their δ¹³ C and δ¹⁸ O isotope compositions in order to establish the presence and trend of the Shuram Excursion in the Flinders Ranges (Figure 12). Husson et al.,

(2015) data was in the center of minibasins and away from the salt diapirs in order to avoid any potential diagenetic alteration of the fluids often association with salt bodies. Husson et al., (2015) stratigraphic correlation begins with samples equivalent to Haines (1988) unit 2-3 and ends in Haines (1988) unit 11 (Figures 12 & 13). Husson et al., (2015) did not take into consideration the stratigraphic update by Reid & Preiss (1999), however a correlation can be made between the previous work and the $\delta^{13}C$ and $\delta^{18}O$ stable isotope data collected and analyzed for this study (Figure 13).

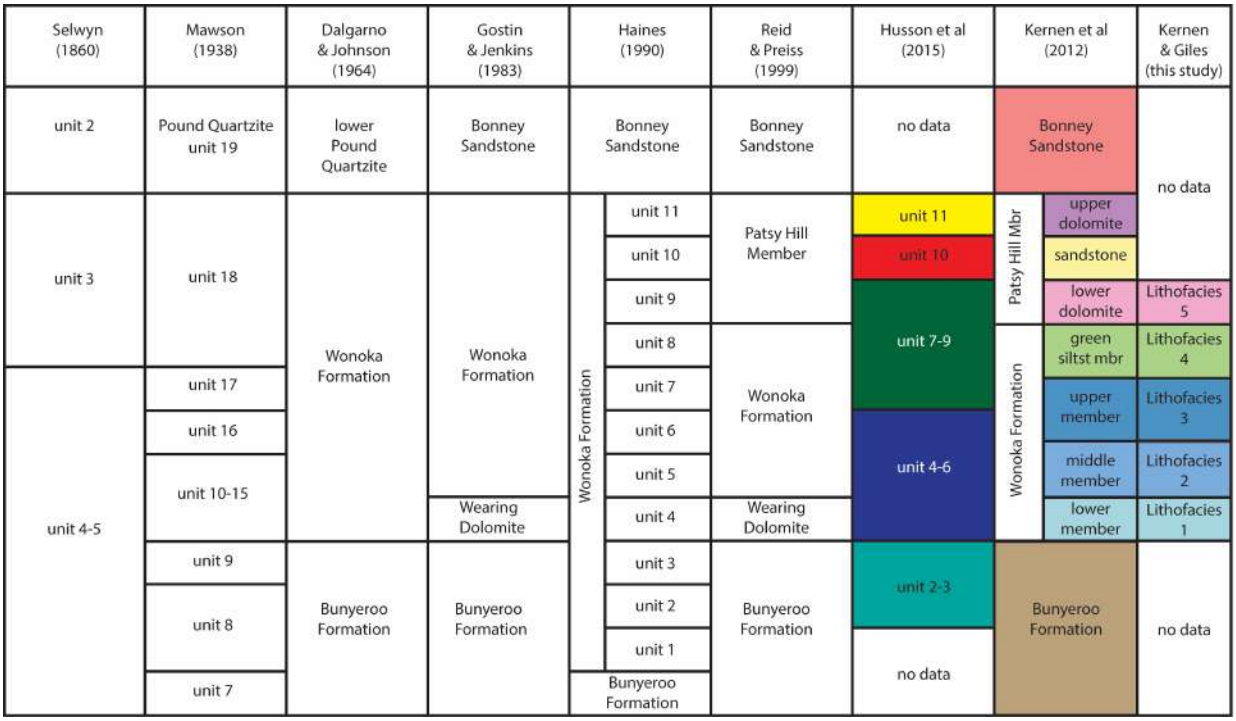

Figure 13: Stratigraphic correlation chart of the different studies and authors on the Bunyeroo, Wonoka, and Bonney Sandstone (Wilpena Group; modified from Kernen et al., 2012; Kernen et al., 2018).

3.4 METHODS

A geological map of the limestone inclusions in the Patawarta diapir was created and added to the previous work from Kernen et al. (2012) and Gannaway (2014) at 1:36,000. The 1:60,000 COPLEY and 1:250 000 ANGEPENA geologic map sheets (Coats, 1973, 2009a), aerial photographs, Quickbird 4-band (60 cm resolution) and HYMAP 126-band (4 m resolution) satellite imagery, and Google Earth imagery were used as base materials for the geologic map. Five measured sections recorded the lithology, grain size, fresh and weathered colors, bedding orientation and formational contacts. Approximately 200 samples were collected to document the range of lithologies and varying mineralogies of the inclusions in the Patawarta diapir. 100 petrographic thin sections were cut from the samples and stained for calcite and iron with alizarin red-S and potassium ferricyanide. The thin sections were petrographically analyzed in both plane and polarized light for groundmass, cements, and grain mineralogy. The results of the limestone inclusion sedimentology and stratigraphy were compared and correlated to the previous work from Gannaway (2014) and Kernen et al (2012).

Fifty-eight limestone and dolomite samples were analyzed for $\delta^{13}C$ and $\delta^{18}O$ isotopes by the University of Michigan and University of Kansas Stable Isotope laboratories. Samples were slabbed perpendicular to bedding and 5 to10 milligrams (mg) of powder were micro-drilled from the diapiric matrix, rim dolomite, inclusion 3, and lower-upper Wonoka Formation, and Patsy Hill member of the Bonney Sandstone from the suprasalt and subsalt minibasins. The diapiric matrix near the salt-sediment

interface and each rim dolomite capstone fabric were sampled. Because inclusion 3 contained all the varying carbonate inclusion lithologies, 2 samples were collected from Lithofacies 1 and 1 sample from each Lithofacies 2-5. All powders were heated to 110°C to remove volatile contaminants and water in individual borosilicate reaction vials. Carbonate samples weighing a minimum of 10 micrograms were placed in stainless steel boats. Samples were transferred to individual borosilicate reaction vessels and reacted at 77° ± 1°C with 4 drops of anhydrous phosphoric acid for 8 minutes in a Finnigan MAT Kiel IV preparation device coupled directly to the inlet of a Finnigan MAT 253 triple collector isotope ratio mass spectrometer. Δ^{13} C and δ^{18} O were acquired simultaneously on both systems, and isotopic data are reported in the standard delta notation as the ‰ difference from the VPDB standard (Vienna Pee Dee Belemnite). Precision and accuracy of data were monitored through daily analysis of a variety of powdered carbonate standards. At least four standards were reacted and analyzed daily. All samples are measured relative to an internal gas standard, and then converted to the VPDB scale using the known composition of NBS-19 (δ^{13} C σ 1.95; δ^{18} O σ 2.20). Measured precision is maintained at better than 0.1 ‰ for δ^{13} C isotope compositions.

3.5 RESULTS

Limestone Sedimentary Inclusions

Because of the previous detailed sedimentological and stratigraphic study of the suprasalt and subsalt minibasins adjacent to Patawarta diapir from Gannaway (2014)

and Kernen et al. (2012), the carbonate inclusions inside the diapir were recognized as possibly being much younger than the Callanna Group stratigraphy. Our approach to this study is to use the detailed observations from Gannaway (2014) and Kernen et al (2012) as a guide for identifying and correlating the lithologies of the inclusions to the regional stratigraphy. Five sedimentary inclusions containing primarily limestone, calcareous siltstone and shale are identified within the southwestern part of Patawarta diapir (Figure 14). The inclusions are bounded by diapiric matrix or mafic igneous inclusions (Figure 14). The inclusions display internally coherent bedding trends that define an internal stratigraphy, though inclusions 2 and 5 display tight folding. Inclusion1 is located the furthest north in Patawarta Diapir. It is 1.5km long and 0.3km wide and displays steep dips (vertical) that gradually decrease northward to approximately 45 degrees (Figure 14; Table 2-4). Inclusion 2 is located south of inclusion 1. It is 1.0km long and 0.4km wide and displays a recumbent fold with steep dips (50-60 degrees) to the west and shallow dips to the east (20-30 degrees; Figure 14; Table 2-4). Inclusion 3 is located directly south of inclusion 2. It is 0.8km long and 0.25km wide and displays steeper dips (50-75 degrees) to the west and shallower dips to the east (30-50 degrees). Inclusion 4 is located south of inclusion 3 and southwest of inclusion 5. It is 1.0km long and 0.20km wide and displays relatively consistent NW-SE trending 40-50 degrees dips on the northwestern side that steepen to vertical and are tightly folded on the southeastern side. Inclusion 5 is directly northeast of inclusion 4 and is the largest inclusion. It is 1.1km long and 1.2km wide and displays varying dips (30-60 degrees) that form a large recumbent fold (Figure 14; Table 2-4). The northern,

western, and southern margins of the 5 inclusions are in contact with the diapiric matrix and the eastern portion is covered by recent alluvium (dark gray on map; Figure 14).

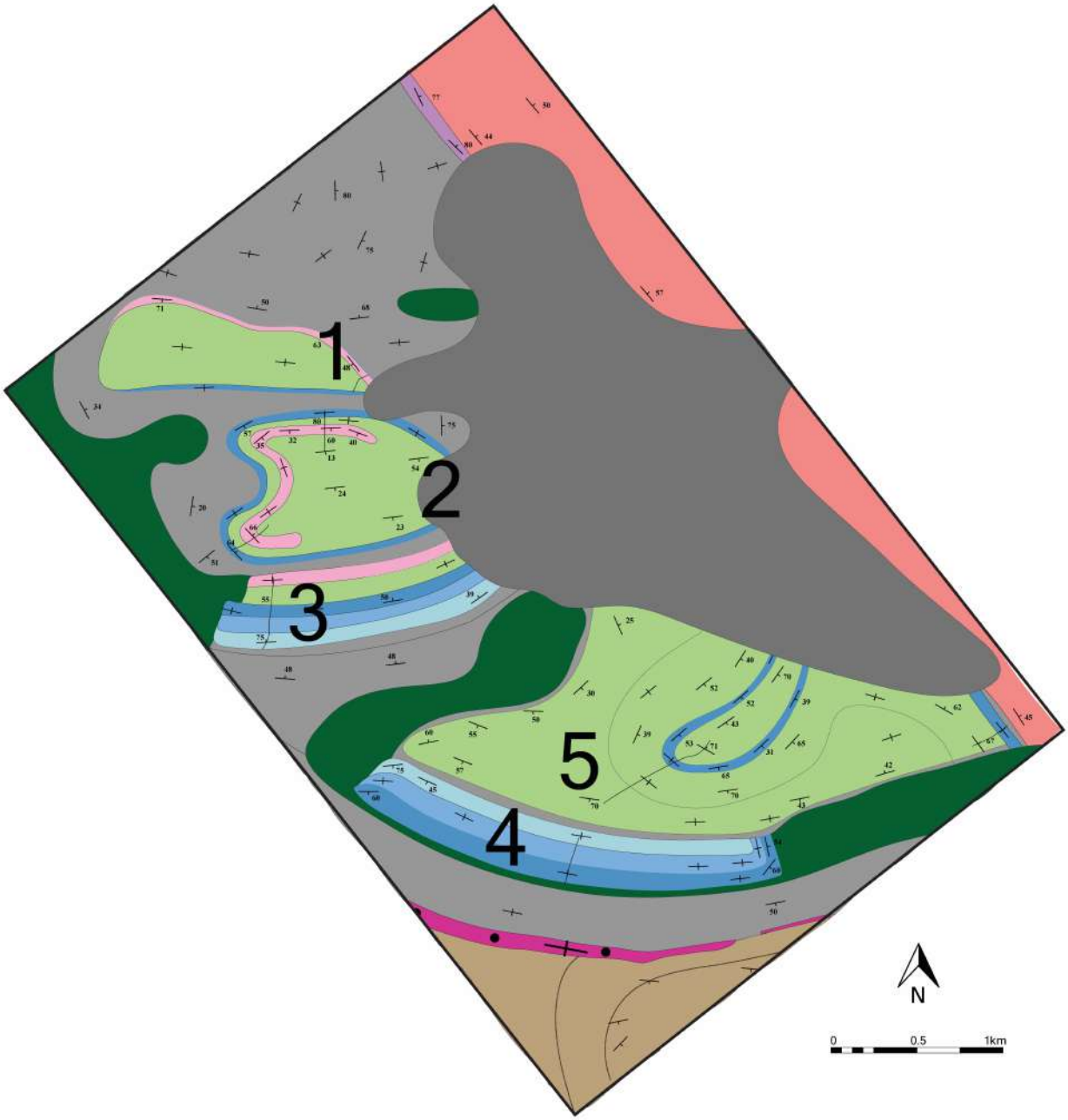

Figure 14: Detailed geologic map of limestone inclusions (1-5) in Patawarta diapir. Lithofacies 1 is defined by the dark blue; Lithofacies 2 is defined by the medium-light

blue; Lithofacies 3 is defined by the light blue; Lithofacies 4 is defined by the green; Lithofacies 5 is defined by the pink.

Table 3: Characteristics of carbonate inclusions in the Patawarta diapir.

INCLUSION CHARACTERISTICS					
Inclusion	Length	Width	Dip	Folds	Stratigraphy
1	1.5km	0.3km	45-90	none	
2	1.0km	0.4km	20-60	recumbent	
3	0.8km	0.25km	30-75	none	
4	1.0km	0.2km	40-90	none	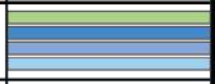
5	1.1km	1.2km	30-60	recumbent	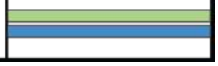

Table 4: Characteristics of the inclusion lithofacies in the Patawarta diapir.

INCLUSION LITHOFACIES CHARACTERISTICS					
Lithofacies	Color	Bedding	Inclusion	Dominant Lithology	δ13C
1	gray & tan	1mm-5cm	3 & 4	silty limestone	-6.36‰ -3.92‰
2	gray & tan	1mm-10cm	3 & 4	silty limestone	-3.66‰
3	tan	5mm-30cm	1-5	silty limestone	-2.32‰
4	green	1-5cm	1-5	shale	-1.09‰
5	tan	5-10mm	1-3	sandy dolomite	-0.12‰

The inclusions contain five distinct lithofacies (1-5), which were mapped in detail throughout the inclusions (Figures 14-17). The lithofacies are arranged in stratigraphic succession within the inclusions and are described here in stratigraphic ascending order starting with Lithofacies 1. Lithofacies 1 is 22-60m thick and is composed of gray to tan, thinly laminated (1-3 mm) calcareous siltstone and silty lime mudstone that form beds 1-5 cm thick (Figures 14, 15a, 16a, 17). It is dominated by calcareous siltstone at the base and decreases in quartz silt content up stratigraphic section where the beds become more carbonate rich. Lithofacies 1 is always in contact with the diapiric matrix and is only found in inclusion 3 and 4 whereas the upper boundary is in contact with lithofacies 2 in both inclusions (Figures 14; Table 1, 2-4). Lithofacies 2 is 30-55m thick and composed of tan and gray, thinly laminated (1-5 mm) silty lime mudstone interbedded with lime mudstone that forms beds 5-10 cm thick (Figures 14, 15b, 16b, 17). It is dominated by silty lime mudstone at the base and decreases in quartz silt content up section where the beds become primarily lime mudstone. Lithofacies 2 is only found in inclusion 3 and 4 where it is stratigraphically above Lithofacies 1 and below Lithofacies 3 (Figures 14; Table 1, 2-4). Lithofacies 3 is 6-70m thick and composed of tan, thinly laminated (5-10mm) silty lime mudstones interbedded with lime mudstone that forms beds 10-30 cm thick (Figures 14, 15c, 16c, 17). It is dominated by silty lime mudstone at the base and decreases in the quartz silt content up section. Lithofacies 3 is in limestone inclusions 1-5 where it consistently lies stratigraphically below Lithofacies 4. Lithofacies 3 is stratigraphically above Lithofacies 2 in inclusions 3 and 4 (Figures 14; Table 1, 3-4). Lithofacies 4 is 6-200m thick and is composed of dark

greenish black to light green, thinly laminated (3-5mm) calcareous siltstone to shale that form beds 1-5 cm thick (Figures 14, 15d, 16d, 17). It is dominated by calcareous siltstone at the base with apparent thin bedding while the upper portion is dominated by a massive green siltstone that is non-calcareous. Lithofacies 4 is found in inclusions 1-5 and stratigraphically above Lithofacies 3 (Figures 14; Table 1, 3-4). Lithofacies 5 is 3-30m thick and is composed of tan, thinly laminated (1-3 mm) sandy dolomite (calcite cement) that forms beds 5-10 mm thick with local symmetrical wave ripped horizons and rare massive bedding (Figures 14, 15e, 16e, 17). Lithofacies 5 is found in inclusions 1-3 and stratigraphically above Lithofacies 4 (Figures 14; Table 1, 3-4). Due to the dominance of horizontal laminae and the general lack of wave and current sedimentary structures in the limestone inclusions, Lithofacies 1-5 are interpreted to be deposited in an overall shelfal carbonate ramp depositional environment (Table 2).

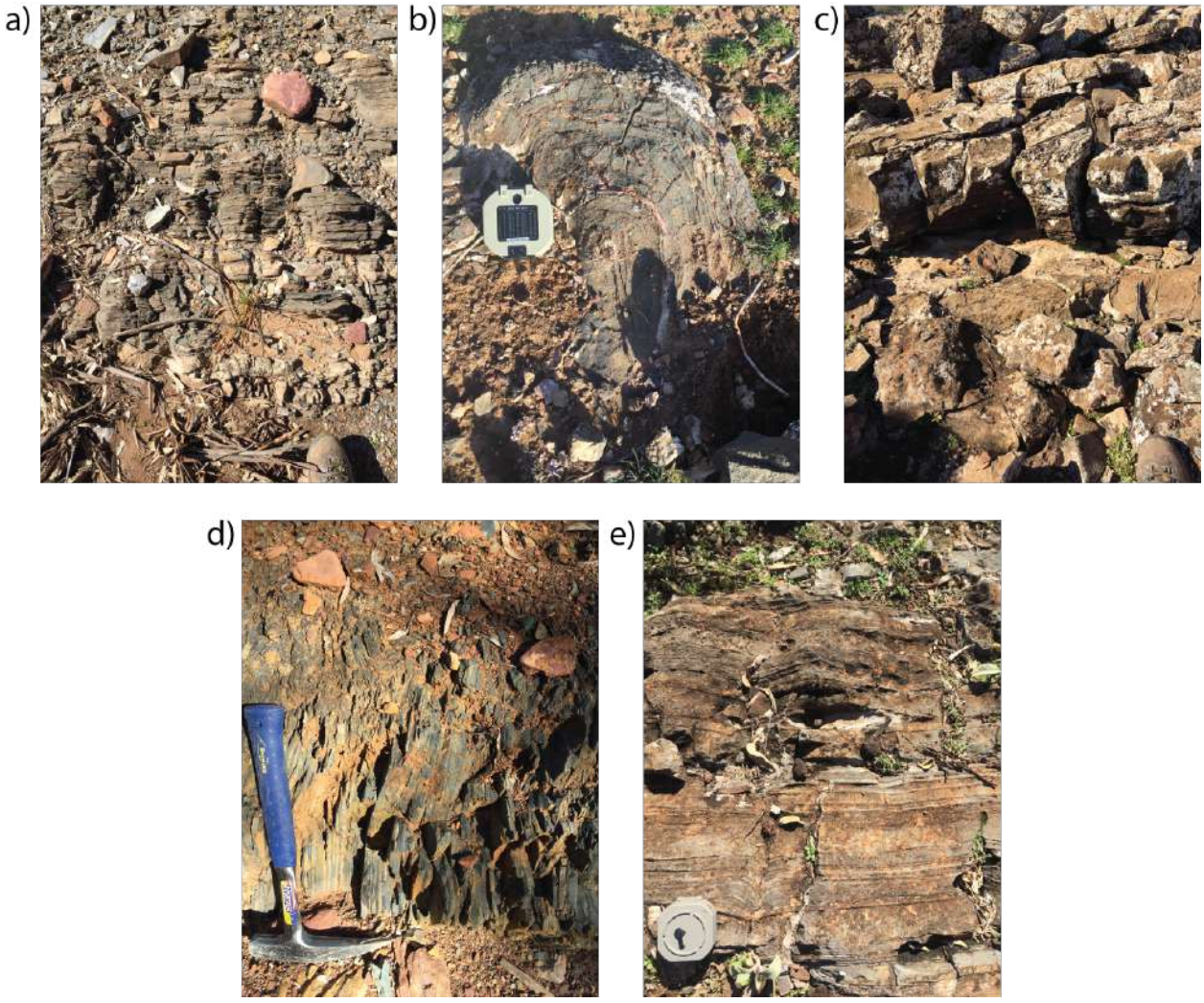

Figure 15: Outcrop of a) Lithofacies 1, b) Lithofacies 2, c) Lithofacies 3, d) Lithofacies 4, and e) Lithofacies 5, located in limestone inclusion 3 in Patawarta diapir in Figure 8.

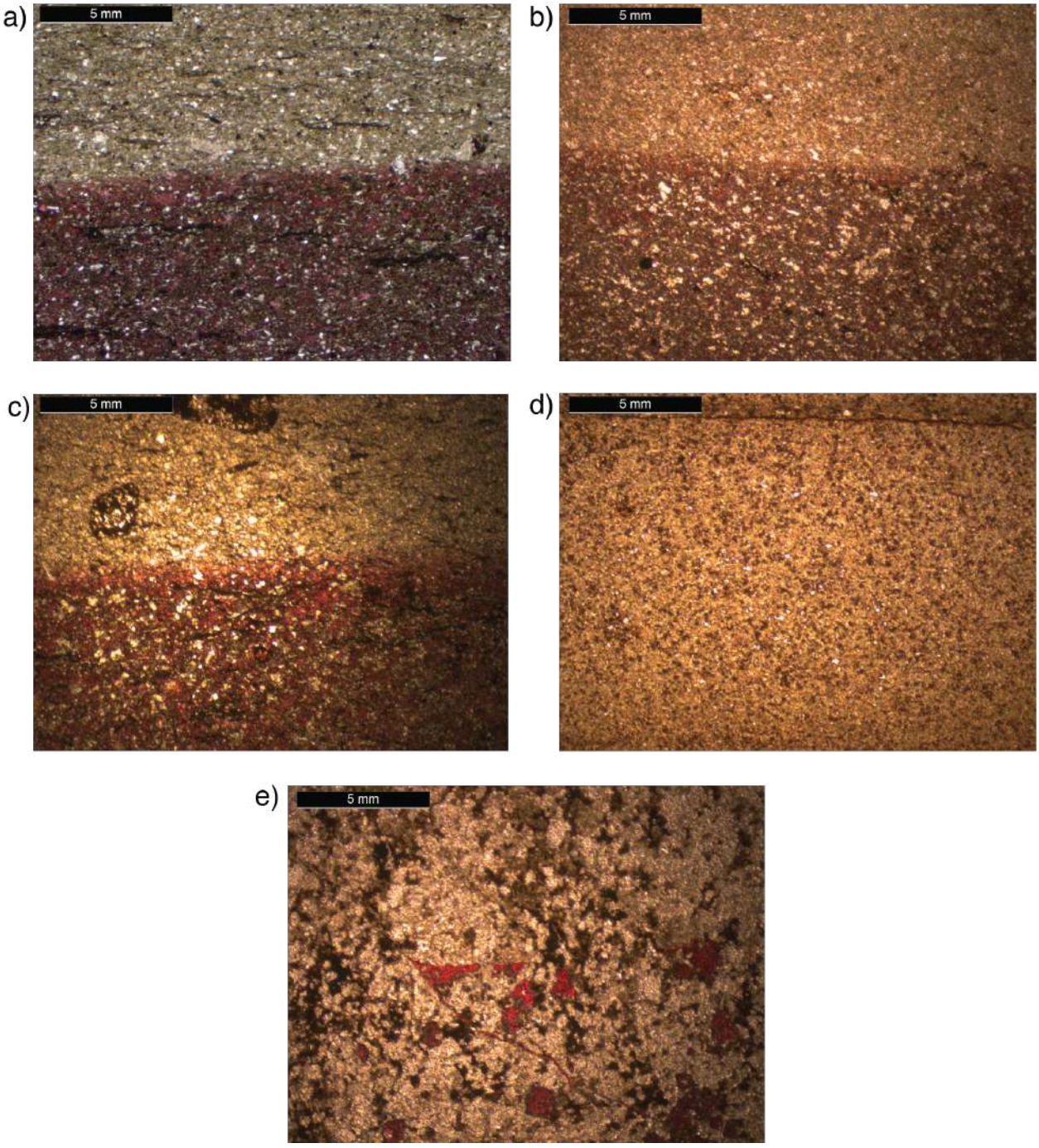

Figure 16: Photomicrographs of a) Lithofacies 1, b) Lithofacies 2, c) Lithofacies 3, d) Lithofacies 4, and e) Lithofacies 5, located in limestone inclusion 3 in Patawarta diapir. Each photomicrograph corresponds to the lithofacies in Figure 8. Thin sections have

been stained with alizarin red-S in order to identify the calcite (limestone) of the Wonoka Formation.

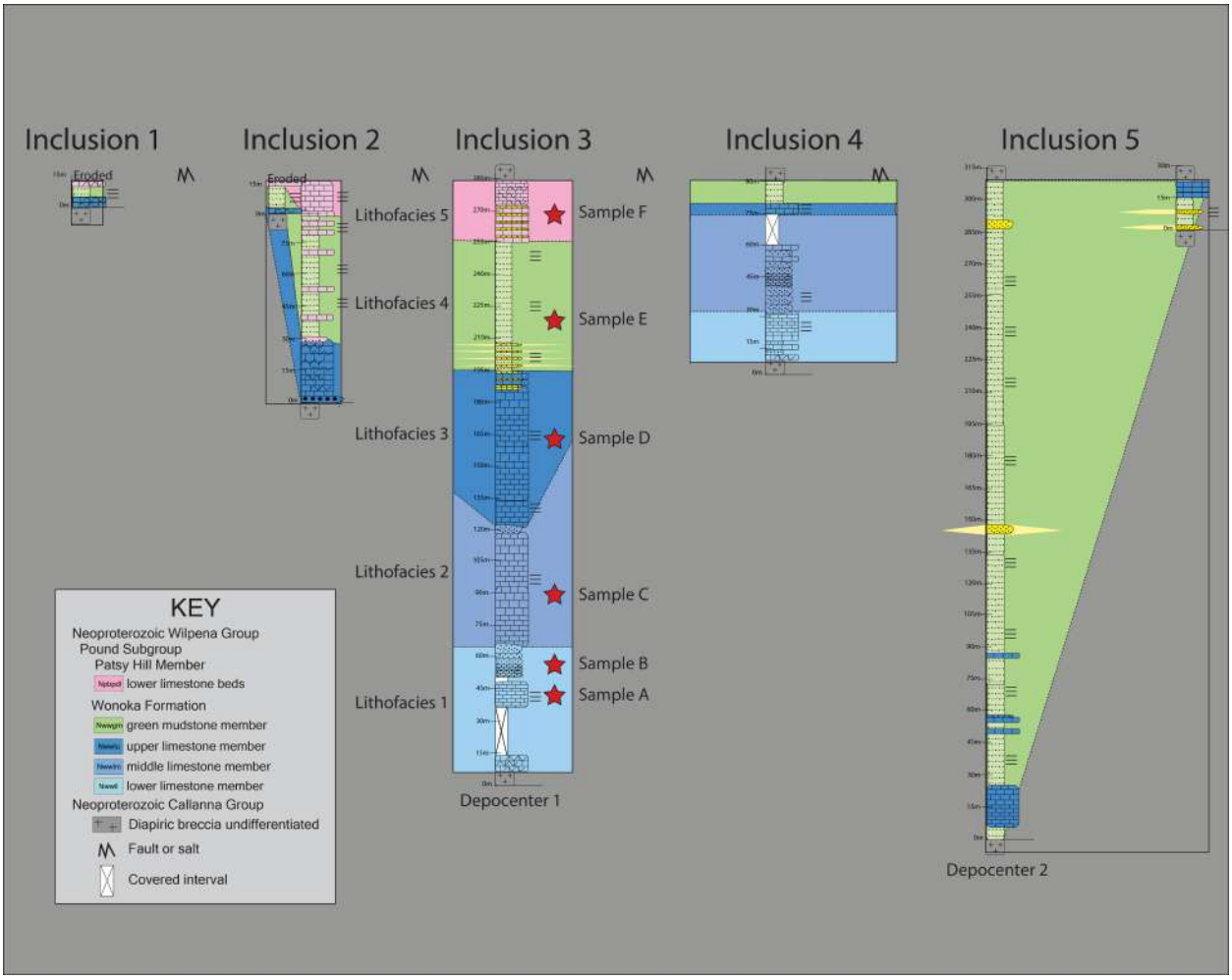

Figure 17: Detailed fence diagram of the intrasalt Ediacaran-aged Wonoka Formation and lower dolomite beds of the Patsy Hill member limestone inclusions. Samples were collected from inclusion 3 in order to complete the outcrop, petrographic, and carbon isotope study.

Based on outcrop and petrographic lithologic attributes and stratigraphic order, Lithofacies 1-5 are lithostratigraphically correlated to Wonoka and Patsy Hill Member of the Bonney Sandstone stratigraphic map units in the suprasalt and subsalt minibasins. In ascending order: (1) Lithofacies 1 is equivalent to the lower limestone member of the Wonoka Formation; (2) Lithofacies 2 is equivalent to the middle limestone member of the Wonoka Formation; (3) Lithofacies 3 is equivalent to the upper limestone member of the Wonoka Formation; (4) Lithofacies 4 is equivalent to the green mudstone member of the Wonoka Formation; and (5) Lithofacies 5 is equivalent to the lower dolomite beds of the Patsy Hill member (Figure 17; Table 4). Because the stratigraphy lacks wave and current sedimentary structures, 'stratigraphic up' was determined by specific order of lithologies. The order of Lithofacies 1-5 matched the order of the lower-green siltstone members of the Wonoka Formation and lower dolomite beds of the Patsy Hill member (Bonney Sandstone). The results of these analyses were used as a chemostratigraphic tool to correlate the inclusion lithologies to the Wonoka Formation and Patsy Hill member of the Bonney Sandstone in suprasalt section A and subsalt section P (Table 1).

Results Chemostratigraphy

The $\delta^{13}C$ carbon isotopes were calculated from Lithofacies 1-5 within inclusion 3 (Figures 12 & 15). Six samples were collected in total; two samples from lithofacies 1 and one sample each from lithofacies 2-5 (Figures 12 & 15). $\Delta^{13}C$ carbon isotopes values for each Lithofacies are the following: 1) Lithofacies 1 are -6.36‰ and -3.92‰, 2)

Lithofacies 2 is -3.66‰, 3) Lithofacies 3 is -2.32‰, 4) Lithofacies 4 is -1.09‰, and 5) Lithofacies 5 is -0.12‰ (Figures 18; Table 4). When comparing the $\delta^{13}C$ carbon inclusion isotope results to the regional Wonoka Formation and Patsy Hill Member data from Husson (2015), Lithofacies 1-3 is more positive or heavy (Figure 18; Table 4). Lithofacies 4 sample has nearly a perfect match and Lithofacies 5 is slightly more negative or light (Figures 18; Table 4). The $\delta^{13}C$ carbon values of the diapiric matrix and rim dolomite are isotopically heavy compared to Husson (2015) $\delta^{13}C$ carbon of the regional Wonoka Formation and the results of the Wonoka Formation from this study (Figures 18; Table 4). An explanation of the isotopically heavy results from the diapiric matrix and rim dolomite are yet to be published. The lower Wonoka Limestone member correlates to the regional δ^{18} O isotope values from the previous work, however there is no obvious correlation with the other members of the carbonate inclusion stratigraphy.

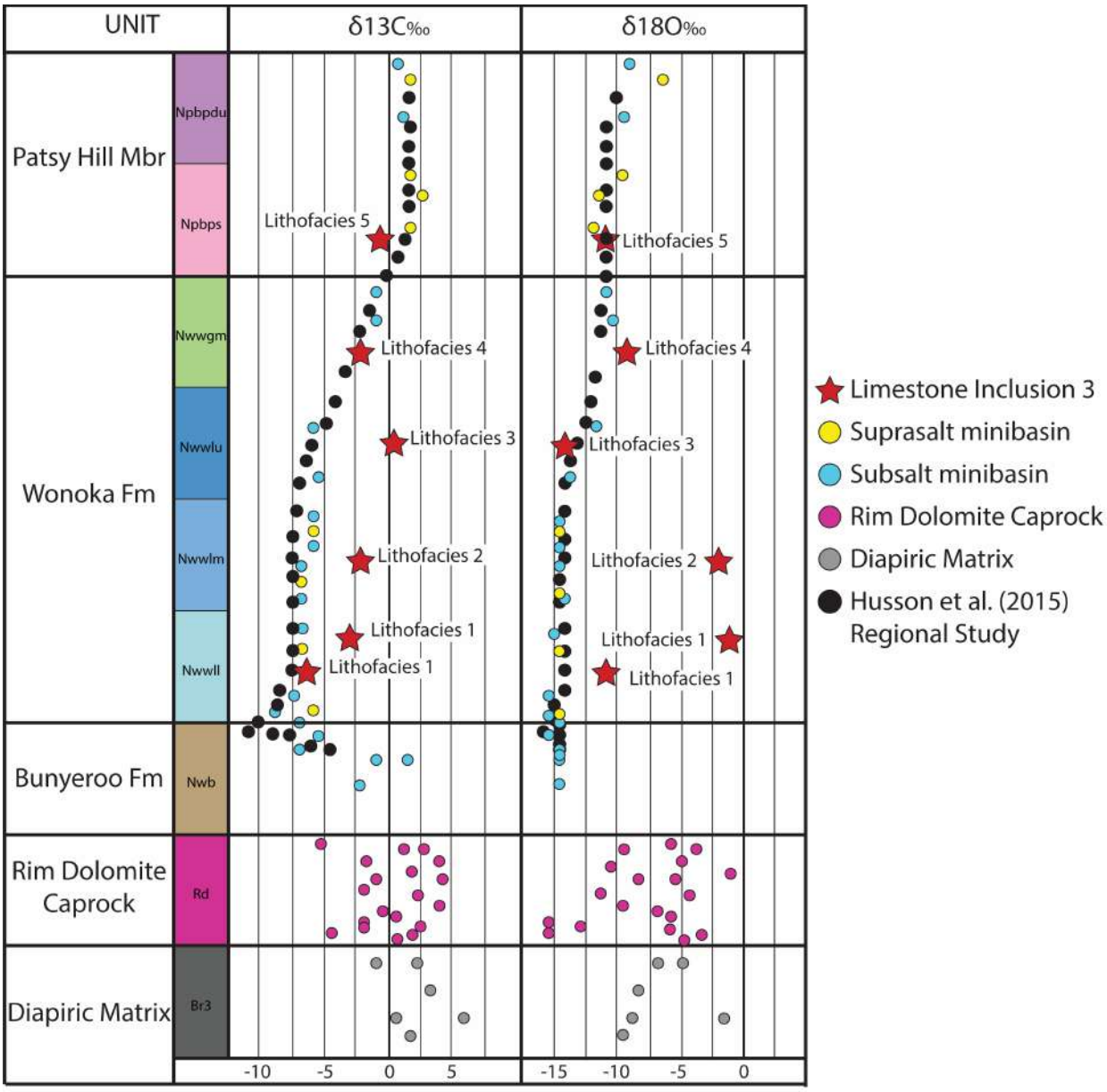

Figure 18: δ[13]C (Shuram Excursion) & δ18O used as a chemostratigraphic tool to identify Wonoka Formation and Patsy Hill member stratigraphy in the Patawarta diapir.

3.6 DISCUSSION

Previous studies of the suprasalt and subsalt minibasins from Kernen et al., (2012) and Gannaway (2014) establish the Wonoka Formation as an overall wave-

dominated sequence that shallows upward into a terrestrial coastal plain deposit. The lower dolomite beds of the Patsy Hill Member (Bonney Sandstone) are interpreted to be tidally influenced main tidal channel inlet (Kernen et al., 2012; Gannaway, 2014). The subsalt and suprasalt Wonoka Formation lower limestone member displays horizontal laminae and reduction spots in the lime mudstone beds and hummocky cross-stratification in the silty lime mudstone and micaceous siltstone beds allow it to be interpreted as an outer shelf deposit below storm wave-base that shallows to a lower shoreface depositional environment (Preiss, 1987; Haines, 1988, 1990; Walker and Plint, 1992; Kernen et al., 2012; Gannaway, 2014). The subsalt and suprasalt Wonoka Formation middle limestone member displays hummocky cross stratification in the calcareous siltstone beds overlain by calcareous siltstone beds and low angle cross-bedding, asymmetrical and symmetrical ripples in the quartz arenite sandstones beds allow it to be interpreted as being deposited within the lower to upper shoreface depositional environment with the sandstone beds deposited in the foreshore (Haines, 1990; Walker and Plint, 1992; Kernen et al., 2012; Gannaway, 2014). The upper limestone member of the Wonoka Formation is interpreted to be deposited in the foreshore depositional environment (Haines, 1988, 1990; Walker and Plint, 1992; Kernen et al., 2012; Gannaway, 2014) based on the presence of abundant low angle cross bedding in the litharenite sandstones. The green mudstone member of the Wonoka Formation lacks current and wave sedimentary structures and is therefore interpreted to be deposited in a coastal plain depositional environment (Haines, 1988; 1990; Kernen et al., 2012; Gannaway, 2014). The local development of the

conglomeratic sandstone beds in the green mudstone member suggests that they were derived from the underlying stratigraphy of a local topographic high over of the adjacent Patawarta diapir. The Patsy Hill lower dolomite beds are interpreted to be deposited in a tidally-dominated main tidal channel inlet depositional environment (Colquhoun, 1995; Kernen et al., 2012; Gannaway, 2014), based on the rhythmically interbedded dark gray dolomite and fetid black shale and quartzite pebble conglomerate and sand stringers that scour into the underlying crypt algal-laminite. The quartzite pebble conglomerate clasts are derived from the exposed diapir.

The inclusions are interpreted to be more akin to the subsalt stratigraphy based on the lithologic and petrographic character. Because the sedimentary structures of the lower, middle, upper, and green siltstone member of the Wonoka Formation inclusions are limited (horizontal laminae almost exclusively) and they are interpreted to be deposited in either a terrestrial to lagoon depositional environment or on the shelf, below wave base. The lower dolomite beds of the Patsy Hill member display wavy bedding which may indicate crypt-algal laminae; therefore, it is most likely that Lithofacies 5 was deposited in shallow water which is nearly identical to the subsalt and suprasalt minibasins. The inclusions display a 500m thick section that has horizontal bedding and planar laminations that lack growth stratigraphy or halokinetic sequences (Giles & Lawton, 2002). In comparison, the same stratigraphic section in the suprasalt minibasin to the north is 1,000m thick and the subsalt minibasin to the south is 1,300m thick (Figure 8; Table 1 & 2). Because the thickness of each member/bed within the inclusions is stratigraphically thinner (Table 1), it can be interpreted that the inclusions

were likely deposited on top of a salt body as a condensed section, which is termed carapace (Hart et al., 2004).

The inclusions display two depocenters (Figure 17) interpreted to represent differential deposition on a rugose top salt. The Wonoka Formation and Patsy Hill Member lithostratigraphy established as inclusions in the Patawarta salt diapir are interpreted to represent carapace (Hart et al., 2004) that later form a suture zone (Dooley et al., 2012; Figure 5) encased in the Patawarta diapir. A suture zone separates the two coalesced salt sheets (allosuture) or two lobes from a single salt sheet (autosuture), including any trapped sediments (Dooley et al., 2012). Our first line of evidence to support an allosuture interpretation is that the distribution of the layered evaporite sequence Curdimurka Subgroup inclusions are concentrated to the northern side of the diapir and significantly younger Wonoka Formation and Patsy Hill Member inclusions are concentrated to the southern side of the diapir. An equal distribution of inclusions would suggest that all the inclusions are relatively the same age. Our second line of evidence to support an allosuture interpretation is the detailed stratigraphic changes from the suprasalt minibasin (Giles et al., 2017) and subsalt minibasin (Lehrmann et al., 2017) suggest the suprasalt minibasin was not depositionally connected to the subsalt minibasin (Figures 9 & 10). Because the detailed stratigraphy of the Wonoka Formation and lower dolomite beds of the Patsy Hill member from the suprasalt and subsalt minibasins (Figure 9 & 10) are slightly different in terms of water depth and thickness than the stratigraphy of the inclusions, the carapace is interpreted to represent either a lateral or frontal allosuture, possibly forming during the initial

stages of the Delamerian Orogeny (Preiss, 2000). For example, the sedimentary structures within the minibasins capture the overall shallowing upward sequence of the Highstand Systems Tract that is not seen in the inclusion stratigraphy (Table 2). If the detailed stratigraphy of the Wonoka Formation and Patsy Hill member were identical in the suprasalt and subsalt minibasins and inclusions, an autosuture (Dooley et al., 2012) would be a more likely interpretation. Our third line of evidence to support an allosuture interpretation is that one salt sheet is thought to be sourced from the northwest, with internal flow represented by the layered evaporite sequence Curdimurka Subgroup sheath fold (Figure 19; Rowan et al., 2019), and the other sheet was likely sourced from the southeast based on the orientation of the halokinetic fold in the subsalt Bunyeroo Formation established by (Figure 19; Hearon et al., 2015a).

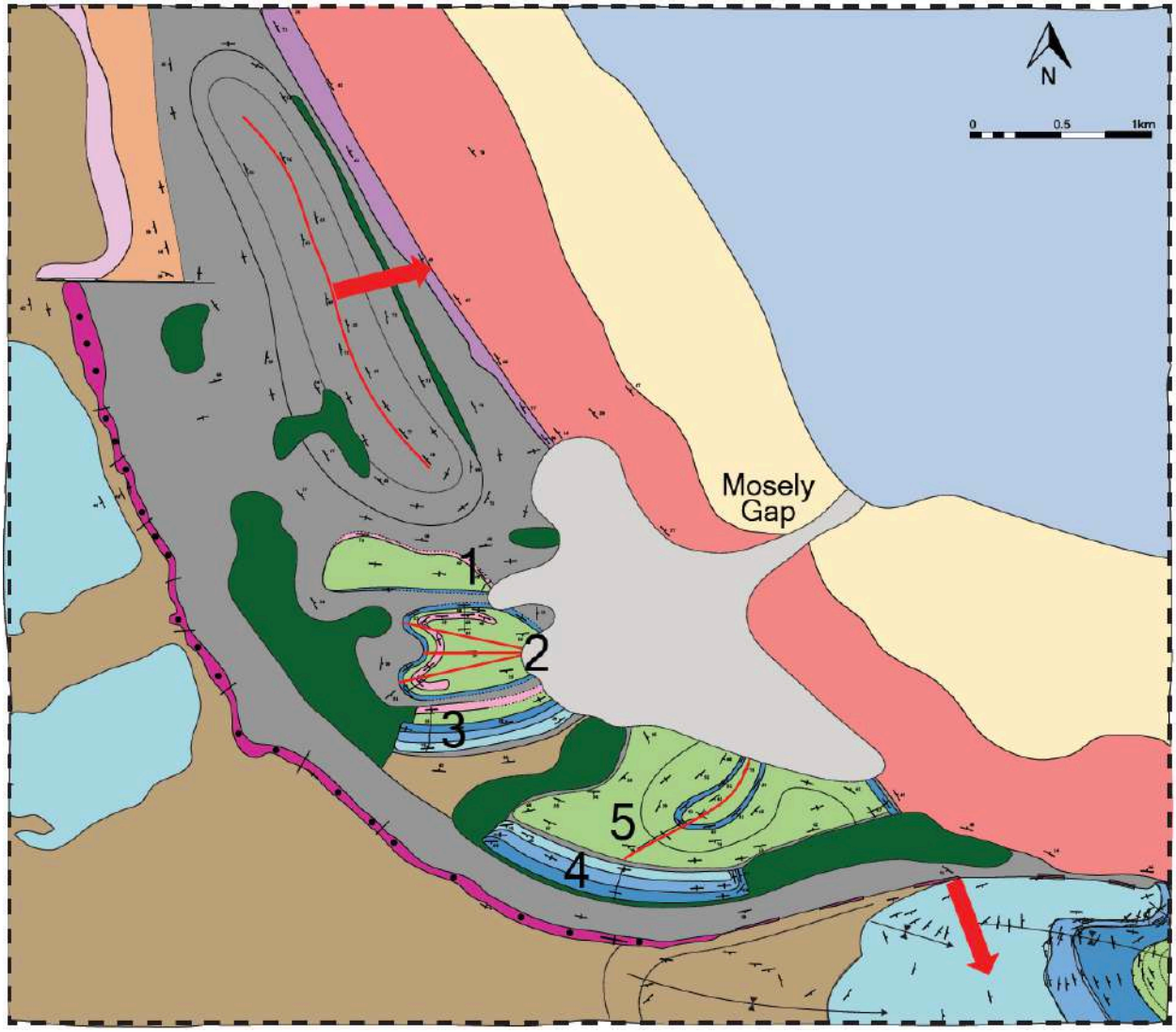

Figure 19: Geologic Map of the Patawarta diapir, Central Flinders Ranges, South Australia (modified from Kernen et al., 2018; Rowan et al., 2019). Stratigraphic units match the key on Figure 4. Red lines in inclusions 2 & 5 are refolded folds, red line to the north is the axial trace of a sheath fold with the red arrow indicating the direction of salt flow (Rowan et al., 2019). The red arrow to the south is from (Hearon et al., 2015) that indicates the direction of salt flow (using the outboard halokinetic sequence fold plane to calculate direction).

The frontal or lateral allosuture at Patawarta diapir could have formed by the following salt tectonic processes: 1) encasement of one salt sheet overriding another salt sheet, 2) encasement of one salt sheet overriding a flared diapir, or 3) encasement by which two or more diapirs or salt sheets amalgamated. It is likely that a salt body was sourced from the northern side of Patawarta diapir and the thickened suprasalt Wonoka Formation provided the sedimentary loading mechanism for a salt body to override the downdip salt body to the south, thus encasing the inclusions in the diapiric matrix. With the interpretation of an allosuture, Patawarta diapir is reinterpreted to represent at least two diapirs instead of a single diapir originally mapped by Coats (1973) and Hall (1984).

The results of the $\delta^{13}C$ geochemistry (along with the outcrop and petrographic observations) suggest that the inclusions are the limestones from the Wonoka Formation and Patsy Hill member. The results of the $\delta^{13}C$ isotopes of the inclusions are not as negative as Husson et al., (2015) regional study, and this could be due to several reasons. Husson et al., (2015) states a -12‰ value in the lowermost part of the lower limestone member of the Wonoka Formation (Figure 18). This value is not captured in our results and could be for two reasons: 1) the lowermost part of the lower member limestone member of the Wonoka Formation or the lowermost part of Lithofacies 1 could be missing (because of erosion, was never deposited) or 2) the $\delta^{13}C$ isotope results are diagenetically altered from post-encasement fluid flow. The heavier $\delta^{13}C$ isotope values of the diapiric matrix and rim dolomite is an indication that a post-encasement fluid flow event likely took place and only altered the lower, middle, and

upper limestone inclusions partially, making those values more positive. Additionally, the $\delta^{18}O$ isotope results are not consistent with Husson et al., (2015) also suggesting that post-encasement fluid flow took place. After close examination of the petrographic sections, there is rhombohedral dolomite cement present in the lower-upper limestone inclusions supporting the post-encasement fluid flow argument to explain the isotopically heavy results (Figures 16a-c). Our outcrop and petrographic data are the strongest arguments for identifying Wonoka Formation and Patsy Hill member age stratigraphy in the Patawarta diapir.

3.7 CONCLUSION

Patawarta Diapir is reinterpreted to contain inclusions of Wonoka Formation and Patsy Hill Member stratigraphy approximately 250 years younger than the Callanna Group stratigraphy (Curdimurka Subgroup). This study utilized outcrop, petrographic, & the presence of the negative $\delta^{13}C$ Shuram excursion to identify Wonoka Formation stratigraphy in the Patawarta Diapir. The current map view of the inclusions comprise folded and faulted Wonoka Formation and Patsy Hill beds that are stratigraphically thinner than the equivalent strata in either subsalt or suprasalt minibasins and are interpreted to represent disrupted remnants of carapace entrained at a suture during the amalgamation of at least two salt bodies (Dooley et al., 2012). The inclusions are interpreted as a suture zone between the northern and southern portion of the diapir with the Callanna Group sheath fold flowing in a different direction than the halokinetic fold in the subsalt Bunyeroo Formation. The difference in salt flow direction support the

interpretation that the carbonate inclusions are forming an allosuture rather than an autosuture. Due to the inclusion distribution and stratigraphic evidence of the suprasalt and subsalt minibasins, the suture is interpreted to separate at least two salt bodies. The Wonoka Formation forms a depositional syncline in the suprasalt minibasin that initiated loading which provided the salt budget to encase the inclusions along with shortening from the Delamerian Orogeny (Preiss, 2000). The results of the $\delta^{13}C$ stable isotope geochemistry suggest that the green siltstone member and lower dolomite beds of the Patsy Hill member and the $\delta^{18}O$ of the middle limestone and green siltstone member and lower dolomite beds directly correlated to the regional stratigraphy from Husson et al., (2015). The $\delta^{13}C$ of the lower and middle limestone member inclusions of the Wonoka Formation do not correlate to the regional stratigraphy from Husson et al., (2015). One possible explanation for this difference in values are that they were diagenetically altered from post-encasement fluid flow.

CHAPTER 4: ORIGIN AND CHARACTERIZATION OF INTRASALT INCLUSIONS

4.1 ABSTRACT

Classification schemes are created in order to communicate pertinent information, especially if there is jargon with loose definitions that vary between academic and industry research groups and teams. Presented here is a classification system for identifying and understanding the origin and nature of intrasalt inclusions. Previously, intrasalt inclusions have variously been termed clasts, rafts, chips, stringers, sutures, or encased minibasins, or can be misinterpreted as seismic anomalies or noise. These terms convey various levels of genetic interpretation and thus implications that become problematic when trying to communicate effectively. The intrasalt inclusion classification scheme presented here divides intrasalt inclusions into three time-stratigraphic sequences relative to depositional age of the salt within the layered evaporite sequence (LES) that the inclusion originated from: 1) *presalt* inclusions originate from the sedimentary, igneous, and metamorphic rocks that form the "basement" framework of the salt basin or the initial infill prior to LES deposition and are thus older than the salt; 2) *synsalt* inclusions originate from non-evaporite lithologies interbedded in the LES, including siliciclastics, carbonates, volcanic flows, and shallow sills and are roughly the same age as the salt; and 3) *postsalt* inclusions originate from the stratigraphy deposited above the layered evaporite sequence and any igneous activity that postdates the layered evaporite sequence.

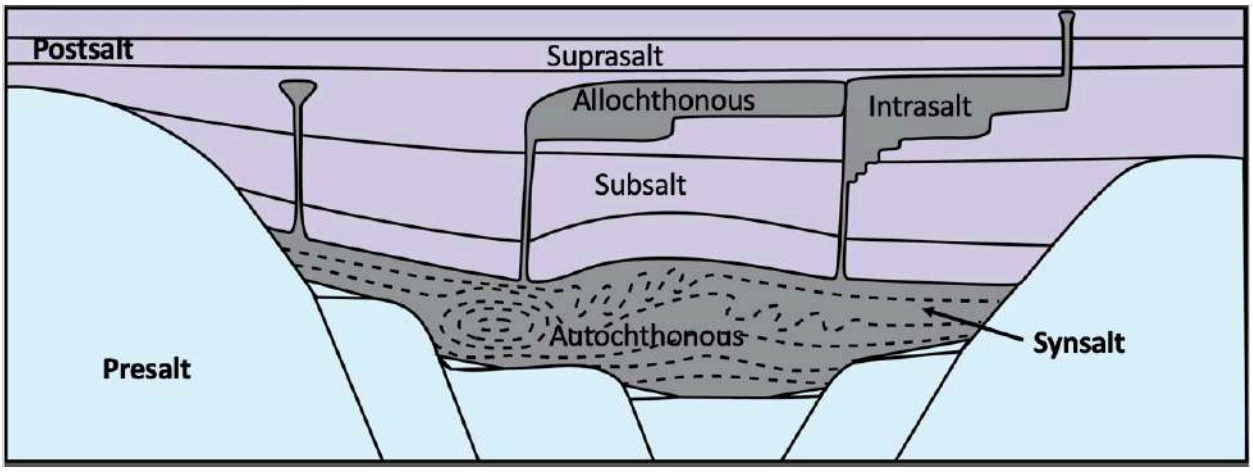

Figure 4.1- Tectonostratigraphic sequences of potential inclusion-type lithologies.

4.2 INTRODUCTION

The characteristics, distribution, and origin of non-halite carbonate intrasalt inclusions within Patawarta Diapir serve as an outcrop analog for inclusions in seismically imaged allochthonous salt bodies. In order to establish the origin, the age of the lithologies must first be correlated to the regional stratigraphy of the Adelaide Basin. The Adelaide Basin fill is grouped into 3 informal lithologic packages. In ascending order these sequences are referred to as the: 1) *presalt*, 2) *synsalt*, and 3) *postsalt*. Intrasalt inclusions from the presalt have three possible modes of origin: 1) *Subsalt plucking* (Harrison, 1930) during salt flow, 2) *Subsalt thrusting* (Couzens-Schultz, 2003) on detachment below the salt horizon thrusting strata up into the salt, and 3) *Mass-wasting* and depositional inter-fingering of clasts derived from the rift basin shoulders or structural highs (Laudon, 1984; Garrison and McMillian, 1999). Intrasalt inclusions of the synsalt origin have 3 possible modes of origin: 1) *Depositional interbedding* of non-halite sediments with the depositional layers of evaporites (Fiduk and Rowan 2012); 2*)*

Syn-depositional volcanic extrusion of lavas onto the surface of the layered evaporite sequence (LES; Mackay, 2011) and 3) *Early post-depositional or coeval magmatic injection* of igneous magmas as dikes or sills along LES bedding plans (Stern et al., 2011, McPhie, 2011). Intrasalt inclusions of the postsalt origin have six possible modes of origin with the first four involving post-depositional diapiric salt encasement of the stratal package: 1) *Primary minibasin* encased in salt (Fernandez et al., 2017; Pilcher et al., 2011), 2) *Secondary minibasin* encased in salt (Pilcher et al., 2011), 3) *Drop-in minibasin* encased in salt (Pilcher et al., 2011), 4) *Carapac*e encased in salt (Hart et al., 2004; Dooley et al., 2012), 5) *Caprock* (Halbouty, 1979), and 6) *Salt Karst* (Rodriguez et al., 2017 & Mueller et al., 2018).

4.3 ORIGIN OF PRESALT INCLUSIONS

The classification of intrasalt inclusions in outcrop and well data is relatively straightforward but is more problematic in seismic reflection datasets due to the lack of age constraining data, possible imaging effects, and the lithologic and geometric similarity of presalt, synsalt, or post-salt stratal packages contained within inclusions. Therefore, there is a need to establish key parameters to aid in their identification. Presalt inclusions could be incorporated into the layered evaporite sequence by 'Subsalt Thrusting' whereby the presalt stratigraphy is thrusted into the salt because of an older shale or salt detachment surface (Table 1; Couzens-Schultz, 2003). Alternatively, the emplacement of presalt inclusions via 'Subsalt Plucking' is an undocumented process by which flowing salt lifts & entrains or "plucks" basement blocks (Table 1; Harrison,

1930). More likely Presalt inclusions originate as lithologies present in salt basin bounding, basement topographic highs that are transported as gravity-driven mass wasting deposits (slide blocks, slumps, and landslides) into the LES depositional system (Table 1; Garrison & McMillian, 1999).

Table 1-Presalt inclusion origins.

Name	Origin	Lithology	Bedding Geometry	Inclusion Geometry
1. Subsalt Plucking (Harrison, 1930)	Presalt material plucked from 'basement' by flowing salt	siliciclastic carbonate evaporites volcanoclastic intrusive igneous metamorphic	parallel concordant growth strata syn-rift	equal length/width ratio high length/width
2. Subsalt Thrusting (Couzens-Schultz et al., 2003)	Presalt material thrusted from basement Pre-salt detachment surface	siliciclastic carbonate evaporites volcanoclastic intrusive igneous metamorphic	parallel concordant growth strata syn-rift	equal length/width ratio high length/width
3. Mass - wasting of salt basin margin or structural high (Garrison & McMillian, 1999)	Presalt reworked into alluvial fan or mass wasting deposit	siliciclastic carbonate evaporites volcanoclastic intrusive igneous metamorphic	cross cut stratigraphy (laccolith or pluton) parallel concordant (sill or extrusive flow)	equal length/width ratio high length/width

Presalt lithologies include siliciclastic, carbonate, evaporite, metamorphic, and intrusive/extrusive igneous rock types (Fig. 2). Presalt inclusions may vary in size from tens to hundreds of meters depending on the scale of the mass wasting event. If the inclusions comprise igneous or metamorphic basement, they will lack internal reflectors; if they are sedimentary, any internal bedding might be difficult to see due to disruption and faulting during the mass wasting event. The bedding geometry of these inclusions will likely be parallel concordant (sedimentary strata, metamorphic lineation, volcanic flows) or bedding-less. It is expected that most inclusion geometries will be equal in their length to width ratio but potentially some variation depending on their lithologic origin.

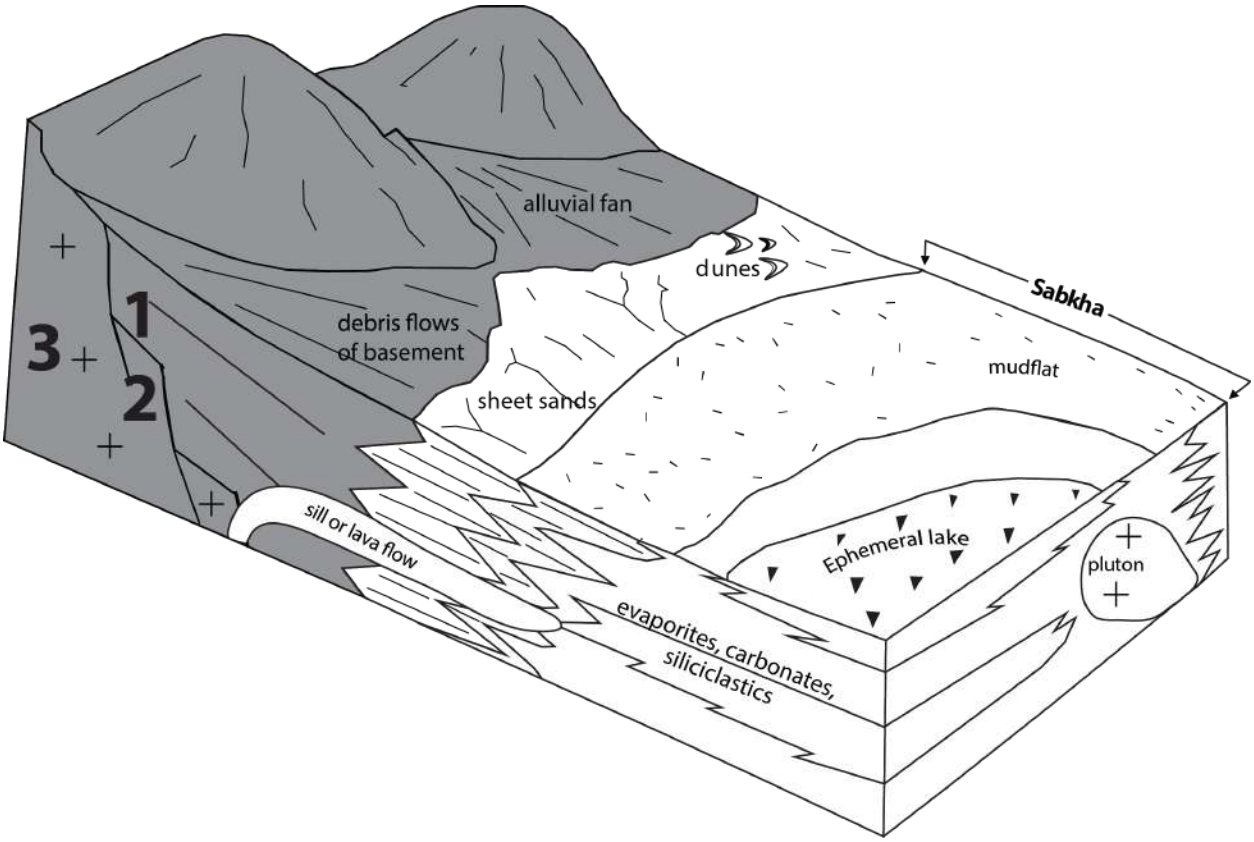

Figure 4.2- schematic cartoon of presalt inclusion types derived from a rift basin topographic high (modified from Warren, 2006).

4.4 ORIGIN OF SYNSALT INCLUSIONS

Synsalt inclusions represent ruptured strong layers, within a ductile matrix of halite and bittern salts, that may form complex folds and boudins (Fiduk & Rowan, 2012). Synsalt inclusions may vary in size from tens to thousands of meters and will display parallel to subparallel reflectors if it is thick enough and comprises sediments that seismically contrast with halite (Fiduk & Rowan, 2012: *showed the carnalite evaporites in Santos Basin gives nice layering contrast with halite*). Intrasalt deformation

generates boudins and variable fold geometries that commonly include isoclinal and sheath folds(refs). Synsalt inclusions most likely are the result of these processes and later salt movement (Table 2; Fiduk & Rowan, 2012; Jackson et al., 2015). Additionally, it is possible and highly likely that igneous plutons in the form of shallow sills and flows could be interbedded with the synsalt LES sequence (Table 2; McPhie, 2011; Stern et al., 2011).

Table 2- Synsalt inclusion origins.

Name	Origin	Lithology	Bedding Geometry	Inclusion Geometry
1. Non-halite interbeds in layered evaporites (Fiduk & Rowan, 2012; Jackson et al., 2015)	autothonous salt extrusive igneous assemblages intrusive sills karst breccia, debris flow, mass wasting, non-halite sedimentary deposites	siliciclastic carbonate volcanoclastic halite, sylvite, carnallite anhydrite potash shale	convergent, onlap truncation, toplap, downlap, halokinetic sequences, megaflaps, parallel concordant	equal length/width ratio high length/width
2 & 3. Igneous Plutons (Stern el al., 2011; McPhie, 2011)	injected into layered evaporite sequence or deposited as a flow	any combination of igneous lithologies	Cross cut stratigraphy (laccolith or pluton), parallel concordant (sill or extrusive flow)	equal length/width ratio low length/width

Synsalt lithologies include siliciclastic, carbonate, evaporite, metamorphic (contact metamorphism from igneous emplacement sills or lava flows (Fig. 3). Synsalt inclusions may vary in size from tens of meters to tens of kilometers. If the inclusions comprise volcanoclastic flows, there will likely be strong reflectors; if they are sedimentary it is highly likely that internal bedding and deformation will be recognizable. The bedding geometry of these inclusions could potentially encompass a wide variety of geometries and scale (Table 2). It is expected that most synsalt inclusion geometries will be tabular or longer than they are wide as LES competent strata are precipitated or settle out into layers that are relatively continuous across the basin, but form relatively thin packages of non-halite lithologies before returning to halite deposition (Warren, 2006).

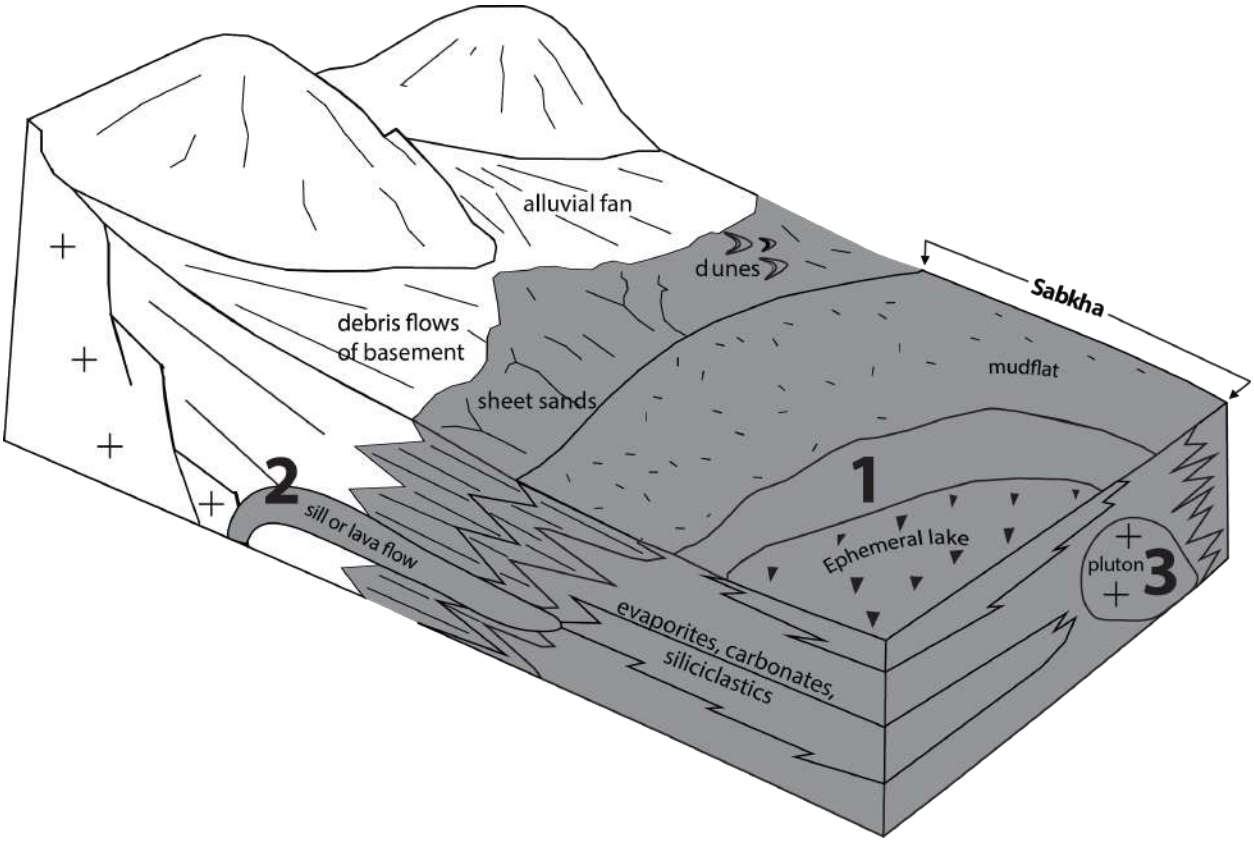

Figure 4.3- Schematic cartoon of synsalt inclusion types derived from a rift basin (modified from Warren, 2006).

4.5 ORIGIN OF POSTSALT INCLUSIONS

Postsalt inclusions may represent: 1) primary minibasins that subside into autochthonous salt; 2) secondary minibasins that subside into allochthonous salt; 3) drop-in basins that subside into a diapir; 4) suprasalt carapace that becomes entrained during amalgamation and suturing of two salt sheets (Table 3; Hart el al., 2004; Dooley et al., 2012). Additionally, caprock and salt karst (the diagenetic carbonate residue from

a salt diapir; Kyle & Posey, 1991) can be incorporated into a salt body as an arbitrary carbonate inclusion (Table 3).

Table 3 - Postsalt inclusion origins.

Name	Origin	Lithology	Bedding Geometry	Inclusion Geometry
1. Primary minibasin (Pilcher et al., 2011)	subside into autothonous salt, may contain: extrusive igneous assemblages or intrusive sills	siliciclastic carbonate evaporites volcanoclastic	convergent, onlap truncation, toplap, downlap, halokinetic sequences, megaflaps	variable
2. Secondary minibasin (Pilcher et al., 2011)	subside into allochthonous salt	siliciclastic carbonate evaporites volcanoclastic	convergent, onlap truncation, toplap, downlap, halokinetic sequences	variable
3. Drop-In minibasin (Pilcher et al., 2011)	subside into primary diapir	siliciclastic carbonate evaporites volcanoclastic	convergent, onlap truncation, toplap, downlap, halokinetic sequences	variable
4. Carapace or Suture (Hart el al., 2004 & Dooley et al., 2012)	condensed, sub-parallel strata on bathymetrical salt high	siliciclastic carbonate evaporites volcanoclastic	parallel concordant	high length/width
5. Caprock (Halbouty, 1979; Kyle & Posey, 1991)	dissolution & accrettion on flanks of diapirs, allochtons & namakiers	gypsum anhydrite carbonate	parallel concordant to edge of diapir, allochtons & namakiers	high length/width
6. Salt karst (Rodriguez et al., 2017 & Mueller et al., 2018)	solution collapse breccia of caprock and roof sediments (carapace)	evaporite carbonate siliciclastic	becciated, infill of karst, sub-parallel, absent	n/a

Postsalt lithologies include siliciclastic, carbonate, and extrusive igneous rock types (Fig. 4). Postsalt inclusions may vary in size from tens of meters to tens of kilometers, depending on the size of the minibasin geometry and/or caprock continuity. If the inclusions comprise volcanoclastic flows, there will likely be strong reflectors; if they are sedimentary it is highly likely that internal bedding and deformation will be recognizable. The bedding geometry of these inclusions could potentially encompass a wide variety of geometry and scale (Table 3). Postsalt inclusions will vary in size and aspect ratio, ranging from thin slivers (carapace along sutures) up to thousands of meters long to thick and broad minibasins that may have halokinetic sequences or growth strata (Table 3). The slivers of carapace can form boudins and folds similar to those of synsalt inclusions (Table 3).

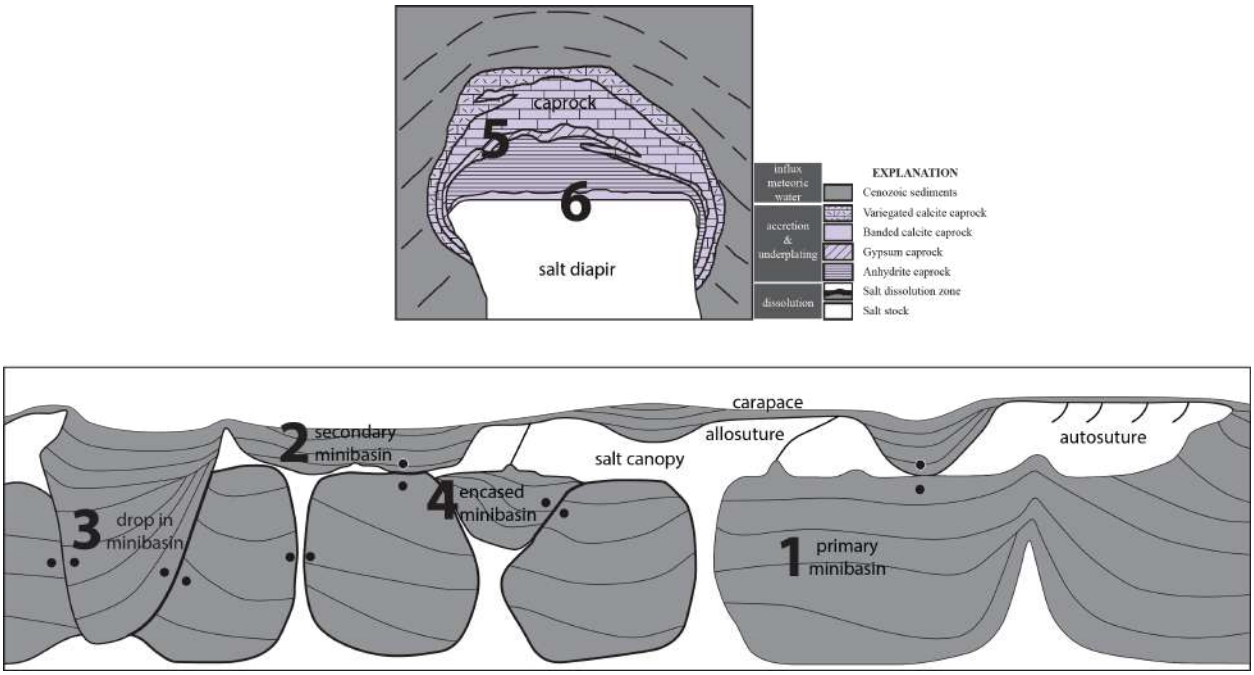

Figure 4.4- Postsalt inclusions types 1-4 different types of minibasin from the deepwater Gulf of Mexico (modified from Pilcher et al., 2011) and 5-6 shallow marine-coastal caprock from the Gulf of Mexico (modified from Kyle & Posey, 1991).

4.6 CONCLUSION

The range of inclusions described above can be present in any basin type and salt tectonic setting, however, Figure 4 of minibasin types is present in highly advanced salt tectonic systems like the Gulf of Mexico. Identification of inclusion origins can potentially be difficult because some of the criteria from Tables 1-3 are non-unique. Moreover, an inclusion origin interpretation on seismic reflection data may be complicated by creating a false image through an incorrect velocity model, stress-induced effects, acquisition limitations resulting in poor illumination, and/or complex salt

geometries. Nevertheless, these guidelines are proposed to help the seismic interpreter and field geologist predict the lithologic and stratigraphic origin of inclusions and thereby reduce the risk associated with drilling through salt. Based on this classification scheme, the inclusions at Patawarta diapir are from the both the synsalt and postsalt category. Chapter 3 described and characterized five limestone inclusions in further detail and provided a mechanism for salt encasement.

4.7 FUTURE WORK

Future work could include detailed outcrop-based descriptions and interpretations of the depositional origin(s) of non-halite sedimentary packages within an allochthonous salt tongue at Pinda diapir and a vertical stock at Beltana diapir in the Flinders Ranges, South Australia. The specific goal of this future work is to map the inclusion distribution, geometry, lithology, stratigraphy, and deformation style within the entire confines of the Pinda and Beltana diapirs and to model the field interpretations using drone data. Once more data is collected from other diapirs in the region, a detailed classification scheme could potentially be created and added to the material presented in this chapter.

A geologic map of the inclusion boundaries and internal stratigraphic and structural data within Pinda and Beltana diapirs will be created in ArcGIS and Adobe Illustrator. Lithologic and structural data will be collected with a Brunton Compass and iPhone 10 using Midland Valley's Clino application. Drone imagery will be used as base materials for the geologic map. To document thickness and facies changes of the

inclusions inside the Beltana and Pinda diapirs a series of stratigraphic sections will be measured within each inclusion type using a Jacob‘s Staff, Brunton Compass, iPhone 10 with Midland Valley Clino application. The measured sections will be correlated by lithology and stratigraphic stacking patterns to the regional stratigraphic units. Each measured section recorded the lithology, grain size, fresh and weathered colors, bedding orientation and formation contacts. Where applicable, a correlation diagram of the intrasalt inclusions will be created from the stratigraphic sections. Samples will be collected to document the range of lithologies and varying mineralogies of the inclusions in Beltana and Pinda diapir. Petrographic thin sections will be stained for calcite and iron with alizarin red-S and potassium ferricyanide and analyzed in both plane and polarized light for groundmass, cements, and grain mineralogy which will be used as a stratigraphic correlation tool.

Drone imagery will be collected, and a 3D model will be built using digital mapping techniques and terrestrially based 3D structure-from-motion based photogrammetry and Light Detection and Ranging (LiDAR). The spatial accuracy of photogrammetrically generated terrain models is evaluated relative to point-cloud derived terrain models obtained by terrestrial laser scanner (TLS) LiDAR system (Bush et al., 2015). The photogrammetric models will be constrained by utilizing the following ground controls (GC): (1) GPS-determined camera positions only (no GC); (2) GC points at prominent natural objects located with a GPS-enabled laser rangefinder and photos; (3) GC points at artificial targets located with differential GPS unit and photos; and (4) GC points at prominent natural objects identified in the LiDAR terrain model and

photos (Bush et al., 2015). The photogrammetric model accuracy depends primarily on the baseline (line that connects the camera positions) length and the distance to the farthest feature (BTD) ratio (Bush et al., 2015). The Clair Camp model with a <200 m position error has a 0.35 BTD, whereas the Noonday model with a 1.0 BTD has <45 m (Bush et al., 2015). BTD may be improved with GC points, more frequent overlapping photographs from more positions, GPS accuracy, and software processing (Bush et al., 2015).

The use of a drone can streamline field work and potentially identify stratigraphic and structural features that are difficult to map inside a complexly deformed salt body. It is difficult to overemphasize the potential impact of this technology on the future of field geology. Inaccessible cliff faces can now be rendered in high-resolution 3D for geologic mapping; the technology affords incredibly detailed mapping in 3D with resolution to a few cm; and even in areas with poor outcrop all key outcrops can be recorded as 3D objects embedded in a spatial database for better documentation of structure (Pavlis et al., 2015). Presently, a two-phase field procedure is required that begins with a data acquisition phase with preliminary interpretations of the terrain model followed by a second field session to finalize interpretations (Pavlis et al., 2015). Drone technology in the field has the capacity to completely revolutionize how geologists complete field work and enables them to continue making observations and collecting from the computer after the field season is complete.

CHAPTER 5: CONCLUSION

In conclusion, two types of anomalous postsalt carbonate inclusions have been identified in the Patawarta Diapir in the central Flinders Ranges, South Australia: 1) rim dolomite lateral caprock at the salt-sediment interface and 2) Wonoka Formation and Patsy Hill member of the Bonney Sandstone inclusions forming a suture zone in the southern part of the Patawarta diapir. The results of these studies are significant because their historic interpretations vary drastically and were not placed into a modern salt tectonics context. The rim dolomite was originally described as 'metamorphic differentiation' by Coats (1973) and was later reinterpreted to be a local carbonate facies in the lower Bunyeroo Formation by Hall (1980). The idea that the rim dolomite is carbonate caprock is a completely new hypothesis and significantly adds to the overall understanding of Precambrian salt diapirism in the Flinders Ranges. The Wonoka Formation and Patsy Hill member inclusions were originally interpreted to be a part of the synsalt Callanna Group, which is approximately 250-300 million years older by Hall (1984). The only inclusions in the Flinders Ranges that were known to be younger than the synsalt Callanna Group are the limestones of the Cambrian that contain Archaeocyathid index fossils. Otherwise, all other inclusions have been assumed to be 'unknown' or part of the Callanna Group stratigraphy. There is no mention of the salt tectonic processes and mechanisms required to encase those inclusions, therefore recognizing the inclusions as a suture zone is historically significant for the overall geological understanding of diapiric history in the Flinders Ranges, South Australia.

The proposed classification system of intrasalt inclusions is geologically significant to the salt tectonics community because it is an attempt to provide a detailed explanation of the intrasalt inclusion origins that can be used for identifying inclusions on seismic reflection data for industry purposes and in the field for future academic studies. The goal is to refine and add data from other salt diapirs in the Flinders Ranges to the proposed classification system prior to publication in order to add depth and completeness so it can be used in a world-wide context where biostratigraphic or well data is not available.

REFERENCES

Cailteux, J.L.H., Muchez, P., De Cuyper, J., Dewaele, S., and De Putter, T., 2018, Origin of megabreccias in the Katanga Copperbelt (D.R. Congo): Journal of African Earth Sciences, v. 140, p. 76-93.

Coats, R.P., 1973, COPLEY map sheet and explanatory notes, Geological Atlas of South Australia 1:250,000 series, Geological Survey of South Australia.

Coats, R. P., Preiss, W.V. 1987, Stratigraphy of the Callanna Group. IN Preiss W.V. (compiler) The Adelaide Geosyncline, Late Proterozoic stratigraphy, sedimentation, palaeontology and tectonics. Part II. The Warrina Supergroup. Chapter 5. Geological Survey of South Australia. Bulletin 53 p. 43-72.

Coats, R. P., 2009, Angepena, South Australia: Adelaide, South Australia Geological Survey, sheet 6636, scale 1:100 000, 1 sheet.

Colquhoun, G.P, 1995, Siliciclastic sedimentation on a storm- and tide-influenced shelf and shoreline, Early Devonain Roxburgh Formation, northeastern Lachlan Fold Belt, southeastern Australia. Sedimentary Geology, v. 97, p. 63-93.

Condon, D., Zhu, M., Bowring, S., Wang, W., Yang,A., Jin, A., 2005, U–Pb ages from the Neoproterozoic Doushantuo Formation, China, Science, 308, p. 95-98.

Couzens-Schultz, B.A., Vendeville, B.C., Wiltschko, D.V., 2003, Duplex style and triangle zone 711 formation: insights from physical modeling. Journal of Structural Geology 25, p. 1623-1644.

Dalgarno, C. R., & Johnson, J. E., 1968, Diapiric structures and Late Precambrian–Early Cambrian sedimentation in Flinders Ranges, South Australia. In J. Braunstein & G. D. O'Brien (Eds.), AAPG Memoir. Diapirs and diapirism p. 301–314. Tulsa, OK: American Association of Petroleum Geologists.

Davison, I., 2009, Faulting and fluid flow through salt, Journal of the Geological Society, London, 166, p. 205-216.

Dooley, T. P., Hudec, M. R., Jackson, M. P. A., 2012, The structure and evolution of sutures in allochthonous salt, AAPG Bulletin, v. 96, No. 6, p. 1045–1070.

Dyson, I. A., 1992, Stratigraphic nomenclature and sequence stratig-raphy of the lower Wilpena Group, Adelaide Geosyncline: The Sandison Subgroup. Geological Survey of South Australia, Quarterly Geological Notes, 122, 2–13.

Dyson, I. A., 1996, Stratigraphy of the Neoproterozoic Aruhna and Depot Springs subgroups. Adelaide Geosyncline, Transactions of the Royal Society, South Australia, 120(3), p. 101–115.

Dyson, I. A., 1998, The ‘Christmas tree diapir’ and salt glacier at Pinda Springs, central Flinders Ranges. MESA Journal, 10, p. 40–43.

Dyson, I. A., 2004, Geology of the eastern Willouran Ranges – evi-dence for earliest onset of salt tectonics in the Adelaide Geosyncline. MESA Journal, 35, p. 48–56.

Dyson, I. A., 2005, Evolution of allochthonous salt systems during development of a divergent margin: The Adelaide Geosyncline of South Australia. In P. P. Post, N. C. Rosen, D. L. Olson, S. L. Palmes, K. T. Lyons, & G. B. Newton (Eds.), Proceedings of the 25th Annual Bob F. Perkins Research Conference. Petroleum systems of divergent continental margin basins p. 69–89. Houston, TX: Gulf Coast Section, SEPM.

Edwards, U., Moore, V., Odumah, U., 2014, Encased Secondary Minibasins: An Emerging Play in the Deepwater Gulf of Mexico, American Association for Petroleum Geologists Annual Convention and Exhibition, Houston, Texas.

Evans, D.G., Nunn, J.A. & Hanor, J.S., 1991, Mechanisms driving groundwater flow near salt domes. Geophysical Research Letters, 18, p. 927-930.

Fernandez, N., Duffy, O.B., Hudec, M.R., Jackson, M.P.A., Burg, G., Jackson, C.A.-L., Dooley, T.P., 2017, The origin of salt-encased sediment packages: Observations

from the SE Precaspian Basin (Kazakhstan), Journal of Structural Geology, doi: 10.1016/j.jsg.2017.01.008.

Fletcher, R. C., M. R. Hudec, and I. A. Watson, 1995, Salt glacier and composite sediment-salt glacier models for the emplacement and early burial of allochthonous salt sheets, in M. P. A. Jackson, D. G. Roberts, and S. Snelson, eds., Salt tectonics: a global perspective: AAPG Memoir 65, p. 77–108.

Fiduk C. J., Clippard, M., Power, S., Robertson, V., Rodriguez, L., Ajose, O., Fernandez, D., Smith, D., 2014, Origin and Transportation and Deformation of Mesozoic Carbonate Rafts in the Northern Gulf of Mexico, Gulf Coast Association of Geological Societies Journal, v. 3, p. 20-32.

Fiduk, C. J., Rowan, M. G., 2012, Brazil Analysis of folding and deformation within layered evaporites in Blocks BM-S-8 & -9, Santos Basin, Brazil, Geological Society, London, Special Publications 2012, v. 363, p. 471-487.

Fike, D. A., Grotzinger, J. P., Pratt, L. M., Summons, R. E., 2006, Oxidation of the Ediacaran ocean, Nature, 444, p. 744-747.

Forbes, B.G., 1971, Stratigraphic subdivision of the Pound Quartzite (late Precambrian, South Australia), Transactions of the Royal Society, Southern Australia, v. 95, p. 219-225.

Forbes, B. G., & Preiss, W. V., 1987, Stratigraphy of the Wilpena Group. In W. V. Preiss (Ed.), The Adelaide Geosyncline – Later Proterozoic stratigraphy, sedimentation, paleontology, and tectonics. Geological Society of Australia Bulletin Vol. 53, p. 211–248. Adelaide, SA: Department of Mines and Energy, Geological Survey of South Australia.

Fyfe, W. S., & Bischoff, J. L., 1965, The calcite–aragonite problem. In: L. C. Pray & R. C. Murray (Eds.), Dolomitization and limestone diagen-esis: A Symposium p. 3–13. Tulsa, Oklahoma: Society of Economic and Paleontologists Mineralogists, Special Publication, 13.

Gannaway, C. E., Giles, K.A., Kernen, R.A., Rowan, M.G., Hearon, T.E., IV, 2014, Comparison of Suprasalt and Subsalt Depositional and Halokinetic History of Patawarta Diapir, Flinders Ranges, South Australia: American Association of Petroleum Geologists 2014 Annual Conventions Abstracts Volumes, Houston, TX.

Garrison, J. M., and McMillan, N. J., 1999, Jurassic continental rift magmatism in northeast Mexico: Allogenic metaigneous blocks in the El Papalote evaporite diapir, La Popa basin, Nuevo Le6n, Mexico, in Bartolini, C., Wilson, J. L., and Lawton, T. F., eds., Mesozoic Sedimentary and Tectonic History of North-Central Mexico: Boulder, Colorado, Geological Society of America Special Paper 340.

Giles, K. A., & Lawton, T. F., 2002, Halokinetic sequence stratigraphy adjacent to the El Papalote diapir, northeastern Mexico. AAPG Bulletin, 86, p. 823–840.

Giles, K. A., and Rowan, M. G., 2012, Concepts in halokinetic–sequence deformation and stratigraphy, in G. I. Alsop, S. G. Archer, A. J. Hartley, N. T. Grant, and R. Hodgkinson, eds., Salt Tectonics, Sediments and Prospectivity, Geological Society of London Special Publications, v. 363, p. 7-31, doi: 10.1144/SP363.2.

Giles, K.A., Lawton, T., Shock, A., Kernen, R., Hearson, T., and Rowan, M.G., 2012, A Halokinetic Drape-Fold Model for Caprock in Diapir-Flanking and Subsalt Positions, in Search and Discovery Article #40956, AAPG, Long Beach, California.

Giles, S. A., Kernen, R.A., Lehrmann, A., Giles, K., 2017, Evolution of a suprasalt minibasin: Neoproterozoic (Ediacaran) Patawarta salt sheet, Flinders Ranges, South Australia, Geological Society of America South Central Annual Conventions Abstracts Volumes, San Antonio, TX.

Gloyna, T. D. and Reynolds, E. F., 1961, Permeability Measurements of Rock Salt, Journal of Geophysical Research v. 66, no. 11.

Gostin, V. A., McKirdy, D. M., Webster, L. J., & Williams, G. E., 2010, Ediacaran ice-rafting and coeval asteroid impact, South Australia; insights into the terminal

Proterozoic environment. Australian Journal of Earth Sciences, 57(7), p. 859–869. doi:10.1080/ 08120099.2010.509408

Grotzinger, J. P., Fike, D. A.,Fischer, W. W., 2011, Enigmatic origin of the largest-known carbon isotope excursion in Earth's history, Nature Geoscience, 4, p. 285-292.

Grover, J. E., 1968, Significance of stylolites in dolomitic limestones. Nature, 217, p. 835–836.

Grover, J. E., 1969, Observations on stylolites in Western Australian rocks. Journal of the Royal Society, Western Australia, 52, p. 12–17.

Haines, P. W., 1987, Carbonate shelf and basin sedimentation, late Proterozoic Wonoka Formation, South Australia (Ph.D. thesis (unpublished)). University of Adelaide, Adelaide, SA.

Haines, P. W., 1988, Storm-dominated mixed carbonate/siliciclastic shelf sequence stratigraphy displaying cycles of hummocky cross-stratification, late Proterozoic Wonoka Formation, South Australia. Sedimentary Geology, 58(2–4), p. 237–254. doi:10.1016/0037-0738(88)90071-1

Haines, P. W., 1990, A late Proterozoic storm-dominated carbonate shelf sequence: The Wonoka Formation in the central and southern Flinders Ranges, South Australia. In J. B. Jago & P. S. Moore (Eds.), The evolution of a Late Precambrian–Early Paleozoic rift complex: Adelaide geosyncline p. 117–198. Sydney, NSW: Geological Society of Australia, Special Publication v. 16.

Halbouty, M. T., 1979, Salt domes—Gulf region, United States and Mexico, 2nd edition: Houston, Texas, Gulf Publishing, p. 561.

Hall, D., 1984, The mineralization and geology of Patawarta Diapir, northern Flinders Ranges, South Australia, Honours thesis, University of Adelaide, (unpublished).

Hall, D., Both, R.A., Daily, B., 1986, Copper Mineralization in the Patawarta Diapir, northern Flinders Ranges, South Australia, Bulletin of Australasian Institute of Mining and Metallurgy, v. 291, no. 7, p. 55-60.

Halverson, G., Wade, B., Hurtgen, M., & Barovich, K., 2010, Neoproterozoic chemostratigraphy. Precambrian Research, 182(4), p. 337-350.

Han, G., Hunter, K., Osmond, J., Ressler, J., Zambonini, M., 2008, Drilling through bitumen in the Gulf of Mexico: the shallower vs. the deeper: Offshore Technology Conference, Houston, 5-8 May, OTC 19307, p. 11.

Harrison, J.V., 1930. The Geology of some Salt-Plugs in Laristan, Southern Persia, Quarterly 743 Journal of the Geological Society 86, p. 463-522.

Hart, W., Jaminski, J., and Albertin, M., 2004, Recognition and Exploration Significance of Suprasalt Stratal Carapaces, Salt-Sediment Interactions and Hydrocarbon Prospectivity: Concepts, Applications, and Case studies for the 21st century, p. 166-199.

Hayes, J., & Waldbauer, J., 2006, The carbon cycle and associated redox processes through time. Philosophical Transactions of the Royal Society of London. Series B, Biological Sciences, 361(1470), p. 931-950.

Hearon, T. E., IV, Lawton, T. F., & Hannah, P. T., 2010, Subdivision of the upper Burra Group in the eastern Willouran Ranges, South Australia. MESA Journal, 59, p. 36–46.

Hearon, T.E., IV, Rowan, M.G., Giles, K.A., Kernen, R.A., Gannaway, C.E., Lawton, T.F., Fiduk, C.J., 2015, Allochthonous salt initiation and advance in the northern Flinders and eastern Willouran ranges, South Australia: using outcrops to test subsurface-based models from the northern Gulf of Mexico, American Association of Petroleum Geologists Bulletin.

Hearon, T. E., IV, Rowan, M. G., Lawton, T. G., Hannah, P. T., & Giles, K. A., 2015, Geology and tectonics of Neoproterozoic salt diapirs and salt sheets in the eastern Willouran Ranges, South Australia. Basin Research, 27(2), p. 183–207.

Helgesen, H. K., Tang, J., Liu, J., Salama, A., Pepper, R., Madden, S., Woodward, M., Klebleeva, A., Frugier-Dorrington, E., El Sabaa, A., Yarman, C. E., Fournier, A., Yang, Y., Osypov, K. S., 2013, Dirty Salt Velocity Model Building: Society of Exploration Geophysicists Annual Meeting, Houston, p. 5.

Huang, W., Jiao, K., Vigh, D., Kapoor, J., Watts, D., Hongyan, L., Derharoutian, D., Cheng, X., Application of full-waveform inversion for salt sediment inclusion inversion: Society of Exploration Geophysicists Annual Meeting, Las Vegas, p. 5.

Husson J. M., Maloof A. C., Schoene B., Chen C. Y. and Higgins J. A., 2015, Stratigraphic expression of Earth's deepest d13C excursion in the Wonoka Formation of South Australia. Am. J. Sci. 315, 1–45.

Jackson, C. A. L., and Lewis, M.M., 2012, Origin of an anhydrite sheath encircling a salt diapir and implications for the seismic imaging of steep-sided salt structures, Egersund Basin, Northern North Sea: Journal of the Geological Society, v. 169, no. 5, p. 593–599.

Jackson, C. A., Lewis, M. M., and Mannie, A. S., 2013, Characterization and Origin on Anhydrite-Rich 'Lateral Caprock' Adjacent to Halite-Cored Salt Diapirs; Implications for Prospectivity in Salt Basins. Oral presentation at AAPG 2013 Annual Convention and Exhibition Pittsburgh, Pennsylvania, May 19-22, 2013.

Jackson, C. A. L., Jackson, M. P. A., Hudec, M. R., Rodriguez, C., R., 2015, Enigmatic structures within salt walls of the Santos Basin—Part 1: Geometry and kinematics from 3D seismic reflection and well data, Journal of Structural Geology, Volume 75, 2015, Pages 135-162, ISSN 0191-8141, https://doi.org/10.1016/j.jsg.2015.01.010.

Jackson, M. P. A., and Talbot, C. J., 1991, A glossary of salt tectonics: The University of Texas at Austin: Bureau of Economic Geology Geological Circular, 91-4, p. 44.

Jackson, M. P. A., and Hudec, M.R., 2004, A new mechanism for advance of allochthonous salt sheets, in P. J. Post, D. L. Olson, K. T. Lyons, S. L. Palmes, P. F. Harrison, and N. C. Rosen, eds., Salt–sediment interactions and hydrocarbon prospectivity: Concepts, applications, and case studies for the 21st century: 24th Annual Gulf Coast Section, SEPM Foundation Bob F. Perkins Research Conference, p. 220–242.

Kaebe, R. M., 2015, The palaeoenvironmental context of Neoproterozoic carbon-isotope excursions, The University of Adelaide School of Physical Sciences (PhD Dissertation unpublished). Adelaide, South Australia.

Kernen, R. A., 2011, Halokinetic sequence stratigraphy of the Neoproterozoic Wonoka Formation at Patawarta Diapir, Central Flinders Ranges, South Australia: Master's thesis, New Mexico State University, Las Cruces, New Mexico (master's thesis unpublished).

Kernen, R.A., Giles, K.A., Lawton, T.F., Rowan, M.G., Hearon, T.E., IV, 2012, Depositional and halokinetic sequence stratigraphy of the Neoproterozoic Wilpena Group adjacent to Patawarta allochthonous salt sheet, central Flinders Ranges, South Australia in G. I. Alsop, S. G. Archer, A. J. Hartley, N. T. Grant, and R. Hodgkinson, eds., Salt Tectonics, Sedimentation and Prospectivity: London, Geological Society of London Special Publication 363, p. 81-105.

Kernen, R. A., Giles, K. A., Fischer, M. P., Giles, S. A., Lehrmann, A., & Rowan, M. G., 2017, Evaluating exploration potential of suture zones or encased minibasins using an outcrop example from the Neoproterozoic Patawarta Salt Canopy, Central Flinders Ranges, South Australia. American Association of Petroleum Geologists Annual Conventions Abstracts Volumes, Houston, TX. Tulsa, OK: American Association of Petroleum Geologists.

Kernen, R. A., Giles, K. A., & Rowan, M. G., 2018, Origin, characteristics, and distribution of intrasalt non-halite stratal packages at Patawarta diapir, Flinders Ranges, South Australia. Paper presented at the Geological Society of America Penrose Conference on “Advances in salt tectonics: Observations, applications, and perspectives: In honor of Martin P. A. Jackson”, Sedom, Israel. Boulder, CO: Geological Society of America.

Knoll, A. H., 1985, The distribution and evolution of microbial life in the Late Proterozoic era. Annual Review of Microbiology, 39, 391–417. doi:10.1146/annurev.mi.39.100185.002135

Kyle, J. R., & Posey, H. H., 1991, Halokinesis, cap rock development, and salt dome mineral resources. In J. L. Melvin (Ed.), Evaporites, petroleum and mineral resources p. 413–474. Amsterdam, Netherland: Elsevier.

Kukla, P.A., Reuning, L., Becker, S., Urai, J.L. and Schoenherr, J., 2011b. Distribution and mechanisms of overpressure generation and deflation in the late Neoproterozoic to early Cambrian South Oman Salt Basin. Geofluids, 11(4): p. 349-361.

Lagabrielle, Y., Labaume, P., de Saint Blanquat, M., 2010, Mantle exhumation, crustal denudation, and gravity tectonics during Cretaceous rifting in the Pyrenean realm (SW Europe): Insights from the geological setting of the lherzolite bodies. Tectonics, 29 (2010), p. TC4012, 10.1029/2009TC002588

Laudon, R. C., 1984, Evaporite diapirs in the La Popa basin, Nuevo Leon, Mexico: Geological Society of America Bulletin, v. 95, p. 1219-1225.

Le Guerroué, E., 2010, Duration and synchroneity of the largest negative carbon isotope excursion on Earth: the Shuram/Wonoka anomaly Comptes Rendus Geoscience, 342 (2010), pp. 204-214.

Lehrmann, A., Kernen, R. A., Giles, S., Giles, K., 2017, Timing of allochthonous salt emplacement of the Neoproterozoic (Ediacaran) Patawarta salt sheet, Flinders Ranges, South Australia: Evidence from the subsalt minibasin, Geological Society of America South Central Annual Conventions Abstracts Volumes, San Antonio, TX.

Lemon, N. M., 1988, Diapir recognition and modelling with examples from the late proterozoic Adelaide Geosyncline, Central Flinders Ranges, South Australia. Ph.D. thesis, University of Adelaide, Department of Geology and Geophysics.

Lemon, N. M., 2000, A Neoproterozoic fringing stromatolite reef complex, Flinders Ranges, South Australia: Precambrian Research, v. 100, no. 13, p. 109–120 doi:10.1144/SP363.5.

Li, Z., Ji, S., Bai, B., Wu, Q., Han, W., Dirty Salt Tomography Using RTM 3D Angle Gathers; Society of Exploration Geophysicists Annual Meeting, San Antonio, p. 5.

Machel, H. G., 1989, Relationships between sulphate reduction and oxidation of organic compounds to carbonate diagenesis, hydrocar-bon accumulations, salt domes, and metal sulphide deposits. Carbonates and Evaporites, 4(2), p. 137–161. doi:10.1007/BF03175104

Mackay, W. G., 2011, Structure and sedimentology of the Curdimurka Subgroup, northern Adelaide Fold Belt, South Australia: Ph.D. thesis, University of Tasmania, Hobart, p. 420.

Mast, A. M., 2016, The origin of the anomalous carbonate units out-cropping at the salt-sediment interface of the southern end of Gypsum Valley Salt Wall, Paradox Basin, Colorado (Master's Thesis (unpublished)). University of Texas at El Paso, El Paso TX.

Mawson, D., 1938, Cambrian and sub-Cambrian formations at Parachilna Gorge. Transactions of the Royal Society, South Australia, 62, p. 255–262.

Mawson, D., 1939, The late Proterozoic sediments of South Australia. Report Australian NZ Association for the Advancement of Science, 24, p. 79–88.

Mawson, D., 1941, The Wilpena Pound Formation and underlying Proterozoic sediments. Transactions of the Royal Society, South Australia, 65, p. 295–303.

Mawson, D., & Segnit, E. R., 1949, Purple slates of the Adelaide System. Transactions of the Royal Society, South Australia, 72, p. 276–280.

McPhie, J., Kamenetsky, V., Chambefort, I., Green, N., 2011, Origin of the supergiant Olympic Dam Cu-U-Au-Ag deposit, South Australia: Was a sedimentary basin involved? Geology, August, 2011; vs. 39; no. 8; p. 795-798.

Milliken, K. L., 1979, The silicified evaporite syndrome—two aspects of silicification history of former evaporite nodules from southern Kentucky and northern Tennessee. Journal of Sedimentary Petrology, 49(1), p. 245–256.

Moore, V. and Douglas, H., 2013, Secondary Basins and Sediment Pathways in Green Canyon, Deepwater Gulf of Mexico, American Association of Petroleum Geologists Annual Convention and Exhibition, Pittsburgh, Pennsylvania.

Murrell, B., 1977, Statigraphy and Tectonics across the Torrens Hinge Zone Between Andamooka and Marree, South Australia. Victoria University of Wellington (BSc unpublished).

Neely, J., Mironova, A., Hearon, T. E., 2017, Structural Evolution of Encapsulated Oligocene Minbasins and Allochthonous Salt in the Northern Gulf of Mexico,

American Association of Petroleum Geologists Annual Convention and Exhibition, Houston, Texas.

Peles, O., Bartana, A., Kosloff, D., Koren, Z., 2004, Limitations of the exploding reflector model in sub-salt imaging, Society of Exploration Geophysicists Annual Meeting, Denver, p. 3.

Pilcher, R. S., Kilsdonk, B., Trude, J., 2011, Primary basins and their boundaries in the deep-water northern Gulf of Mexico: Origin, trap types, and petroleum system implications, AAPG Bulletin, v. 95, n. 2, p. 219–240.

Poe, P. L., Giles, K. A., Brunner, B., Kernen, R. A., Labrado, A., & Lerer, K., 2018, Classification of caprock associated with salt diapirs. Poster. Penrose conference “Advances in salt tectonics: observations, applica-tions, and perspectives: In honor of Martin P.A. Jackson.” Ein Boqeq, Dead Sea, Israel. Poster. Boulder, CO: Geological Society of America.

Preiss, W. V., 1987, The Adelaide Geosyncline-late Proterozoic stratigraphy, sedimentation, palaeontology and tectonics: Geological Survey of South Australia Bulletin v. 53, p. 438.

Preiss, W. V., 2000, The Adelaide Geosyncline of South Australia and its significance in Neoproterozoic continental reconstruction: Precambrian Research, v. 100, p. 21-63.

Read, R., 1971, Geological Report on the Patawarta Diapir, Part S.M.L. 557 (formerly S.M.L. 292), North Flinders Mines Limited, Open File Envelope n. 1638, Progress Reports to Licence Expiry/Renewal for the Period 25/3/1971-24/3/1972.

Reid, P. W., & Preiss, W. V., 1999, PARACHILNA map sheet (second ed.): Geological Atlas 1:250 000 Series, Sheet SH54-13. Adelaide SA: South Australia Geological Survey.

Rodriguez, C. R., Jackson, C. A., Bell, R. E., Rotevatn, A., & Francis, M., 2017, Submarine salt dissolution in the Santos Basin, offshore Brazil. https://doi.org/10.31223/osf.io/en4x7

Rowan, M. G., Lawton, T. F., Giles, K. A., & Ratliff, R. A., 2003, Near-salt deformation in La Popa basin, Mexico, and the northern Gulf of Mexico: A general model for passive diapirism. AAPG Bulletin, 87(5), p. 733–756. doi:10.1306/01150302012

Rowan, M. G., & Vendeville, B. C., 2006, Foldbelts with early salt with-drawal and diapirism: Physical model and examples from the north-ern Gulf of Mexico and the

Flinders Ranges, Australia. Marine and Petroleum Geology, 23(9–10), p. 871–891. doi:10.1016/j.marpetgeo. 2006.08.003

Rowan, M.G., Inman, K.F., 2011, Salt-related deformation recorded by allochthonous salt rather than growth strata. Gulf Coast Association of Geological Societies Transactions 61, p. 379-390.

Rowan, M. G., Hearon, T. E., Kernen, R. A., Giles, K. A., Gannaway, C. E., Williams, N. J., Hannah, P. T., 2019, A review of allochthonous salt tectonics in the Flinders and Willouran ranges, South Australia. Australian Journal of Earth Sciences, 66. doi:10.1080/08120099. 2018.1553063

Roy, A., and Chazalnoel, 2011, RTM technology for improved salt imaging in the Santos Basin, Brazil: Society of Exploration Geophysicists Annual Meeting, San Antonio, p. 5.

Schmid, S., 2017, Neoproterozoic evaporites and their role in carbon isotope chemostratigraphy (Amadeus Basin, Australia). Precambrian Research, 290, p. 16-31.

Schwerdtner, and Troeng, 1978, Strain Distribution within Arcuate Diapir Ridges of Silicone Putty. Tectonophysics 50, p. 13-28.

Selwyn, A. R. C., 1860, Geological notes of a journey in South Australia from Cape Jervis to Mount Serle, Park. Adelaide, SA: Parliamentary Papers., no. 20.

Sprigg, R. C., 1952, Sedimentation in the Adelaide Geosyncline and the formation of a continental terrace, in M. F. Glaessner and E. A. Rudd, eds., Sir Douglas Mawson Anniversary Volume: Adelaide, University of Adelaide, p.153–159.

Stern, R.J., Anthony, E.Y., Ren, M., Lock, B.E., Norton, I., Kimura, J. I., Miyazaki, T., Hanyu, T., Chang, Q., and Hirahara, Y., 2011, Southern Louisiana salt dome xenoliths: First glimpse of Jurassic (ca. 160 Ma) Gulf of Mexico crust, Geology, April 2011; v. 39; no. 4; p. 315-318.

Thompson Jobe, J. A., K. A. Giles, B. Trudgill, T. E. Hearon IV, C. E. Gannaway, Z. R. Jobe, & M. G. Rowan, 2019 Structural and Stratigraphic Evolution of the Sinbad Valley Salt Wall, NE Paradox Basin, SW Colorado (in press).

von der Borch, C. C., Grady, A. E., Eickhoff, K. H., Dibona, P., & Christieblick, N., 1989, Late proterozoic patsy springs Canyon, Adelaide Geosyncline – submarine or subaerial origin. Sedimentology, 36(5), p. 777–792. doi:10.1111/j.1365-3091.1989.tb01746.x

Walker, R.G. and Plint, A.G., 1992, Wave- and Storm-Dominated Shallow Marine Systems, In: Facies Models Response to Sea Level Change, Memorial University of Newfoundland St. John's, Newfoundland and Labrador, Geological Association of Canada, p. 219-238.

Walther, J., 1894, Einleitung in die Geologie als historische Wissenschaft. In Lithogenesis der Gegenwart p. 535–1055. Jena, Germany: G. Fischer Verlag.

Warren, J.K., 2006, Evaporites: Sediments, Resources and Hydrocarbons: Springer Science & Business Media.

Webb, B. P., 1960, Diapiric structures in the Flinders Ranges, South Australia. Australian Journal of Science, 22, 390–391.

Weijermars, R., Jackson, M.P.A., and Dooley, T.P., 2014, Quantifying drag on wellbore casings in moving salt sheets: Geophysics Journal International, v. 198, p. 965-977.

Williams, N. J., 2017, Structural evolution and paleohydrology of a ter-tiary salt weld, Willouran Ranges, South Australia (Unpublished mas-ter's thesis). Northern Illinois University, DeKalb, IL.

Zdanovsky, A. B., 1956, Kinetics of dissolution of natural salts in condi-tions of forced convection. Leningrad USSR: Goskhimizdat, 219 p. (in Russian).

VITA

Rachelle Ann Kernen was born in Upland, California and later moved to Neenah, Wisconsin where she attended primary school. Rachelle graduated from Neenah High School in May 2003 and later attended undergraduate university at The University of Wisconsin Oshkosh. While pursuing a degree in education, she fell in love with geology and changed her major to a bachelor's in science majoring in geology. After graduating in August 2008, she moved to Las Cruces, New Mexico and pursued a master's degree in geology at New Mexico State University. In the summer of 2009, Rachelle began her research in the Flinders Ranges, South Australia and later finished her degree in spring 2011. Rachelle interned for Samson Resources for the first half of 2011 and later started a full-time position as an exploration geologist at the Royal Dutch Shell in Houston, Texas. At Shell, Rachelle completed the 3-year Shell Graduate Program and had many experiences traveling around the globe. During this time, she continued her research in South Australia and later took an academic leave of absence from Shell and began her Ph.D. in Geological Sciences at the University of Texas at El Paso in the fall of 2015. Rachelle continued to work on research in South Australia and presented at conferences and published papers. While at UTEP, Rachelle received numerous awards and scholarships from the geology department and through other professional organizations. Rachelle obtained funding for a postdoc position at the University of Adelaide's Australian School of Petroleum and Natural Resources where she will continue her research in Australia and continue to build her career as an academic.

Contact Information: rachellekernen@gmail.com